Preparation of Nano-Structured Catalysts

Thesis submitted in accordance with the regulations of the

University of Cardiff for the degree of

Doctor of Philosophy

By

Mosaed Saud S. Alhumaimess

2012

In The Name Of Allah, The Most Compassionate,
The Most Merciful

Declaration

This work has not previously been accepted in substance for any degree and is not being concurrently submitted in candidature for any degree.

Signed…….. (Candidate)

Date…….

Statement 1

This thesis is the result of my own investigations, except where otherwise stated.
Other sources are acknowledged by footnotes giving explicit references. A bibliography is appended.

Signed……. (Candidate)

Date……..

Statement 2

I hereby give consent for my thesis, if accepted, to be available for photocopying and for inter-library loan, and for the title and summary to be made available to outside organizations.

Signed…….. (Candidate)

Date……...

To the memory of my father

To my mother

To my wife

To my sons Bakr, Saud, Khalid and Asim

Acknowledgements

I would like to begin with praising and thanking the god, Allah, the almighty for all his bounties upon me and for his assistance in my life and my study which without him this work would not have been achieved.

I would like to greatly thank my supervisor, Professor Graham Hutchings, for his great guidance and support during my study. I am deeply thankful to Dr. Stuart Taylor, Dr. Jonathan Bartley, Dr. Nicolas Dummer and Dr. Marco Conte for their guidance and support on resolving technical problems and revising my thesis. Thanks to all technical staff in Chemistry Department.

I also would like to thank all people in Lab. 1.88 and 1.86 who helped me during my study. Special thanks to my friends Salem Bawaked, Hamed Alshammari, Moataz Morad and Obaid Aldosari who made this study more enjoyable. My thanks to my neighbour Raee Alqahtani with whom I spent a lovely time in Cardiff.

Thanks are due for my sponsor, Al-Jowf University, in Saudi Arabia for their financial support and for giving me this opportunity to increase my knowledge.

Finally, my sincere prays are to my father, Allah's mercy upon him, who devoted his life to provide me a happy life and an excellent education. I ask Allah to bless you and admit you to his paradise. My great thanks are due to my beloved mother, who knows what she means to me, for her emotional support. I would like to thank my wife and sons for their unlimited patience and sacrifices and without them I do not think I would have completed this journey.

Abstract

Gold catalysts have been found to be effective for many oxidation reactions and it is known that the performance of these catalysts depends strongly on the particle size of Au nanoparticles. However, other factors have strong influence on the catalytic activity such as the preparation methods, choice of support, the structure and morphology of supports. The effect of support morphology and structure on the activity of Au catalysts was investigated using two hydrothermally prepared supports, CeO_2 and MnO_2.

Ceria foams as a support for nano-clusters of gold were synthesised hydrothermally at 160 °C by the reaction of L-Asparagine and $CeCl_3.7H_2O$ at different crystallisation times. The effect of the reaction time on the morphology of prepared CeO_2 was investigated. The morphology varied remarkably and it was found to change from spherical particles to foam and eventually to a collapsed foam as the crystallisation time increased. Gold catalysts were prepared by sol-immobilisation, supported on the foam ceria and examined for solvent free oxidation of benzyl alcohol using molecular O_2 as an oxidant and the effect of the support was compared with commercial ceria. Au/CeO_2 foam catalysts were more active than the Au/commercialCeO_2 although the Au nanoparticles were larger in ceria foam supports. This was due to the greater lability of surface oxygen in the foam support compared with commercial CeO_2 materials. The Au/CeO_2 foam catalyst was found to be reusable over three experiments. The effect of catalyst loading, oxygen pressure and reaction time-online were also studied. It was found that there was no mass transfer limitation when the mass of catalyst varied from 5 to 40 mg under the reaction conditions. The conversion of benzyl alcohol decreased as the oxygen pressure decreased which shows that oxygen was involved in the oxidation process. For time-online study, the conversion increased as the reaction time increased with slightly increase.

MnO_2 supports were synthesised by reacting $MnSO_4.H_2O$ with $(NH_4)_2S_2O_8$ hydrothermally at 160 °C. Two different phases and morphologies of MnO_2 were formed and as the reaction time increased the morphology changed from microspheres to nanowires and the MnO_2 phase changed from α- to β-. Gold was deposited on all prepared MnO_2 materials and the catalysts were examined for solvent free benzyl alcohol and CO oxidation. The influence of the preparation method on the catalytic activity was studied and sol-immobilisation was found to be the best for benzyl alcohol

oxidation whereas the deposition-precipitation was found to be the best for CO oxidation. Impregnation method exhibited poor activity for both reactions. The effect of the morphology and phase on the catalyst activity for both reactions was researched and Au/α-MnO_2 microspheres catalysts were best for benzyl alcohol oxidation while Au/β-MnO_2 nanowires catalysts exhibited better performance for CO oxidation due to their smaller Au nanoparticles and easier surface reduction. The catalysts reusability, time-online and the effect of catalyst loading were also studied of an Au/MnO_2 microsphere catalyst for benzyl alcohol oxidation reaction.

Vanadium phosphate catalysts have been extensively studied for the selective oxidation of butane to maleic anhydride. The catalytic activity of vanadium phosphates is greatly dependant on the preparation method of the catalyst precursor $VOHPO_4 \cdot 0.5H_2O$. Poly (acrylic acid-co-maleic acid) copolymer, PAAMA, was employed as a structure directing agent in the preparation of $VOHPO_4.0.5H_2O$ via two routes. The effect of PAAMA concentration on the structure morphology of $VOHPO_4 \cdot 0.5H_2O$ was studied in both preparation routes. As the concentration of PAAMA increased the morphology changed from rosette like for the standard precursors to rosette-like agglomerates with isolated rhomboidal platelets and eventually to isolated rhomboidal platelets at highest concentration of PAAMA. The XRD confirmed that all precursors were $VOHPO_4 \cdot 0.5H_2O$ but as the concentration of PAAMA increased the (001) reflection increased and the (220) reflection decreased. When these precursors were tested for butane selective oxidation, the standard precursors that contain rosettes VPO0 and VPD0 activated to the active phase ($(VO)_2P_2O_7$) over typically observed time (> 100 h). While the precursors that had rosette-like agglomerates with isolated rhomboidal platelets and a relative intensity ratio of the (001)/(220) reflections of around 1.4, VPO5 and VPD15, activated much faster, less than 20 h with a comparable conversion and selectivity. The isolated rhomboidal platelets precursors which had a high relative intensity ratio of the (001)/(220) reflections, VPO15, VPO25 and VPD25, displayed very poor activity because the thin platelets were rapidly oxidised to α_{II}-$VOPO_4$ phase as confirmed by the XRD and Laser Raman Spectroscopy.

Table of contents

Chapter 1 Introduction……. 1-57

1 Historical background of catalysis…….. 1

1.2 Importance of catalysis…… 3

1.3 Categories of catalysis……. 5

1.3.1 Homogeneous catalysis……... 5

1.3.2 Heterogeneous catalysis……... 5

1.3.3 Biocatalysis…….. 7

1.4 Oxidation catalysis…….. 8

1.5 Gold catalysis…….. 12

1.5.1 Historical background…….. 12

1.5.2 Preparation method of supported gold catalysts…….. 15

1.5.2.1 Impregnation……... 15

1.5.2.2 Co-precipitation……... 16

1.5.2.3 Deposition-precipitation (DP)……. 16

1.5.2.4 Sol-immobilisation…….. 17

1.5.3 Reactions catalysed by gold…… 18

1.5.3.1 Selective oxidation of benzyl alcohol……. 18

1.5.3.2 CO oxidation…….. 26

1.5.4 Preparation methods of CeO_2 and MnO_2 supports…….. 33

1.6 Vanadium Phosphorus Oxide Catalysts…….. 36

1.6.1 Background……. 36

1.6.2 Preparation of catalyst precursors $VOHPO_4.0.5H_2O$…….. 38

1.6.2.1 The VPA method (preparation in aqueous media)…….. 38

1.6.2.2 The VPO method (preparation in organic media)……... 39

1.6.2.3 The VPD method (preparation in organic media via $VOPO_4 \cdot 2H_2O$)…… 40

1.6.3 Reaction mechanism…… 44

1.7 The aims of this study…….. 47

1.8 References……... 49

Chapter 2 Experimental…… 58-84

2 Experimental…… 59

2.1 Preparation of supports…… 59

2.1.1 Preparation of CeO_2 foams…….. 59

2.1.2 Preparation of MnO_2 nanowire microspheres…….. 59

2.2 Preparation of gold catalysts……... 60

2.2.1 Sol-immobilisation method……. 60

2.2.1.1 Sol-immobilisation using THPC stabiliser…….. 60

2.2.1.2 Sol-immobilisation using PVA stabiliser…… 60

2.2.1.3 Reflux Sol-immobilisation method……. 61

2.2.2 Impregnation method……... 61

2.2.3 Deposition precipitation……... 61

2.3 Preparation of vanadium phosphate catalysts…….. 62

2.3.1 Preparation of $VOHPO_4.0.5H_2O$ precursor via VPO route……. 62

2.3.1.1 Standard procedure…….. 62

2.3.1.2 Copolymer modified procedure…….. 62

2.3.2 Preparation of $VOHPO_4.0.5H_2O$ precursor via VPD route……. 63

2.3.2.1 Preparation of $VOPO_4.2H_2O$……... 63

2.3.2.2 Preparation of $VOHPO_4 \cdot 0.5H_2O$ via $VOPO_4.2H_2O$ using the standard procedure…… 63

2.3.2.3 Preparation of $VOHPO_4 \cdot 0.5H_2O$ via $VOPO_4.2H_2O$ using copolymer modified procedure……... 64

2.4 Characterisation techniques……. 65

2.4.1 Powder X-ray diffraction (XRD)……. 65

2.4.2 Laser Raman Spectroscopy…….. 67

2.4.3 Electron microscopy (SEM, TEM and STEM)……... 69

2.4.4 Surface area measurements (BET)…….. 74

2.4.5 Temperature-Programmed Reduction (H_2-TPR)……. 75

2.4.6 Gas Chromatography (GC)…….. 76

2.5 Catalyst evaluation…….. 78

2.5.1 Oxidation of benzyl alcohol……. 78

2.5.2 CO oxidation…… 80

2.5.3 Oxidation of n-butane…….. 81

2.6 References……... 84

Chapter 3 Oxidation of benzyl alcohol using gold nanoparticles supported on CeO_2 foam……... 85-117

3.1 Introduction……. 86

3.2 Experimental…… 87

3.2.1 Preparation of CeO_2 foams…….. 87

3.2.2 Preparation of the gold sol and the supported gold catalyst…… 87

3.2.3 Oxidation of benzyl alcohol……. 88

3.2.4 Characterisation……... 88

3.3 Results and discussion……. 88

3.2.1 Preparation of CeO_2 foams and Au/CeO_2…… 88

3.3.2 Oxidation of benzyl alcohol using Au/CeO_2 catalysts…… 98

3.3.2.1 The effect of catalyst mass…….. 107

3.3.2.2 Time on-line analysis of Au/foamCeO_2-4h……. 108

3.3.2.3 The effect of oxygen pressure……. 110

3.3.2.4 The reaction in the absence of oxygen…… 111

3.3.2.5 Reusability of Au/foamCeO_2-4h……. 112

3.4 Conclusions……. 113

3.5 References……... 115

Chapter 4 Oxidation of benzyl alcohol and CO using gold nanoparticles supported on MnO_2 nanowire micro spheres……. 118-161

4.1 Introduction……. 111

4.2 Experimental…… 119

4.2.1 Preparation of MnO_2 nanowire microspheres…….. 119

4.2.2 Preparation of gold catalysts…… 119

4.2.2.1 Sol-immobilisation method (SI)…….. 119

4.2.2.2 Reflux Sol-immobilisation method (RSI)……... 119

4.2.2.3 Impregnation method (IM)…….. 120

4.2.2.4 Deposition precipitation method (DP)…… 120

4.2.3 Oxidation of benzyl alcohol……. 120

4.2.4 Oxidation of CO…….. 120

4.2.5 Characterisation……... 120

4.3 Results and discussion……. 122

4.3.1 Preparation of MnO_2 and Au/MnO_2…… 122

4.3.2 Catalyst testing……. 128

4.3.2.1 Oxidation of benzyl alcohol using Au/MnO_2 catalysts…... 128

4.3.2.1.1 The effect of the preparation method……... 128

4.3.2.1.2 The effect of the catalyst structure and morphology…….. 130

4.3.2.1.3 The effect of catalyst mass……... 138

4.3.2.1.4 Time on-line analysis of Au/MnO_2-12h……... 139

4.3.2.1.5 Reusability of Au/MnO_2-12h……... 140

4.3.2.2 Oxidation of CO using Au/MnO_2 catalysts…… 143

4.3.2.2.1 The effect of the preparation method…….. 143

4.3.2.2.2 The effect of the support structure and morphology…….. 149

4.4 Conclusions……. 155

4.5 References……... 157

Chapter 5 The synthesis of highly crystalline vanadium phosphate catalysts using PAAMA as a structure directing agent……. 162-199

5.1 Introduction……. 163

5.2 Experimental…… 164

5.2.1 Preparation of vanadium phosphate catalysts……. 164

5.2.1.1 Preparation of $VOHPO_4.0.5H_2O$ precursor via VPO route. 165

5.2.1.1.1 Standard procedure……... 165

5.2.1.1.2 Copolymer modified procedure……... 165

5.2.1.2 Preparation of $VOHPO_4.0.5H_2O$ precursor via VPD route. 165

5.2.1.2.1 Preparation of $VOPO_4.2H_2O$…… 165

5.2.1.2.2 Preparation of $VOHPO_4 \cdot 0.5H_2O$ via $VOPO_4.2H_2O$ using the standard procedure… 166

5.2.1.2.3 Preparation of $VOHPO_4 \cdot 0.5H_2O$ via $VOPO_4.2H_2O$ using copolymer modified procedure…….. 166

5.3 Characterisation……... 166

5.4 Catalyst testing…… 167

5.5 Results and discussion……. 167

5.5.1 Catalyst precursor characterisation…….. 167

5.5.1.1 Characterisation of precursors synthesised via VPO route. 167

5.5.1.2 Characterisation of precursors synthesised via VPD route. 172

5.5.2 Butane oxidation studies and post-reaction characterisation……... 178

5.5.2.1 Butane oxidation studies using the precursors synthesised via VPO route……. 178

5.5.2.2 Butane oxidation studies using the precursors synthesised via VPD route……. 186

5.6 Conclusion……... 195

5.7 References……... 196

Chapter 6 Conclusion and future work……... 200-209

6.1 Conclusion……... 201

6.1.1 Gold catalysts…….. 201

6.1.2 Vanadium phosphate catalysts……. 205

6.2 Future work……. 207

6.2.1 Gold catalysts…….. 207

6.2.1.1 Au/CeO_2 foam……. 207

6.2.1.2 Au/MnO_2 nanowire microspheres……... 207

6.2.2 Vanadium phosphate catalysts……. 208

6.3 References……... 209

Chapter 1

Introduction

1. Introduction

1.1 Historical background of catalysis

The first observation of a catalytic reaction occurred in 1552 when Valerius Cordus converted alcohol to ether using sulfuric acid. In 1794, Fulhame was the first to present the basic aspects of catalysis when he found that water was needed for CO oxidation yet was not consumed. Kirchhoff came to a similar conclusion in 1812 with respect to the acids used for the hydrolysis of starch to sugars. In 1817, Sir Humphry Davy supposed that mixing oxygen with flammable gases can lead to an explosion if they were passed over platinum when heated at lower than the combustion temperature. In 1818, Thendard illustrated the possibility of the stabilising hydrogen peroxide in acidic solutions, whereas, it decomposed in water. Furthermore, he showed that by adding noble metals the rate of decomposition could be decreased. Edmund Davy in 1820 studied the role of noble metals on alcohols oxidation. He showed that the oxidation of alcohols can rapidly take place over platinum exposed to air. This was confirmed by Dobereiner in 1822 that burnt oxygen and hydrogen over platinum at room temperature. Dulong and Thenard were inspired by Dobereiner's work and they examined some materials other that platinum (e.g. Au and Ag) for the reaction of oxygen and hydrogen and they found that the activity depended on the material used. In 1825, Henry discovered some materials such as hydrogen sulfide that prohibited the combustion of hydrogen. Furthermore, he found that platinum based catalysts were inactive for CO oxidation. Turner illustrated that the combination of hydrogen with chlorine was achievable when platinum based catalysts were used. This promoted Peregrine Phillips

to patent the commercial production of sulphuric acid by oxidizing the sulphur dioxide over platinum based catalysts [1]. However, the first effort to explain these observations was made by Berzelius in 1836 who coined the word catalysis; he reported "*I shall therefore call it the catalytic power of substances, and the decomposition by means of this power catalysis, just as we use the word analysis to denote the separation of the component parts of bodies by means of ordinary chemical process. Catalytic power actually means that substances are able to awake affinities which are asleep at this temperature by their mere presence and not by their own affinity*" [2].

The origin of word catalysis is from Greek words, the prefix cata and the verb lysein. Cata means down and the meaning of lysein is split. A catalyst splits down the forces that impede the molecules to react [2].

More precise definitions have been made as a result of the development in understanding the catalysis process. According to G. C. Bond, the catalyst is "a substance that increases the rate at which a chemical system approaches equilibrium, without being consumed in the process" [2].

1.2 Importance of catalysis

Catalysts are a class of materials that enhance the rate of a reaction and the process of catalysis is that of a catalyst involved in a reaction. The main role of a catalyst is to enhance the rate of reaction. The rate for any chemical reaction is the step at which the reactants transform to products. This step is the slowest step and often determines the

rate of reaction. The reactant must form an activated complex where there are no reactants but are not yet transformed to products. This is a transitional state and the energy needed to reach this state is named the activation energy. The reactants must reach and pass the energy barriers to transform to products. The catalyst provides another path that is more complex but has an activation energy that is remarkably lower than that of the uncatalysed reaction so the rate is much larger for the catalysed one (Fig. 1.1). As the catalyst is not consumed in the reaction, it does not exist in the final chemical equation and it accelerates the reactions that are kinetically possible. This suggests that if the reaction is thermodynamically impossible, catalysts cannot make it possible [2].

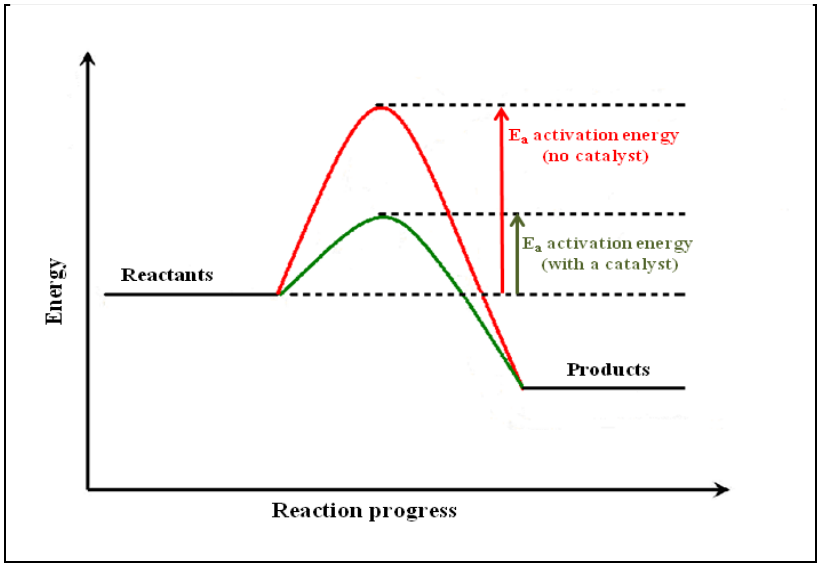

Fig. 1.1 Activation energy for catalysed reaction and uncatalysed reaction

Catalysis is essential for academic study and industry. It is very important in our life. Many industrial processes such as plastics manufacturing, fuel production and pollution reduction depend on catalysis. It is estimated that ca. 90 % of materials produced is achieved using catalysis. Therefore, the efficacy of a modern chemical industry can be said to be intimately tied to catalysis [3, 4].

1.3 Categories of catalysis

Catalysis can be classified to three kinds: homogeneous catalysis, heterogeneous catalysis and bio-catalysis [5].

1.3.1 Homogeneous catalysis

In homogeneous catalysis both the catalyst and the reactant have the same phase, e.g. ozone destruction by chloride [3]. The main benefit of homogeneous catalysis is that all of the active sites of the catalyst are reachable by the reactant so a greater selectivity can be achieved. However, due to the difficulty of separating the catalysts from the reaction mixture some homogeneous catalytic processes could not be achieved industrially [6].

1.3.2 Heterogeneous catalysis

In heterogeneous catalysis the catalyst and the reactant have different phases. The catalyst is usually solid while the reactant is liquid or gas, for example the production of ammonia from N_2 and H_2 using solid Fe catalysts [3]. Table 1.1 shows the main variations between homogeneous and heterogeneous catalysis.

Table1.1 The main differences between homogeneous and heterogeneous catalysis [7].

	Homogeneous	**Heterogeneous**
Catalyst phase	Dissolved metal complex	Usually solid
Activity	High	Variable
Selectivity	High	Variable
Stability	Decomposes at high temperatures	Usually stable at high Temperature
Recovery	Difficult and expensive	Easy
Application	Limited	Wide

Heterogeneous catalysts can be categorised into three types of compounds: metals, metal oxides and metal sulfides. Metals are broadly utilised in many reactions such as hydrogenation, oxidation and reduction of NO_x with hydrocarbons. Metal oxides are mostly used for the oxidation of hydrocarbons. Metal sulfides are employed in hydrodesulfurization of petroleum [8].

The first step in most heterogeneous catalytic reactions is that the reactants are adsorbed on the surface of the catalyst, particularly on the active sites (Fig. 1.2). Then, the surface reaction takes place between the adsorbed reactants to form the adsorbed product. Finally, the produced is desorbed when the bond between it and the surface of the catalyst is broken [3, 4].

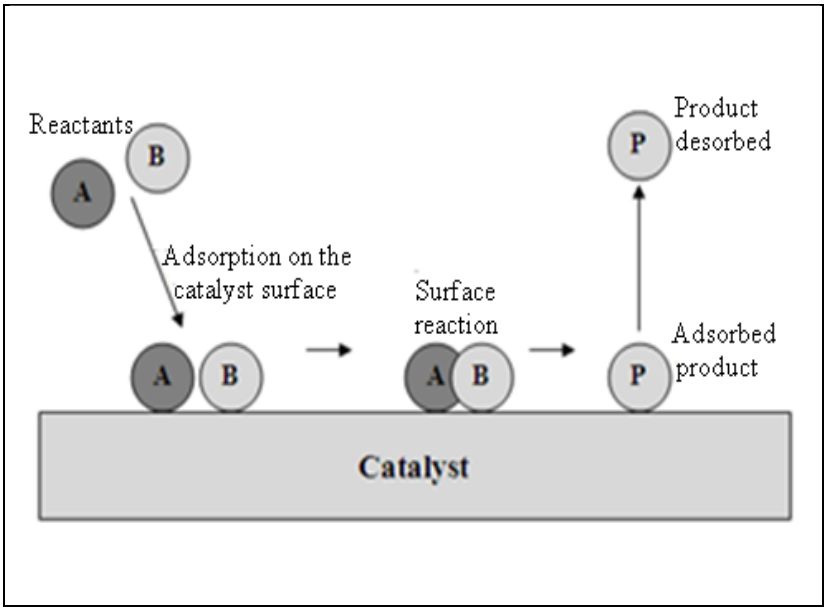

Fig. 1.2 The general reaction steps for the heterogeneous catalytic reactions

Heterogeneous catalysts are easy to recover and reused and are the most used in the petrochemicals industry due to the ease in catalyst separation and reusability [5, 9].

1.3.3 Biocatalysis

Biocatalysis is a special case in which enzymes, which are complex proteins that catalyse the reactions in living organs. Enzymes are effective as catalysts often better than homogeneous and heterogeneous ones due to their high turn-over frequency which is related to their high specificity, often at mild conditions [5].

1.4 Oxidation catalysis

Oxidation is a very important process in the chemical industry. It is used for the production of materials and intermediates in addition to the pollution diminishing and environmental cleaning. A number of valuable products are produced by oxidation processes and, therefore, oxidation has an extreme impact in our everyday life.

There are two kinds of oxidation processes, total oxidation and selective oxidation. In total oxidation, also called complete oxidation, carbon dioxide and water are the thermodynamically stable products of this type of reaction. This process is used in energy production, typically, for the elimination of pollutants from the environment especially from car exhausts. In selective oxidation, also called partial oxidation, the desirable products are not thermodynamically stable and kinetic control must be employed [10, 11]. Table 1.2 demonstrates some common oxidation reactions and their catalysts.

Table1.2 Some common oxidation reactions [10].

Reaction	Catalyst
Total oxidation	
Oxidation of CO to CO_2	$CuMnO_4$, Au/MO_x at 25°C, Pt/MO_x > 200°C
Oxidation of hydrocarbons & NO_x to CO_2, water & Nitrogen	Three way car exhaust catalyst, Pt, Pd
Oxidation of volatile organic compounds (VOCs) to CO_2 & water	Pt, Pd/Al_2O_3
Selective oxidation	
Oxidation of butane to maleic anhydride	Vanadium phosphate
Oxidation of propene to acrolein	$MoOBi_2O$, US_3O_{10}, $FeSbO_4$
Oxidation of propene to acrylonitrile	$MoBi_2O_6$, US_3O_{10}, $FeSbO_4$
Oxidation of o-xylene to phthalic anhydride	V_2O_5
Oxidation of methanol to formaldehyde	Iron molybdate, Ag
Oxidation of ethene to ethylene oxide	Ag
Oxidation of ethyl benzene to styrene	V_2O_5/TiO_2
Oxidation of benzene to phenol	Fe-ZSM-5
Oxidation of toluene to benzaldehyde	Vanadium phosphate
Oxidation of isobutene to methacrylic acid	Molybdophosphoric heteropolyacids
Oxidation of ethene to acetic acid	Pd-silicotungstic heteropolyacid

Selective oxidation of hydrocarbons such as alkanes, alcohols, aldehydes and acids is very important since the products can be used either as intermediates for other chemical reactions or in final important products like paints, plastics, food additives and perfumes

Presently, the chemical and petrochemical industries are growing resulting in a large number of processes operating every day and thus there is a need to minimize the environmental pollution. The term 'Green Chemistry' was first coined by Anastas from US Environmental Protection Agency (EPA) [12] and has since been considered in the chemical industry. The definition of Green Chemistry is as follows: *Green chemistry efficiently utilizes (preferably renewable) raw materials, eliminates waste and avoids the use of toxic and/or hazardous reagents and solvents in the manufacture and application of chemical products* [13]. The concept of green chemistry includes 12 principles [12] as follows:

- It is better to prohibit waste than to treat it after it is produced.
- All chemicals used in the procedure should corporate in the final product by designing proper synthetic methods.
- Wherever possible, synthetic methods should be designed to use and produce less toxic chemicals.
- Chemical products should maintain efficacy of function while reducing toxicity.
- The use of substances such as solvents, separating agents, etc. should be avoided wherever possible.

- The environmental and economic impacts of the energy requirements should be considered and therefore the processes should be carried out at mild temperatures and pressures.
- A renewable raw material or feedstock should be used rather than depleting wherever possible.
- Unnecessary derivatization should be avoided wherever possible.
- Stoichiometric reagents should be replaced by a catalytic cycles (as selective as possible).
- At the end of their function, chemical products should not persist in the environment and should decomposes into safe materials.
- Real-time and on-line analysis should be developed to monitor and control the hazardous materials.
- Processes should be designed to minimize the chance of accidents.

The oxidation processes often use stoichiometric oxygen donors as a source of oxygen at the commercial scales, especially for the selective oxidation of alcohols to their corresponding aldehydes. These oxygen donors such as chromate or permanganate are expensive and toxic which is environmentally unfriendly [14-17]. In addition to the environmental obstacles, in the heterogeneous catalysts the reactions take place only when the reactants make contact with the exposed active sites [18]. Thus, it is a difficult challenge to make active, selective and stable catalysts using a green process.

Metals and metal oxides materials have been extensively used as heterogeneous catalysts for the oxidation reactions in industry. Metal oxides catalysts are used in

several industrial processes: oxidation of o-xylene to phthalic anhydride over supported V_2O_3/TiO_2 catalysts, oxidation of H_2S to sulfur element over supported Fe_2O_3/SiO_2 and MnO_x/SiO_2 catalysts [19]. Mixed metal oxides are considerably utilised in the chemical industry as selective oxidation catalysts. For example, Mo-V-Te-Nb-O catalysts are used for the oxidation of propane to acrylic acid [20] and V-P-O catalysts are used for the commercial production of maleic anhydride from butane oxidation [21]. Metal catalysts are widely used in the chemical and petrochemical industries. Ammonia has been long synthesized using iron catalysts [3], nitric acid is manufactured by Pt-Rh catalysts and Cu is used for methanol synthesis. Another example is the oxidation of dangerous gases that emitted from the combustion of gasoline in automobiles like CO and NO_x into CO_2 and N_2. The catalyst used in the automobile's catalytic converter consists of Pt, Pd and Rh loaded on ceramic. In metal catalysts, the metal particles are usually dispersed in small forms on stable supports such as metal oxides [22]. In fact, metals and metal oxides are very important materials since they are employed as catalysts for many industrial processes.

1.5 Gold catalysis

1.5.1 Historical background

Metals are broadly employed as catalysts for several reactions such as oxidation, hydrogenation and reduction of NO_x with hydrocarbons. The metals widely used as catalysts are the 3d metals (Fe, Co, Ni and Cu), the 4d metals (Rh, Pd and Ag) and a 5d metal (Pt). These metals are prepared in small particles and supported on metal oxides

like Al_2O_3 and SiO_2. Gold (5d) has been a special case and has always been reputed to be catalytically inactive.

The catalysts activity of group VIII metals can be attributed to vacancies in the d-band. Elements in group Ib (Cu, Ag and Au) have d-bands which are completely occupied. However, due to the ease at which they can lose electrons or 'low ionization potentials' by Cu and Ag leading to vacancies in their d-bands, Cu and Ag are used for the industrial production of methanol and ethylene oxide respectively. Au, on the contrary, has a high ionization potential and therefore has a low attraction to other elements [22]. Furthermore, it was illustrated by surface science and density functional theory calculations that H_2 and O_2 cannot be adsorbed over the smooth surface of Au below 473K. The implication being that Au should be a poor catalyst for oxidation and hydrogenation reactions [23, 24].

Practically, the particles of Au in conventional supported gold catalysts which are prepared by impregnation are not well dispersed on the support when compared to Pt. In addition, the size of Au particles was usually larger than 30 nm compared to 3 nm in the case of Pt particles [22]. Accordingly, gold has been regarded as inactive catalytic application and has received less attention in comparison to the other noble metals such as platinum and palladium which both are largely employed as catalysts, moreover, silver and copper, which both are in the same group as gold, are used in many large processes [25].

However, some observations about catalytic activity of gold existed. Thendard and Dulong reported that gold catalysed the decomposition of ammonia [26]. Gold was also

reported to dehydrogenate cyclohexene by Erkelens *et al.* [27] and Chambers and Boudart [28]. Bond and co-workers [29] illustrated that when gold prepared as small particles and supported on silica could hydrogenate alkenes and alkynes successfully. This was the first admit to proof that Au might be an active catalyst when dispersed in small particles. Despite all the previous reports, gold has received a little attention by researchers until 1980s when two major discoveries demonstrated that nano-particulate gold could be the best catalyst for certain reactions. Haruta discovered that gold supported catalysts are very active for low temperature CO oxidation [30]. Hutchings predicted that gold would be the most active catalyst for ethylene hydrochloronation [31]. Subsequently, nano-particulate gold catalysts have attracted remarkable attention due to their distinctive catalytic properties. Figure 1.3 demonstrates the dramatic increase in publications in field of gold catalysis over the years.

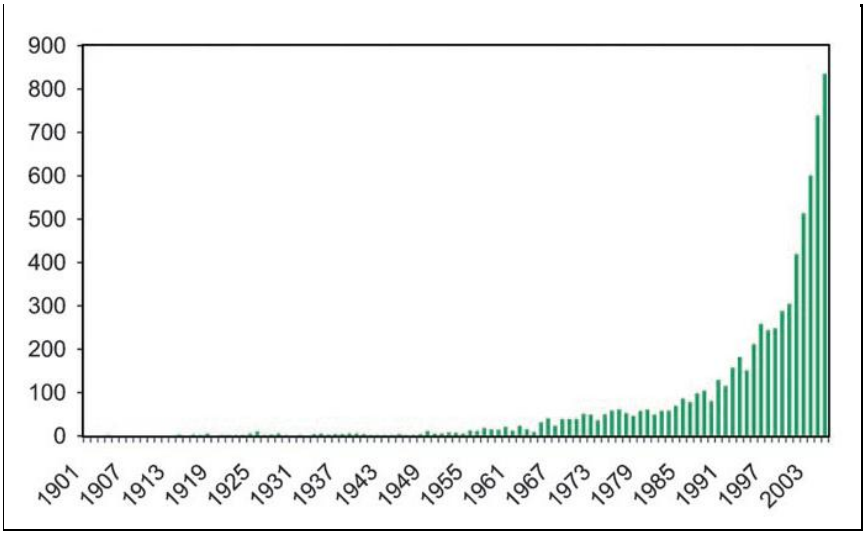

Fig. 1.3 Number of publications on "gold catalysis" from 1900 to 2006 [32].

1.5.2 Preparation method of supported gold catalysts

The catalytic performance of supported gold catalysts essentially relies on the size of gold particles. Nevertheless, there are some factors that could inherently affect the catalyst activity such as gold oxidation state, the preparation method and the choice of support [33]. The particle size is very important in gold catalysis and it was found that catalysts with large gold particles are inactive for many reactions especially for CO oxidation. The preparation method and the choice of support deeply affect the particle size of gold and the catalyst performance [34].

The method of preparation generally includes two main steps, first: the introduction of gold precursor on the support by impregnation, deposition-precipitation, coprecipitation, sol-immobilisation, and second: drying and calcination [34]. As the preparation method is crucial to obtain a very active catalyst for a desired reaction, the following methods: impregnation, deposition-precipitation, coprecipitation and sol-immobilisation will be discussed in more details.

1.5.2.1 Impregnation

It is a very straightforward method and can be applied with any support. In impregnation, a solution of the gold precursor fills the pores of the support. When only the required volume of the gold solution used to fill the pores, the method is then called incipient wetness. However, sometimes an excess volume is used by adding a solvent which is evaporated to increase the concentration of the solution in the pores. The gold precursors usually used in these methods are chloroauric acid ($HAuCl_4$) and gold

chloride ($AuCl_3$). The gold particles produced by these methods after calcination are large (10-35 nm) leading to a catalyst with poor activity for many reactions. The large particles are formed due to chloride ion which helps gold species to move and agglomerate during the thermal treatment. Furthermore, it is known that chloride ions poison many reactions like CO oxidation. It seems that chloride can be removed as HCl by the reduction with hydrogen [34].

1.5.2.2 Co-precipitation

In co-precipitation, sodium carbonate is added the aqueous solution of gold precursor ($HAuCl_4$) and a metal nitrate such that the metal forms the desired oxide. Then, the co-precipitates are washed, dried and calcined in air. Co-precipitation provides small gold particles with high dispersion and higher surface area compared to the analogous oxide before adding gold. The drawback of this method is that some of the gold particles could be placed in the bulk of the support [34].

1.5.2.3 Deposition-precipitation (DP)

The DP method is commonly employed to prepare small gold particles supported on metal oxides. In a typical preparation, a support is added to the aqueous solution of $HAuCl_4$ then the pH of the mixture is raised to a certain value, normally 7 or 8 by adding sodium hydroxide or carbonate. After that, the mixture is heated to a certain temperature and stirred for a fixed time. The product is then washed thoroughly by water to eliminate the sodium and chlorine followed by drying and calcination in air.

DP method can be used with supports having a point of zero charge (PZC) > 5 such as MgO, TiO_2, Al_2O_3, ZrO and CeO_2. It is inapplicable for supports like silica (PZC ~ 2) and activated carbon [34].

1.5.2.4 Sol-immobilisation

The gold particles can be immobilised on a support by adding the support to a colloidal suspension. Typically, a support is added to the aqueous solution of gold precursor and a stabiliser such as poly vinyl alcohol (PVA) or tetrakis (hydroxymethyl) phosphonium chloride (THPC). The catalyst is then washed and dried. Very small particles of gold with narrow distribution can be achieved by this method. Several parameters play a role in the character of the immobilised gold particles and their distribution; such as the nature of the support, the concentration and the nature of the stabiliser and the stabiliser/gold ratio. PVA was found to be suitable for supports like carbon and TiO_2 but it was inapplicable for use with SiO_2 and Al_2O_3. THPC was found to supply smaller gold particles (~2 nm) in many preparations compared to ~ 5 nm for PVA. The benefits of this method are that the particle size is controllable, it provides narrow particle size distribution and the gold is already reduced. Furthermore, the thermal treatment is avoidable for the liquid phase reactions. For the gas phase reactions the removal of the stabiliser which usually covers the gold particles is required. Thermal treatment can remove the stabiliser but this leads the gold particles to sinter easily [34]. However, refluxing the catalyst in water was found to be effective for the facile removal of the stabiliser leading to an active catalyst for CO oxidation [35].

1.5.3 Reactions catalysed by gold

Since the observations of Haruta and Hutchings stated previously, gold catalysts have been reported to perform well for many chemical reactions such as CO oxidation [30], ethylene hydrochloronation [31], oxygen hydrogenation for the direct synthesis of hydrogen peroxide [36], water gas shift reaction (WGSR) [37], epoxidation of olefins [38], selective oxidation of alcohols [9, 39] and total oxidation of hydrocarbons [40].

Gold supported catalysts have been extensively investigated for many oxidation reactions as stated above and they have shown a very high activity at mild reaction conditions for CO oxidation, oxidation of alkenes and alcohols. By using gold catalysis, it could be possible to use greener routes for the selective oxidation of these compounds especially for alcohols [41].

1.5.3.1 Selective oxidation of benzyl alcohol

The selective oxidation of primary alcohols to their corresponding aldehydes is a very important chemical transformation, specifically, the oxidation of benzyl alcohol to benzaldehyde. Benzaldehyde is commercially used for the production of perfumes and pharmaceuticals. The industrial process of the oxidation of alcohols contains electron donors such as chromate or permanganate that are expensive and toxic. Therefore, there is a need to design a green and inexpensive process for this reaction with high activity and selectivity. This can be achieved by using clean oxidant agents like molecular oxygen instead of the toxic donors, using solvent free reaction conditions and active solid catalysts due to their ease of separation and reusability. Some catalysts have been

reported for the oxidation of benzyl alcohol using molecular oxygen such as Pd/C, Pd-Ag/pumice and Ni-hydrotalcite, however, these have been used with a solvent [42].

Gold catalysts have been reported to be effective for the oxidation of alcohols, benzyl alcohol in particular and under solvent free conditions using molecular oxygen. Hutchings and co-workers [43] demonstrated that supported gold catalysts are effective for this reaction and investigated the deposition of gold on several supports by coprecipitation and impregnation. They reported that both procedures were effective and the Au with SiO_2, CeO_2 and TiO_2 supports gave 100 % selectivity to benzaldehyde and Au/CeO_2 gave a TOF 150 h^{-1}. The Au with more acidic supports like Fe_2O_3 produced higher activity with some selectivity to benzyl benzoate. The Au/C displayed poor activity and selectivity.

Choudhary et al [44] prepared Au catalysts by homogeneous deposition precipitation using several oxide supports and examined them for benzyl alcohol oxidation. An Au/Al_2O_3 catalyst was found to exhibit the highest activity (68.9 % conversion) but with lower selectivity to benzaldehyde (65 %). The Au/Fe_2O_3 showed very high selectivity but with low conversion (16.2 %). The best catalyst performance was illustrated by Au/U_3O_8 which performed high conversion 53 % and selectivity to benzaldehyde 95 %. However, when TOF is taken into consideration, the Au/ZrO_2 catalyst was found to demonstrate the highest TOF among these catalysts. Choudhary work clearly shows that the support plays an important role in gold catalysis.

Further investigation of the support effect was carried out by Su and co-workers [45] who used gallia polymorphs (α-, β-, and γ-Ga_2O_3) as supports for Au and Pd using

homogeneous deposition precipitation method. They found that the Au/γ-Ga_2O_3 catalyst had much higher activity for benzyl alcohol oxidation and selectivity towards benzaldehyde as compared to the corresponding catalysts prepared on TiO_2, CeO_2 and Fe_2O_3. The authors attributed the activity of Au/γ-Ga_2O_3 catalyst for benzyl alcohol oxidation to the strong interaction between gold nanoparticles and the γ-Ga_2O_3 support.

More recently, Miedziak *et al.* studied the influence of support morphology and structure on the catalyst activity [46]. They prepared CeO_2 by antisolvent precipitation technique using supercritical CO_2 and used it as support for Au-Pd catalyst. The authors found out that the Au-Pd/scCeO_2 catalyst was much more active and stable for benzyl alcohol oxidation than the catalyst used non-supercritical CeO_2. Au and Pd were found to be highly dispersed in a regular configuration over scCeO_2. Moreover, the particle size of the non-supercritical CeO_2 (unCeO_2) were larger than what they were with the scCeO_2. The Au-Pd/scCeO_2 displayed high stability when reused.

The effect of adding Pd to Au was reported for the oxidation of benzyl alcohol with oxygen under solvent free conditions. Enache *et al.* [47] prepared Au-Pd/TiO_2 catalysts and they found that this catalyst had more initial activity for this reaction than Au/TiO_2 but less than Pd/TiO_2. Nevertheless, the bimetallic catalyst showed higher activity and selectivity than the Pd/TiO_2 over the period of reaction. The analysis of this catalyst by scanning transmission electron microscopy (STEM) and X-ray photoelectron spectroscopy (XPS) showed that the introduction of Au to Pd produced an Au rich core surrounded by a Pd-rich shell. Different supports were investigated for the bimetallic

catalyst and it was found that the formation of byproducts was enhanced when acidic supports such as Al_2O_3 and Fe_2O_3 were used (Table 1.3).

Table1.3 The effect of adding Pd to Au on the oxidation of benzyl alcohol to benzaldehyde as reported by Enache [47].

catalyst	Conversion (%)		Benzaldehyde selectivity (%)	
	0.5 hour	8 hour	0.5 hour	8 hour
2.5%Au-2.5%Pd/Al_2O_3	2.6	83.3	90.5	86.6
2.5%Au-2.5%Pd/TiO_2	3.7	74.5	95.2	91.6
2.5%Au-2.5%Pd/SiO_2	3.6	35.7	97.3	88.0
2.5%Au-2.5%Pd/Fe_2O_3	3.6	63.4	74.9	66.4
2.5%Au-2.5%Pd/C	2.9	69.2	53.9	46.4
2.5%Au/ TiO_2	0.6	15.3	96.7	63.9
2.5%Pd/TiO_2	13.4	60.1	51.3	54.4

Enache *et al.* extended their work and studied the influence of Au–Pd ratio on catalytic performance of Au-Pd/TiO_2 [48]. They prepared catalysts by impregnation with different Au-Pd ratios and found that under reaction conditions the 2.5 wt% Au–2.5 wt% Pd/TiO_2 was the most active catalyst.

To study the influence of preparation method on the catalyst performance Choudhary *et al.* [49] prepared Au supported on U_3O_8 by homogeneous deposition precipitation

(HDP), deposition precipitation (DP), impregnation and co-precipitation (CP). In HDP method, the U_3O_8 was stirred in aqueous solution of urea (instead of NaOH) for 6 h. The mixture was then aged at 30 °C for 12 h followed by washing with water, drying and calcination in air at 400 °C for 2 h. They selected the Au/U_3O_8 catalyst because it showed the best performance for benzyl alcohol oxidation among the supports they investigated in their earlier study [44]. The HDP method provided the smallest gold particles, whereas, impregnation resulted in the largest ones. The gold loading for both HDP and impregnation methods were quantitative while only 60 % of the gold was loaded on the support when the DP and CP methods were used. They reported that the HDP method displayed the best performance (highest conversion, high benzaldehyde yield and excellent reusability). Due to the large particle size of gold the impregnation method showed poor activity although it had similar gold loading to the HDP. The DP and CP methods gave intermediate activity as the particle size of gold was intermediate and the gold loading was found to be lower than with the HDP method. The authors investigated other parameters with the HDP prepared Au/U_3O_8 catalysts that might influence the catalytic performance such as the gold loading and calcination temperature. They reported that the conversion increased almost linear as the gold loading increased in contrast with the selectivity to benzaldehyde that decreased as the gold loading increased. The authors did not provide any explanation about these results. Also, the conversion increased as the calcination temperature increased until 400 °C after which it dropped. They ascribed the drop in conversion when the catalyst calcined higher than 400 °C to the sintering of gold particles. Hutchings and co workers [9] were the first to report gold supported catalysts prepared by the sol immobilisation method

used for the solvent free oxidation of benzyl alcohol with oxygen. They prepared Au on carbon and titania and these catalysts were found to show superior catalytic performance for this reaction. The sol immobilisation procedure provided very small gold particles (mean size = 3nm) and narrow particle size distribution that led to TOF ~ 31,900 h^{-1}. They also reported that the choice of support influenced the gold distribution and the catalyst activity which reinforces the importance of support choice on gold catalysis.

Subsequently, the addition of Pd to Au in sol immobilisation method and used the catalyst for benzyl alcohol oxidation was reported [50]. They found that adding Pd to Au on carbon also led to small gold particles and small particle distribution. That increased the conversion as well as the selectivity to toluene when compared with Au/C or Pd/C. When TOF is considered Au-Pd/C displayed the best performance.

Further investigation then [51] compared sol immobilisation with impregnation and deposition-precipitation methods. It was found that sol immobilised Au-Pd/TiO_2 catalyst demonstrated the best catalyst activity and selectivity, whereas, the impregnated catalyst was found to be the least active. This was attributed the smaller gold particles produced by sol immobilisation as well as the narrow distribution. Impregnated catalyst showed substantial level of toluene formed which could be due to the residual chlorine on the surface that led to more surface acidity and therefore selectivity to side reactions. This was minimised in the sol immobilisation procedure with thorough washing.

Several products can be produced by the oxidation of benzyl alcohol [52]. Benzaldehyde is the main products of the reaction which is also oxidised to benzoic acid (Scheme 1.1).

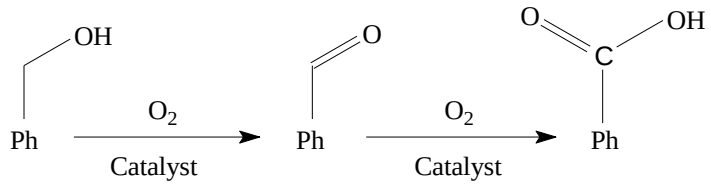

Scheme 1.1

However, there are other byproducts that can be also formed by side reactions. One possible pathway is a condensation reaction between the produced benzaldehyde and benzyl alcohol to produce hemiacetal. This condensation reaction is catalysed by the acid-basic sites on the catalyst. The formed hemiacital is unstable and is further oxidised to an ester (benzyl benzoate) as shown in Scheme 1.2.

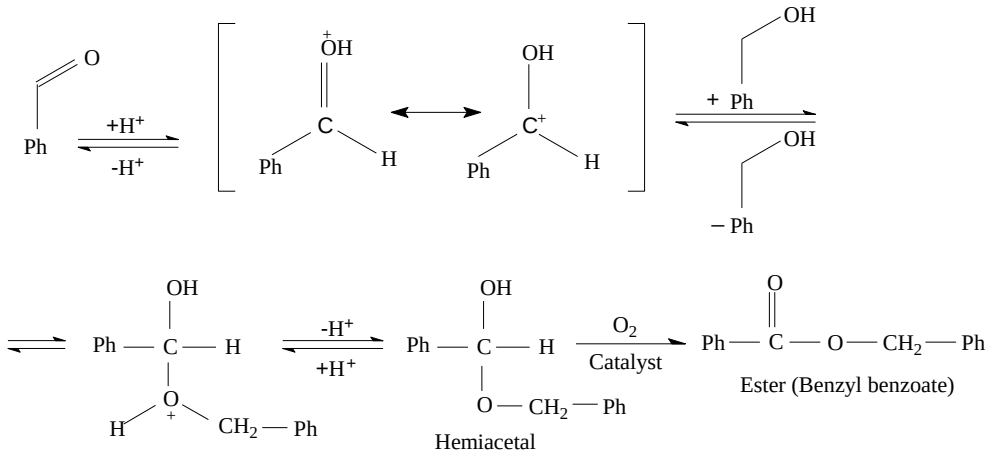

Scheme 1.2

Another possible pathway, which is also catalysed by the acid-basic sites, is the production of dibenzylether (Scheme 1.3).

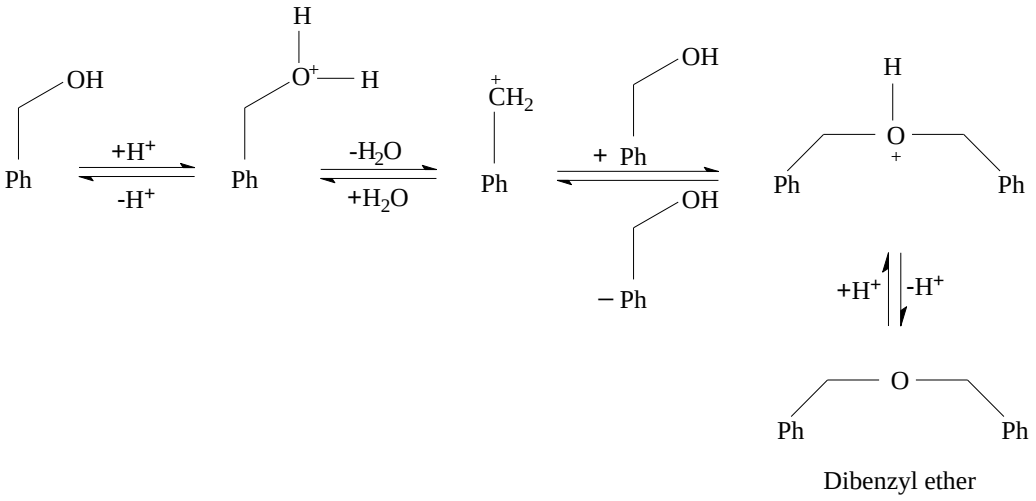

Scheme 1.3

Disproportionation of benzyl alcohol to benzaldehyde, toluene and water is also possible (Scheme 1.4). This reaction is most likely catalysed by the metallic sites of the catalyst and takes place by the removal of the oxygen from benzyl alcohol and thereafter oxidising a molecule of alcohol to aldehydes (Scheme 1.4).

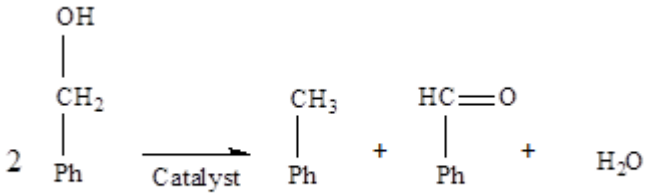

Scheme 1.4

The possibility of the disproportionation reaction increases when high temperature and low oxygen pressure are used.

1.5.3.2 CO oxidation

CO oxidation is a very important process for removing pollutants from air as well as for respiratory equipment. Industrially, this process is carried out using a mixed oxide catalyst (Hopcalite) which is comprised of copper and manganese ($CuMn_2O_3$). This catalyst has drawbacks such as deactivation by water and short life time on-line [53]. Following the demonstration by Haruta that supported gold nanoparticles were active catalysts for CO oxidation at low temperatures [30], supported gold catalysts have been investigated greatly for many reactions. In CO oxidation, like the other reactions

catalysed by supported catalysts, it is generally accepted that the size of the gold particles is essential to achieve an active catalyst. However, the other factors mentioned earlier in this chapter are also crucial and could have a great effect on the catalytic performance.

The size reliance is broadly agreed in gold catalysis. Haruta *et al.* [54] reported that the conversion for CO decreased as the gold particles size increased, below 4 nm. They suggested that the size sensitivity could be because the active sites for adsorbing oxygen are those around the Au particles interfacial perimeter. Tana *et al.* [55] studied the effect of gold nanoparticles by preparing Au/CeO_2 catalysts by deposition precipitation methods. They calcined the catalyst at 673, 773, and 873 K to eliminate any other factors that may affect the catalytic performance except the size effect. They found that the size and shape of CeO_2 in all catalysts were unchanged. The mean size of gold in all catalysts calcined at 673, 773, and 873 K were 3.9, 5.4 and 7.5 nm respectively. When catalysts were tested for CO oxidation, the activity of the catalysts depended strongly on the gold particle size. The conversion of CO was 63 % with Au mean particle size of 3.9 nm whereas it decreased to 30 % and 12 % with Au mean particle size of 5.4 and 7.5 nm respectively. The authors attributed the high activity of catalysts to the $Au\text{-}CeO_2$ interface which takes place easily when smaller Au particles presented. It was found that small Au particles provide effective adsorption of CO and a fast surface reaction of CO with oxygen species supplied by CeO_2.

It is generally noted that a controlled preparation method is important to prepare well dispersed gold nanoparticles on the support. Several preparation methods were reported

in the literature for CO oxidation using gold supported catalysts. The co-precipitation and deposition precipitation methods are commonly used with oxides [56]. Bollinger *et al.* [57] prepared titania-supported gold catalysts by impregnation, deposition precipitation and co-precipitation. All catalysts were found to be active for CO oxidation, however, the impregnated catalyst deactivated after two to three hours of the reaction under the reaction conditions used. The co-precipitation catalysts had the highest activity due to the smaller Au particles when compared to the impregnated analogue.

Bamwenda *et al.* [58] studied the effect of preparation method on Au/TiO_2 catalysts. The catalysts were prepared by deposition precipitation (DP), impregnation (IMP) and photochemical deposition (FD) methods and the activity of Au/TiO_2 samples was found to strongly rely on the preparation method and the activity decreased in the order DP >> IMP ≈ FD. DP methods supplied a very highly dispersed catalyst with small gold particles in contrast with IMP and FD which produced larger particles with poor dispersion. Therefore, they reported that the DP method induced an increased TOF over IMP and FD catalysts by four times. The authors ascribed the higher activity of DP catalyst to the size and the shape of Au particles which were small and hemispherical. This led to a good interaction between Au and TiO_2 giving the longest perimeter interface.

Recently, Ki-Joong *et al.* [59] reported the preparation of Au/Co_3O_4 by deposition precipitation (DP), impregnation (IMP) and coprecipitation (CP). Small Au particles (<

5 nm) prepared by the DP method were more exposed to the surface than the CP and IMP catalysts and hence were more active and stable for CO oxidation.

The importance of the Au support has been well studied and it plays a key role in gold catalysis for CO oxidation. Several factors such as the choice of support, its morphology and even its phase have been reported. The metal oxide supports that have been employed can be categorized as reducible (TiO_2, CeO_2, Fe_2O_3, SnO_2, MnO_x, Co_3O_4, etc.) and irreducible (SiO_2, Al_2O_3, MgO, etc.). In the reducible oxide supports, the Au particles interact with O_2 provided by the support and O_2 is adsorbed in a molecular form and this facilitates the oxidation of CO when it adsorbed on the metal-support interface. While in the case of irreducible supports the activity depends mainly on the size of Au particles as the adsorption of O_2 occurs on the gold particles [60]. Chang *et al.* [61] investigated the effect of the support and they found that when Au was supported on CeO_2 and MnO_2 by deposition precipitation (supports were calcined at 400 °C and Au catalysts were calcined at 180 °C) both catalysts exhibited high activity towards CO oxidation at ambient reaction conditions. The authors attributed the activity to the redox efficiency of both supports. The Au/CeO_2 catalyst showed higher activity than the Au/MnO_2 catalyst due to the presence of Au° and Au^{+3} in the former whereas only the metallic species of Au presented in Au/MnO_2.

Corma and co-workers [62] reported the importance of the structure of ceria support for CO oxidation. By using coprecipitation method, they stated that when Au was loaded on CeO_2- nanocrystalline structure the activity of the resultant catalyst was twice as active when compared to conventional CeO_2 for CO oxidation. They attributed that to the

existence of oxygen vacancies on CeO_2- nanocrystalline which facilitate the adsorption and activation of O_2.

Huang *et al.* [63] investigated the influence of support morphology and its phase on the catalytic performance towards CO oxidation. Two types of CeO_2, namely nanorods and nanoparticles were prepared by hydrothermal processes. Gold nanoparticles were deposited on both prepared ceria by deposition precipitation using the same procedure. They found that Au when supported on CeO_2-nanorods displayed higher activity than when supported on CeO_2-nanoparticles. It was found that CeO_2-nanorods preferentially exposed its (110)/ (100) surfaces which are rich with O_2 whereas CeO_2-nanoparticles exposed (111) and (100) facets. It is well known that the oxygen vacancies which are required for stabilising metal are easier to form on the surfaces following the order (110) < (100) < (111). This facilitated better dispersion of the Au nanoparticles on the CeO_2-nanorods than the CeO_2-nanoparticles and, therefore, efficient redox properties that led to the higher activity to CO oxidation.

Other factors such as preparation conditions (for example; pH, temperature and calcination), pretreatment method [60, 61] were also reported to have an effect. Therefore, preparing active catalysts considering all these factors is a great challenge.

The mechanism of CO oxidation reaction using gold supported catalyst is still under debate as is apparent from the literature cited above. Hutchings and co-workers [64] stated that Au^{3+} in Au/Fe_2O_3 was important for CO oxidation. However, they strongly suggested that the active site for gold catalysts may differ with the composition of the as-prepared catalyst. Bond *et al.* [65] suggested that the active centres for CO oxidation

are Au atoms at the interface between the Au particle and the oxide. The authors demonstrated that both metallic and ionic species of Au exist on the surface of the support and both are responsible for the catalyst activity (Fig 1.4).

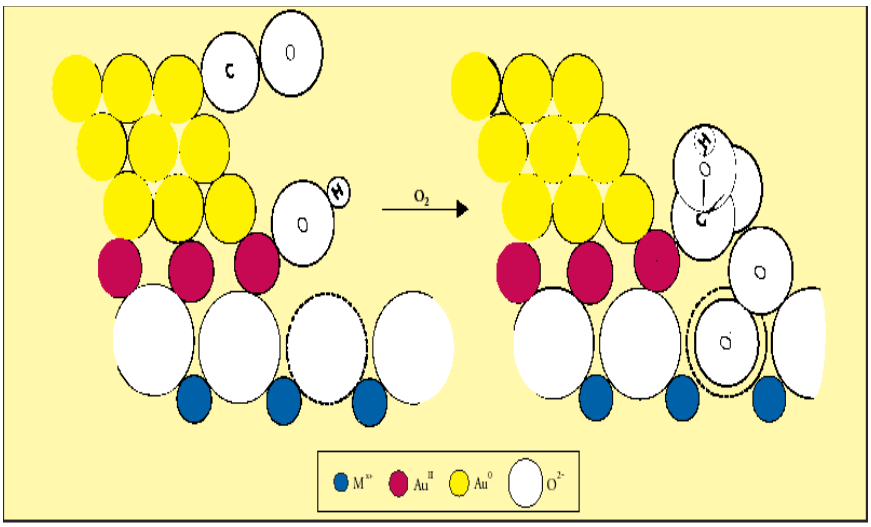

Fig. 1.4 Bond-Thompson mechanism for CO oxidation

Goodman *et al.* [66] reported the size reliance of gold clusters supported on TiO_2 for CO oxidation at low temperature. They stated that only particles from size 2 to 3 nm were active and they attributed this to the electronic properties of the smaller Au nanoparticles when being in contact with the support. The Goodman group [67] later stated that the bi-layer films of Au supported on TiO_2 exhibited unexampled catalytic performance for CO oxidation. They pointed out that gold when deposited on TiO_2 is no longer in the nanoparticles form, but as a supported bi-layer film on TiO_2 and its catalytic performance towards CO oxidation was around 45 times higher than that of Au clusters supported on TiO_2 (Fig. 1.5).

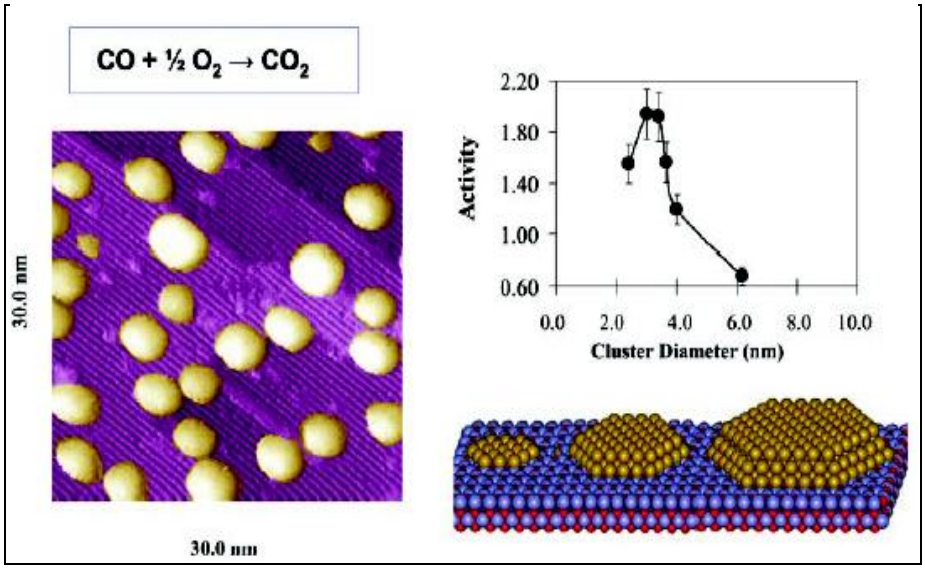

Fig. 1.5 Effect of Au particle size of Au/TiO_2 catalysts for CO oxidation [68].

Haruta *et al.* [69] suggest one probable pathways for CO oxidation over TiO_2 (Fig. 1.6).

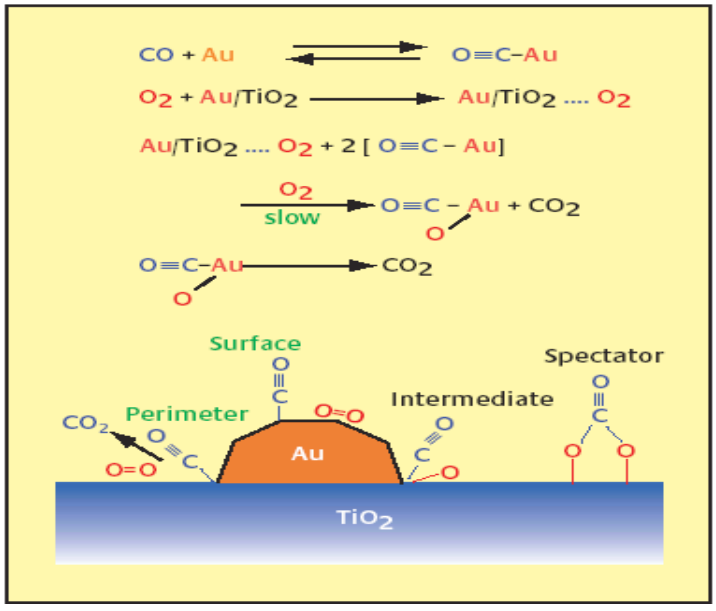

Fig. 1.6 Suggested pathways for CO oxidation over Au/TiO_2 by Haruta.

Recently, Hutchings *et al.* [70] They prepared several iron oxide-supported catalysts and the activity ranged from those with low or no activity to others with high activities towards CO oxidation although the same Au precursor and preparation method were used. The authors illustrated by using aberration-corrected scanning transmission electron microscopy that the samples that had the high activity presented bi-layer clusters that are ~0.5 nm in diameter and contain only ~10 gold atoms.

1.5.4 Preparation methods of CeO_2 and MnO_2 supports

It is well known that the support in gold catalysis plays a key role in determining the catalytic performance. Many supports have been used in gold catalysis, particularly CeO_2 and MnO_2. CeO_2 is broadly used as a support in gold catalysis because of its redox efficiency and high O_2 storage capacity. MnO_2 is also a very important material in both material science and catalysis due to its capacitance as well as redox properties. Different structures and morphologies of these materials were reported in the literature. Mai *et al* [71] prepared nanocrystalline CeO_2 with three different morphologies, nanorods, nanocubes and nanopolyhedra by a hydrothermal reaction of $Ce(NO_3)_3.6H_2O$ and NaOH at 100-180 °C. In this method, the variation of NaOH concentration produced CeO_2 material with different morphologies. Yin *et al.* [72] successfully synthesised rod-like and spherical CeO_2 particles by reacting cerium (III) nitrate with a precipitate reagent such as urea by a mild solution process followed by calcination treatment (Fig. 1.7).

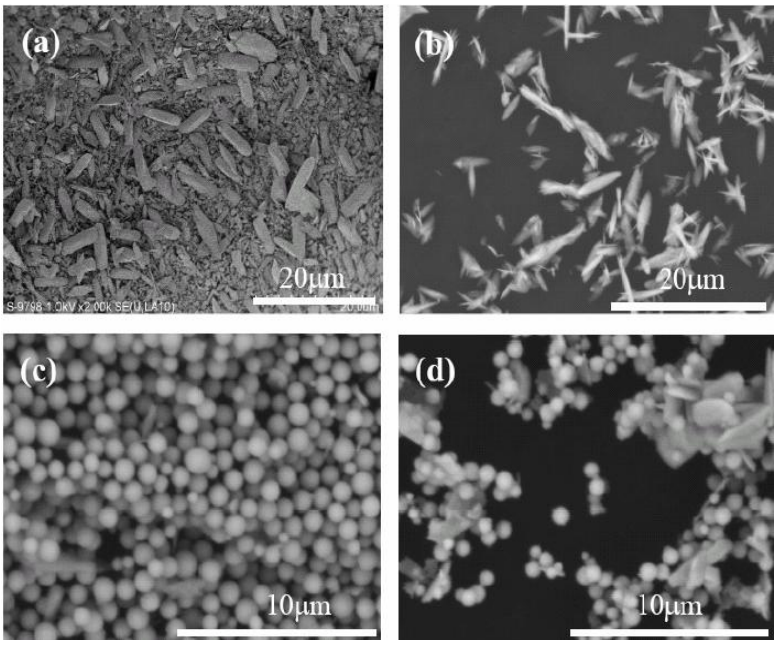

Fig. 1.7 SEM micrographs of ceria particles synthesized in solution at 25°C with different reaction times of (a) 0h, (b) 24h, (c) 72h, (d) 120h. The precipitation reaction was carried out at 90oC for 2h followed by calcination at 400°C in air.

Zhong et al. [73] reported the preparation of flowerlike ceria micro/nanocomposite structure by the reaction of $CeCl_3.6H_2O$, urea and tetrabutylammonium bromide (TBAB) in ethylene glycol at 180 °C for 30 min. Ceria was produced by calcining the as-prepared precursor in air at 450 °C for 2 h. Subramanian *et al.* [74] prepared flowerlike whiskers and rod-like structures of MnO_2 by the hydrothermal synthesis of $MnSO_4.H_2O$ and $KMnO_4$ at 140 °C by varying the reaction time (Fig. 1.8).

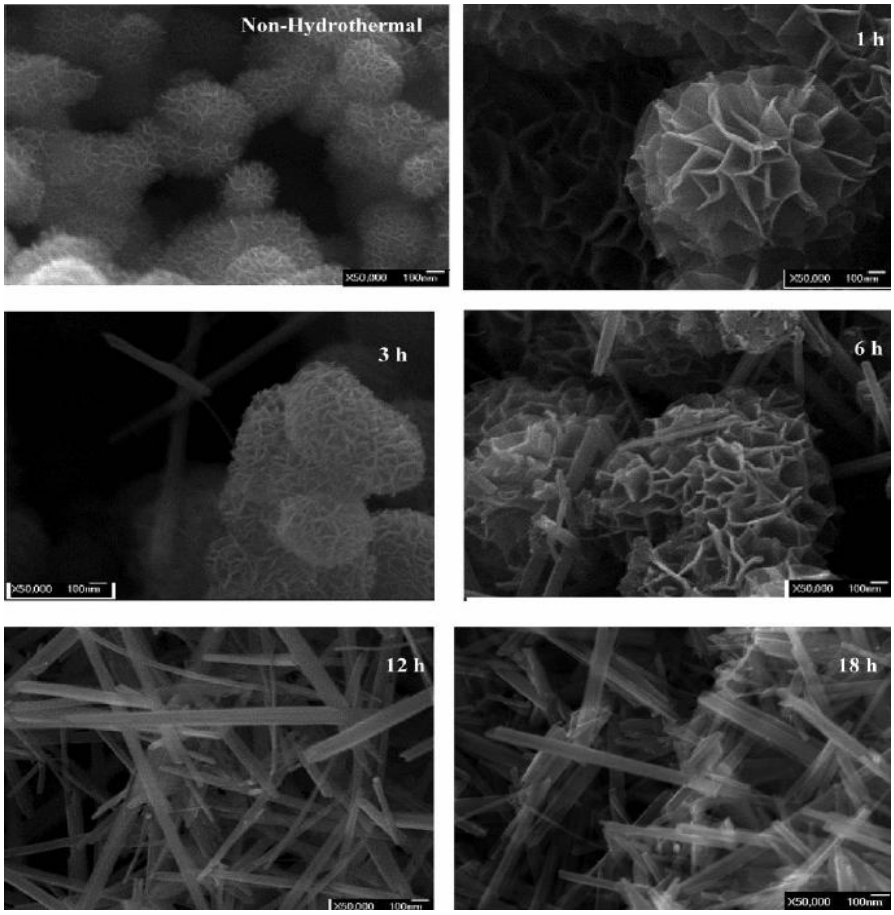

Fig. 1.8 SEM images of MnO_2 prepared at different hydrothermal reaction times.

Hollow spheres, hollow urchins and nanorods of α-MnO_2 were synthesised by Maowen *et al.* [75] by hydrothermally reacting $KMnO_4$ with sulfuric acid in the presence of Cu scraps at 110 °C at different crystallisation times. Many types of morphologies of CeO_2 and MnO_2 were documented in the literature and the above are just examples on some of them. The structure and morphology of the support play a very important role in gold supported catalysts as they can affect the gold particle size [76, 77], the metal-support interaction [62, 78] and the dispersion and reducibility of gold catalysts [63, 79].

1.6 Vanadium Phosphorus Oxide Catalysts

1.6.1 Background

Vanadium phosphate catalysts are used industrially for the production of maleic anhydride (MA) from n-butane oxidation (Fig. 1.9).

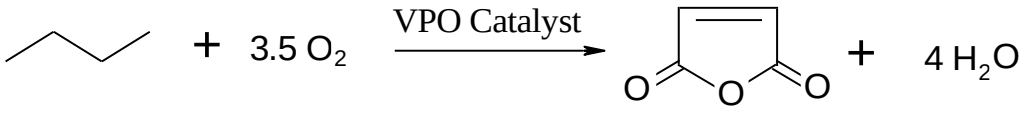

Figure 1.9

In 1966, Bergman and Frisch discovered the vanadium phosphates to be an effective catalyst for the selective oxidation of n-butane [21]. Since 1974 n-butane has been progressively employed as a replacement for benzene as the raw material for maleic anhydride production because of lower price, availability and environmental influence [80]. Due to the beneficial use of maleic anhydride in many fields, such as the production of polyesters, agricultural chemicals such as herbicides and pesticides, food manufacture and oil additives, vanadium phosphates are one of the most attractive industrial catalysts [80].

It is generally agreed that the active catalyst comprises mainly vanadyl pyrophosphate phase, $(VO)_2P_2O_7$. [80]. This phase is achieved by the topotactic transformation of the precursor, vanadyl hydrogen phosphate hemihydrate, $VOHPO_4.0.5H_2O$, in n-butane/air at ca. 400 °C to the final catalyst (Fig. 1.10) [81-83].

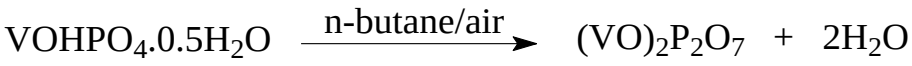

Figure 1.10

Although $(VO)_2P_2O_7$ is agreed to be the only active phase for the formation of maleic anhydride, some V^{5+} and V^{4+} phosphate phases were reported to exist whether crystalline or disordered in the final catalyst. Bordes *et al.* [84] suggested the interfaces between $VOPO_4$ phases and $(VO)_2P_2O_7$ are the active sites for the production of maleic anhydride. Hutchings *et al.* [85] reported the transformation of the hemihydrate precursor to a complex of $(VO)_2P_2O_7$ (V^{4+}) and some V^{5+} phases, namely α_{II}-, γ- and δ-$VOPO_4$. According to the author the existence of $(VO)_2P_2O_7$ in a combination with $VOPO_4$ phases in the active catalyst is widely accepted [86]. Centi *et al.* [87] reported that series of redox couples, V^{3+}, V^{4+} and V^{5+} must be present on the final catalysts for the reaction to occur. They stated that a V^{4+}/V^{3+} couple is essential for butane activation and V^{5+}/V^{4+} is required for the subsequent conversion to maleic anhydride. Batis *et al.* [88] proposed that γ-$VOPO_4$ supported on a $(VO)_2P_2O_7$ matrix was essential for the activation of n-butane as it was confirmed by XRD, ^{31}P MAS and NMR analysis.

The transformation of the precursor $VOHPO_4.0.5H_2O$ to the active phase $(VO)_2P_2O_7$ is usually achieved in situ under reaction condition (1.7 % butane/air, 400 °C) for the oxidation of n-butane. The catalytic performance rises during the reaction period as the transformation to $(VO)_2P_2O_7$ phase takes place. This activation requires around 80-100 hours to obtain a steady state of conversion and selectivity. During the activation period,

a number of $VOPO_4$ phases were observed depending on some factors such as reaction temperature, reaction time, the preparation method of the precursor and the morphology of precursor.

The activated catalyst is formed topotactically from the precursor so it is influenced by the morphology of the precursor. Therefore, the catalytic performance of vanadium phosphates depends on the preparation method of the catalyst precursor and on the reaction conditions of n-butane oxidation [81]. Hence, it is well known that a controlled preparation method of the precursor can play an important role in determining the catalytic performance.

1.6.2 Preparation of catalyst precursors $VOHPO_4.0.5H_2O$

Vanadyl hydrogen phosphate hemihydrate precursor, $VOHPO_4.0.5H_2O$, can be prepared by three methods:

1.6.2.1 The VPA method (preparation in aqueous media)

In this method hemihydrate is produced by reducing V^{5+} (e.g. V_2O_5) to V^{4+} in an aqueous solution of H_3PO_4 (Fig. 1.11). This method is commonly known as the VPA route.

$$V_2O_5 + HCl \xrightarrow[2.\ H_3PO_4]{1.\triangle,\ 2h} VOHPO_4 \cdot {}^1\!/_2\, H_2O$$

Figure 1.11 The VPA preparation method

Typically, V_2O_5 is refluxed with HCl using water as a solvent and this reduces V^{5+} to V^{4+}. Then H_3PO_4 is added [80, 89]. Alternative reducing agents to HCl have also been reported such as oxalic acid [90] and phosphorus acid [91]. However, the $VOHPO_4.0.5H_2O$ prepared by this method has low surface area and lower activity as a result.

1.6.2.2 The VPO method (preparation in organic media)

In this method V^{5+} compounds are reduced to V^{4+} by anhydrous alcohols then followed by H_3PO_4 (Fig. 1.12). In typical preparation, V_2O_5 and H_3PO_4 are refluxed in alcohol and the light blue hemihydrate precursor is produced. Several alcohols have been used but isobutanol is most commonly used.

$$V_2O_5 + H_3PO_4 + \text{alcohol} \xrightarrow{\triangle,\,16h} VOHPO_4 \cdot {}^1\!/_2\, H_2O$$

Figure 1.12 The VPO preparation method

The VPO method is considered the standard preparation method in most academic studies and it is usually referred as the VPO route [80, 89].

1.6.2.3 The VPD method (preparation in organic media via $VOPO_4 \cdot 2H_2O$)

This method consists of two steps; the first one is the formation of the V^{5+} phase $VOPO_4.2H_2O$, vanadyl phosphate dihydrate, by reacting V_2O_5 with H_3PO_4 in water under reflux conditions. The $VOPO_4.2H_2O$ is filtered, recovered and dried and then refluxed in the second step with alcohol to form the precursor $VOHPO_4.0.5H_2O$ (Fig. 1.13) [80, 89].

$$V_2O_5 + H_3PO_4 \xrightarrow[\triangle, 16\,h]{H_2O} VOPO_4 \cdot 2H_2O \xrightarrow[\triangle, 16\,h]{\text{alcohol}} VOHPO_4.\,{}^1\!/_2\,H_2O$$

Figure 1.13 The VPD preparation method

Many studies have been reported regarding the importance of the morphology of the precursor as it can determine the catalytic performance for n-butane oxidation. Typically, V_2O_5 is used as a source of vanadium and H_3PO_4 as a source of phosphorous. The reducing agents are necessary to prepare the V^{4+} precursor phase. Most studies have focused on the VPO and VPD methods as they produce better catalysts.

Hutchings *et al.* [92] investigated several alcohols for preparing the hemihydrate precursor via VPD methods. It was found that using secondary alcohols as reducing agents led the precursors to have platelet morphology. The precursors prepared using

primary alcohols had a rosette morphology with high surface area (40 m^2g^{-1}) and they displayed higher activity and selectivity for n-butane oxidation to maleic anhydride.

Bartley *et al.* [93] reported that when aldehydes or ketones were added instead of alcohols in the VPO methods, $VO(H_2PO_4)_2$ was the only product formed. This exclusive formation of $VO(H_2PO_4)_2$ was noticed with several aldehydes and ketones, typically (C_4-C_{10}) and this phase is well known to exhibit a poor catalytic performance for butane oxidation. They reported that the use of alcohols as reducing agents in the VPO method forms the precursor of the commercial catalyst ($VOHPO_4.0.5H_2O$) used for n-butane oxidation and the alcohols are oxidised to aldehydes or ketones. Once aldehydes and ketones are formed during the preparation method, they will lead to the production of $VO(H_2PO_4)_2$. The presence of $VO(H_2PO_4)_2$ in the final precursors will affect the catalyst activity negatively as it lowers the surface area of the activated catalysts. The authors reported that this phase, $VO(H_2PO_4)_2$, is soluble in water so it can be extracted by water if presented as impurity in the prepared precursor, $VOHPO_4.0.5H_2O$. This clearly confirms that a well controlled preparation method is crucial to avoid by-products in the preparation of heterogeneous catalysts.

Lopez-Sanchez *et al.* [94] prepared vanadium phosphate catalysts in aqueous solution using autoclave at high temperature (145°C). They used H_3PO_3 as a reducing agent and V_2O_4 as vanadium source. It was found that this methodology produced catalysts with higher surface area (20 m^2g^{-1}) compared with those prepared by aqueous methods using HCl as a reducing agent (4 m^2g^{-1}). The catalytic performances of these materials were comparable to these prepared by non-aqueous routes. The authors stated that refluxing

the precursors in water before the activation was essential to obtain these high surface area materials. They found by using ^{31}P spin echo mapping, NMR, SEM and TEM that the reflux step effects the concentration of V^{4+} and V^{5+} in the catalyst.

Griesel *et al.* [95] studied the effect of ageing time of vanadyl phosphate dihydrate, $VOPO_4.2H_2O$, following the reaction of V_2O_5 with H_3PO_4 in water. Three samples were prepared with different ageing times. The first one was filtered straight away after the reaction and was then dried. The filtrate of the first sample was left for 24 h and the formed crystals were filtered and dried and this was the second sample. In the third sample the dihydrate was left to stand after the reaction for 24 h before filtration. It was found that the first sample had oval crystallites with surface area of 17 m^2g^{-1}, the second one contained square platelets (more crystalline) with the same surface area and the third one had square platelets but were much larger than the previous ones which led to lower surface area (13 m^2g^{-1}). The second sample which was more crystalline than the first one and had more surface area than the third one produced the best hemihydrate precursor when reduced by alcohol among these samples for n-butane oxidation.

Taufiq-Yap *et al.* [83] studied the effect of mechanochemical pretreatment on the precursor prepared via the VPD method. Four precursors were prepared with different pre-treatment times: 0, 30, 60 and 120 minutes prior to the calcination in n-butane/air mixture to produce the active phase, $(VO)_2P_2O_7$. It was found that ball milling enhanced the surface area of the catalysts as it reduced the crystallite size especially with the one that was treated at 60 minutes. Therefore, the catalyst showed an enhancement in n-butane conversion. The enhancement in the surface area was ascribed to the ball milling

process that disallows the catalyst platelets from stacking together. Furthermore, the milled catalyst pre-treated for 60 minutes contained high amounts of oxygen species with the active V^{4+} catalyst $(VO)_2P_2O_7$.

Kamiya *et al.* [96] investigated the effect of the precursor ($VOHPO_4.0.5H_2O$) crystallite size on the final catalyst structure and thereby its performance for n-butane oxidation. It was found that the reduction of $VOPO_4.2H_2O$ by intercalation-exfoliation-reduction in 2-butanol led to small crystallites (av. 1 μm (length) × 110 nm (thickness)) of $VOHPO_4.0.5H_2O$ while large crystallites (av. 10 μm × 415 nm) formed when $VOPO_4.2H_2O$ was directly reduced by 2-butanol. The small sized precursor transformed into $(VO)_2P_2O_7$ phase with V^{5+} species dispersed well on the surface and this led to a higher selectivity to maleic anhydride compared to the large-sized precursor which contained an internal layer of α_{II}-$VOPO_4$.

Lin *et al.* [97] used a diblock copolymer, poly(styrene-alt-maleic acid) (PSMA), as a structure directing agent into the VPO method. The addition of PSMA increased the crystallinity of the precursors and changed the morphology. The XRD illustrated that the (220) reflection that was the most intense in the standard precursor, $VOHPO_4.0.5H_2O$, decreased as the concentration of the added PSMA increased whereas the (001) reflection increased until became the most intense. The morphology of the standard precursor was rosette-like whereas the precursors modified by adding PSMA contained characteristic rosette-like agglomerates of angular platelets together with isolated and more crystalline rhomboidal platelets as it was shown by the SEM. This increased the surface area of the precursor and led to a much quicker in situ

transformation to the active catalyst compared to the standard precursor. The steady state of conversion and selectivity was observed in less than 10 hours for the modified precursor.

1.6.3 Reaction mechanism

The oxidation of n-butane to maleic anhydride necessitates abstraction of 8 hydrogen atoms, insertion of 3 oxygen atoms and a transfer of 14 electrons. Many mechanisms have been reported for n-butane oxidation over vanadium phosphate catalysts based on some experimental and theoretical conclusions. Although there are a considerable argument about the active sites, it is generally acknowledged that the vanadyl pyrophosphate ($(VO_2)P_2O_7$) is the main active phase for n-butane selective oxidation.

Pepera *et al.* [98] used labelled compounds to study n-butane oxidation and they concluded the abstraction of methylene hydrogen was the rate-determining step. Centi et al [99] published a comparison study of the rate constants of the C_4-C_7 alkane series on $(VO_2)P_2O_7$ catalyst. They stated that the abstraction of two methylene hydrogen atoms in the 2- and 3- positions in n-butane by a bridging oxygen and Lewis acid site was the rate-determining step (Fig. 1.14). Although they did not present a full mechanism for the oxidation of n-butane to maleic anhydride, they proposed that Brønsted acid sites could be implicated in the intermediates steps after the initial activation. The Brønsted acid sites, ascribed to the P-OH groups in the terminal HPO_4^- and $H_2P_2O_7^{2-}$ species, were suggested to ease the removal of water formed, stabilise the reaction intermediates by producing surface phosphate esters (P-O-C) and ease the desorption of maleic anhydride.

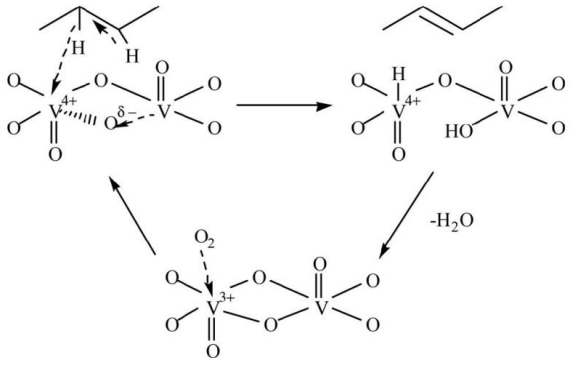

Figure 1.14 Mechanism of n-butane activation on $(VO)_2P_2O_7$ proposed by Centi et al [99].

Schiøtt *et al.* [100, 101] suggested a mechanism at molecular level (Fig. 1.15). They proposed the presence of different kinds of oxygen species for the formation of the intermediates. The electrophilic V=O was required for the initial methylene C-H bond activation in n-butane and it is lost during the cyclo-addition of butadiene resulting in the production of 2,5-dihydrofuran intermediate which was oxidised to maleic anhydride by the insertion of molecular oxygen. However, this mechanism was proposed using fuel rich gas feed conditions which differs from the standard reaction conditions.

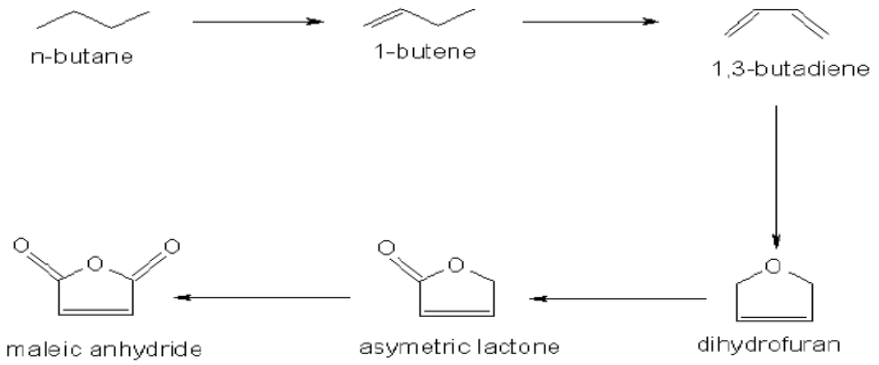

Figure 1.15 Mechanism of n-butane oxidation to maleic anhydride proposed by Schiøtt *et al.* [100, 101]

Zhang-Lin et al [102] reported probable intermediates over different vanadium phosphates and proposed a mechanism. This mechanism, which was confirmed by Rodemerck *et al.* [103], included the sequential oxidation to the products once they were formed in the order:

butane ⟶ butene ⟶ butadiene ⟶ furan ⟶ maleic anhydride

They stated that $VOPO_4$ phases had higher selectivity to by-products that $(VO)_2P_2O_7$. The β phase produced mainly by-products while the δ and γ phases were selective to maleic anhydride.

Taufiq-yap *et al.* [104] reported that by employing TPD/O (Temperature Programmed Desorption/Oxidation) that the existence of oxygen on the surface of $(VO)_2P_2O_7$ lattice is the rate determining step. This conclusion was reached because of the evolved oxygen

from the lattice was the same as removed oxygen from pyrophosphate, suggesting that the lattice oxygen is selective when it is present at the surface.

1.7 The aims of this study

As addressed in the literature review, the morphology of the support used in gold catalysts and the morphology of the precursors in the case of vanadium phosphate catalysts could play an important role in the catalytic performance as well as the catalyst preparation method. Therefore, the main objectives of this study are:

1. The preparation of a material with different morphologies and properties such as porosity, surface area, new phase…etc and use them as supports for gold.

2. The preparation of vanadium phosphate precursors with different morphologies by employing structure directing agents (modifiers).
3. The identification of the best preparation method and its conditions to produce the most effective catalyst.

4. The examination of the prepared catalysts to some important reactions such as benzyl alcohol and carbon monoxide oxidation in case of gold catalysts and n-butane oxidation in case of vanadium phosphate catalysts using green processes and discuss the effect the morphology on the catalytic performance in each case.

Several characterisation techniques were used in this study to explain the effect of the morphology changes on the catalytic performance, including X-ray diffraction (XRD),

BET surface area, Laser Raman Spectroscopy, temperature programmed reduction (TPR) and electron microscopy (SEM, TEM and STEM).

1.8 References

1. Lindstrom, B. and L.L. Pettersson, *A brief history of catalysis.* Cattech, 2003. **7**(4): p. 130-138.

2. Bond, G.C., *Heterogeneous Catalysis: Principles and Applications 2nd Ed*. 1987, Oxford: Clarendon Press.

3. Bowker, M., *The basis and Applications of Heterogeneous Catalysis*. 1998: Oxford University Press.

4. Chorkendorff, I. and J.W. Niemantsverdriet, *Concepts of Modern Catalysis and Kinetics*. 2003: WILEY-VCH GmbH & Co. KGaA.

5. Rothenberg, G., *Catalysis: Concepts and Green Applications*. 2008: WILEY-VCH GmbH & Co. KGaA.

6. Cole-Hamilton, D.J., *Homogeneous Catalysis—New Approaches to Catalyst Separation, Recovery, and Recycling.* Science, 2003. **299**: p. 1702-1706.

7. Cornils, B. and W.A. Herrmann, *Aqueous-Phase Organometallic Catalysis 2nd Ed.* 2004: WILeY-VCH.

8. Haruta, M., *Catalysis of Gold Nanoparticles Deposited on Metal Oxides.* Cattech, 2002. **6**(3): p. 102-115.

9. Dimitratos, N., et al., *Solvent free liquid phase oxidation of benzyl alcohol using Au supported catalysts prepared using a sol immobilization technique.* Catalysis Today, 2007. **122**(3–4): p. 317-324.

10. Hutchings, G.J. and M.S. Scurrell, *Desining oxidation catalysts Are we getting better?* Cattech, 2003. **7**: p. 90-103.

11. Hodnett, B.K., *Heterogeneous catalytic oxidation: fundamental and technological aspects of the selective and total oxidation of organic compounds*. 2000: John Wiley.

12. Anastas, P.T. and M.M. Kirchhoff, *Origins, Current Status, and Future Challenge of Green Chemistry.* Acc. Chem. Res., 2002. **35**(9): p. 686-694.

13. Sheldon, R.A., *Atom utilisation, E factors and the catalytic solution.* Comptes Rendus de l'Académie des Sciences - Series IIC - Chemistry, 2000. **3**(7): p. 541-551.

14. Lopez-Sanchez, J.A., et al., *Au–Pd supported nanocrystals prepared by a sol immobilisation technique as catalysts for selective chemical synthesis.* Phys. Chem. Chem. Phys., 2008. **10**: p. 1921–1930.

15. Dimitratos, N., et al., *Solvent-free oxidation of benzyl alcohol using Au–Pd catalysts prepared by sol immobilisation.* Phys. Chem. Chem. Phys., 2009. **11**: p. 5142–5153.

16. Cainelli, G. and G. Cardillo, *Chromium Oxidants in Organic Chemistry*. 1984, Berlin: Springer.

17. Menger, F.M. and C. Lee, *Synthetically useful oxidations at solid sodium permanganate surfaces.* Tetrahedron Letters, 1981. **22**(18): p. 1655-1656.

18. Klaewkla, R., M. Arend, and W.F. Hoelderich, *A Review of Mass Transfer Controlling the Reaction Rate in Heterogeneous Catalytic Systems.* Mass Transfer - Advanced Aspects, 2011: p. 667-684.

19. Jackson, S.D. and J.S.J. Hargreaves, *Metal Oxide Catalysis*. Vol. 2. 2009, Weinheim: WILEY-VCH VERLAG gMBh & cO. kgAa.

20. Murayama, H., et al., *Structure characterization of orthorhombic phase in MoVTeNbO catalyst by powder X-ray diffraction and XANES.* Applied Catalysis A: General, 2007. **318**(0): p. 137-142.

21. Bergmann, R.L. and N.W. Frisch, *Production of Maleic Anhydride by Oxidation of n-Butane*, U.S.P. Office, Editor. 1966, Princeton Chemical Research.

22. Haruta, M., *When Gold Is Not Noble: Catalysis by Nanoparticles.* The Chemical Record, 2003. **3**: p. 75-87.

23. Sault, A.G., R.J. Madix, and C.T. Campbell, *Adsorption of oxygen and hydrogen on Au(110)-(1 × 2).* Surface Science, 1986. **169**(2–3): p. 347-356.

24. Hammer, B. and J.K. Norskov, *Why gold is the noblest of all the metals.* Nature, 1995. **376**(6537): p. 238-240.

25. Hutchings, G.J., *Catalysis by gold.* Catalysis Today, 2005. **100**: p. 55–61.

26. Thenard, L.G. and P. L. Dulong, *Note Sur La Propriété, Que Possédent Quelques Métaux, De Faciliter La combinasion Des Fluides élastiques.* Annleles De Chimie Et De Physique, 1823. **23**: p. 440-443.

27. Erkelens, J., C. Kemball, and A.K. Galwey, *Some reactions of cyclohexene with hydrogen and deuterium on evaporated gold films.* Transactions of the Faraday Society, 1963. **59**: p. 1181-1191.

28. Chambers, R.P. and M. Boudart, *Selectivity of gold for hydrogenation and dehydrogenation of cyclohexene.* Journal of Catalysis, 1966. **5**(3): p. 517-528.

29. Sermon, P.A., G.C. Bond, and P.B. Wells, *Hydrogenation of alkenes over supported gold.* Journal of the Chemical Society, Faraday Transactions 1: Physical Chemistry in Condensed Phases, 1979. **75**: p. 385-394.

30. Haruta, M., et al., *Gold catalysts prepared by coprecipitation for low-temperature oxidation of hydrogen and of carbon monoxide.* Journal of Catalysis, 1989. **115**(2): p. 301-309.

31. Hutchings, G.J., *Vapor phase hydrochlorination of acetylene: Correlation of catalytic activity of supported metal chloride catalysts.* Journal of Catalysis, 1985. **96**(1): p. 292-295.

32. Hashmi, A.S.K. and G.J. Hutchings, *Gold Catalysis.* Angewandte Chemie International Edition, 2006. **45**(47): p. 7896-7936.

33. Huang, J., W.-L. Dai, and K. Fan, *Remarkable support crystal phase effect in Au/FeO_x catalyzed oxidation of 1,4-butanediol to γ-butyrolactone.* Journal of Catalysis, 2009. **266**(2): p. 228-235.

34. Bond, G.C., C. Louis, and D.T. Thompson, *Catalysis by Gold*. Catalytic Science Series, ed. G.J. Hutchings. Vol. 6. 2006, London: Imperial College Press.

35. Lopez-Sanchez, J.A., et al., *Facile removal of stabilizer-ligands from supported gold nanoparticles.* Nat Chem, 2011. **3**(7): p. 551-556.

36. Ntainjua, E.N., et al., *Direct synthesis of hydrogen peroxide using Au-Pd-exchanged and supported heteropolyacid catalysts at ambient temperature using water as solvent.* Green Chemistry, 2012. **14**(1): p. 170-181.

37. Fu, Q., H. Saltsburg, and M. Flytzani-Stephanopoulos, *Active Nonmetallic Au and Pt Species on Ceria-Based Water-Gas Shift catalysts.* Science, 2003. **301**: p. 935-938.

38. Hayashi, T., K. Tanaka, and M. Haruta, *Selective Vapor-Phase Epoxidation of Propylene over Au/TiO_2 Catalysts in the Presence of Oxygen and Hydrogen.* Journal of Catalysis, 1998. **178**(2): p. 566-575.

39. Abad, A., et al., *A Collaborative Effect between Gold and a Support Induces the Selective Oxidation of Alcohols.* Angewandte Chemie International Edition, 2005. **44**(26): p. 4066-4069.

40. Solsona, B.E., et al., *Supported gold catalysts for the total oxidation of alkanes and carbon monoxide.* Applied Catalysis A: General, 2006. **312**(0): p. 67-76.

41. Dimitratos, N., et al., *Solvent free liquid phase oxidation of benzyl alcohol using Au supported catalysts prepared using a sol immobilization technique.* Catalysis Today, 2007. **122**: p. 317-324.

42. Choudhary, V.R. and D.K. Dumbre, *Solvent-free selective oxidation of primary alcohols-to-aldehydes and aldehydes-to-carboxylic acids by molecular oxygen over MgO-supported nano-gold catalyst.* Catalysis Communications, 2011. **13**(1): p. 82-86.

43. Enache, D.I., D.W. Knight, and G.J. Hutchings, *Solvent-free Oxidation of Primary Alcohols to Aldehydes using Supported Gold Catalysts.* Catalysis Letters, 2005. **103**(1): p. 43-52.

44. Choudhary, V.R., et al., *A green process for chlorine-free benzaldehyde from the solvent-free oxidation of benzyl alcohol with molecular oxygen over a supported nano-size gold catalyst.* Green Chemistry, 2005. **7**(11): p. 768-770.

45. Su, F.-Z., et al., *Aerobic oxidation of alcohols catalyzed by gold nanoparticles supported on gallia polymorphs.* Catalysis Communications, 2008. **9**(6): p. 1027-1032.

46. Miedziak, P.J., et al., *Ceria prepared using supercritical antisolvent precipitation: a green support for gold-palladium nanoparticles for the selective catalytic oxidation of alcohols.* Journal of Materials Chemistry, 2009. **19**(45): p. 8619-8627.

47. Enache, D.I., et al., *Solvent-Free Oxidation of Primary Alcohols to Aldehydes Using Au-Pd/TiO_2 Catalysts.* Science, 2006. **311**(5759): p. 362-365.

48. Enache, D.I., et al., *Solvent-free oxidation of benzyl alcohol using titania-supported gold–palladium catalysts: Effect of Au–Pd ratio on catalytic performance.* Catalysis Today, 2007. **122**(3–4): p. 407-411.

49. Choudhary, V.R. and D.K. Dumbre, *Solvent-free selective oxidation of benzyl alcohol to benzaldehyde by tert-butyl hydroperoxide over U3O8-supported nano-gold catalysts.* Applied Catalysis A: General, 2010. **375**(2): p. 252-257.

50. Lopez-Sanchez, J.A., et al., *Au-Pd supported nanocrystals prepared by a sol immobilisation technique as catalysts for selective chemical synthesis.* Physical Chemistry Chemical Physics, 2008. **10**(14): p. 1921-1930.

51. Miedziak, P., et al., *Oxidation of benzyl alcohol using supported gold–palladium nanoparticles.* Catalysis Today, 2011. **164**(1): p. 315-319.

52. Li, G., et al., *Solvent-free oxidation of benzyl alcohol with oxygen using zeolite-supported Au and Au–Pd catalysts.* Catalysis Letters, 2006. **110**(1): p. 7-13.

53. J. Hutchings, G., et al., *High-activity Au/CuO-ZnO catalysts for the oxidation of carbon monoxide at ambient temperature.* Journal of the Chemical Society, Faraday Transactions, 1997. **93**(1): p. 187-188.

54. Haruta, M., et al., *Low-Temperature Oxidation of CO over Gold Supported on TiO_2, α-Fe_2O_3, and Co_3O_4.* Journal of Catalysis, 1993. **144**(1): p. 175-192.

55. Tana, et al., *Influence of Au particle size on Au/CeO_2 catalysts for CO oxidation.* Catalysis Today, 2011. **175**(1): p. 541-545.

56. Carabineiro, S., et al., *Gold nanoparticles supported on magnesium oxide for CO oxidation.* Nanoscale Research Letters, 2011. **6**(1): p. 435.

57. Bollinger, M.A. and M.A. Vannice, *A kinetic and DRIFTS study of low-temperature carbon monoxide oxidation over Au—TiO_2 catalysts.* Applied Catalysis B: Environmental, 1996. **8**(4): p. 417-443.

58. Bamwenda, G.R., et al., *The influence of the preparation methods on the catalytic activity of platinum and gold supported on TiO_2 for CO oxidation.* Catalysis Letters, 1997. **44**(1): p. 83-87.

59. Kim, K.-J., et al., *Preparation and characterization of nanosized gold catalysts supported on Co_3O_4 and their activities for CO oxidation.* Journal of Nanoscience and Nanotechnology, 2011. **11**(2): p. 1605-1608.

60. Moreau, F. and G.C. Bond, *Influence of the surface area of the support on the activity of gold catalysts for CO oxidation.* Catalysis Today, 2007. **122**(3–4): p. 215-221.

61. Chang, L.-H., et al., *CO oxidation on ceria- and manganese oxide-supported gold catalysts.* Separation and Purification Technology, 2007. **58**(1): p. 211-218.

62. Carrettin, S., et al., *Nanocrystalline CeO_2 Increases the Activity of Au for CO Oxidation by Two Orders of Magnitude.* Angewandte Chemie International Edition, 2004. **43**(19): p. 2538-2540.

63. Huang, X.-S., et al., *Morphology effects of nanoscale ceria on the activity of Au/CeO_2 catalysts for low-temperature CO oxidation.* Applied Catalysis B: Environmental, 2009. **90**(1–2): p. 224-232.

64. M. Finch, R., et al., *Identification of active phases in Au-Fe catalysts for low-temperature CO oxidation.* Physical Chemistry Chemical Physics, 1999. **1**(3): p. 485-489.

65. Bond, G.C. and D.T. Thompson, *Gold-Catalysed Oxidation of Carbon Monoxide.* Gold Bulletin, 2000. **33**(2): p. 41-50.

66. Valden, M., X. Lai, and D.W. Goodman, *Onset of Catalytic Activity of Gold Clusters on Titania with the Appearance of Nonmetallic Properties.* Science, 1998. **281**(5383): p. 1647-1650.

67. Chen, M.S. and D.W. Goodman, *The Structure of Catalytically Active Gold on Titania.* Science, 2004. **306**(5694): p. 252-255.

68. Bell, A.T., *The Impact of Nanoscience on Heterogeneous Catalysis.* Science, 2003. **299**(5613): p. 1688-1691.

69. Haruta, M., *Gold as a novel catalyst in the 21st century: Preparation, working mechanism and applications.* Gold Bulletin, 2004. **37**(1): p. 27-36.

70. Herzing, A.A., et al., *Identification of Active Gold Nanoclusters on Iron Oxide Supports for CO Oxidation.* Science, 2008. **321**(5894): p. 1331-1335.

71. Mai, H.-X., et al., *Shape-Selective Synthesis and Oxygen Storage Behavior of Ceria Nanopolyhedra, Nanorods, and Nanocubes.* The Journal of Physical Chemistry B, 2005. **109**(51): p. 24380-24385.

72. Yoshihiro, M., Y. Shu, and S. Tsugio, *Synthesis of Monodispersed rod-like and spherical CeO 2 particles by mild solution process.* IOP Conference Series: Materials Science and Engineering, 2009. **1**(1): p. 012003.

73. Zhong, L.-S., et al., *3D Flowerlike Ceria Micro/Nanocomposite Structure and Its Application for Water Treatment and CO Removal.* Chemistry of Materials, 2007. **19**(7): p. 1648-1655.

74. Subramanian, V., et al., *Hydrothermal Synthesis and Pseudocapacitance Properties of MnO2 Nanostructures.* The Journal of Physical Chemistry B, 2005. **109**(43): p. 20207-20214.

75. Xu, M., et al., *Hydrothermal Synthesis and Pseudocapacitance Properties of α-MnO_2 Hollow Spheres and Hollow Urchins.* The Journal of Physical Chemistry C, 2007. **111**(51): p. 19141-19147.

76. Zhang, X., H. Wang, and B.-Q. Xu, *Remarkable Nanosize Effect of Zirconia in Au/ZrO_2 Catalyst for CO Oxidation†.* The Journal of Physical Chemistry B, 2005. **109**(19): p. 9678-9683.

77. Ho, K. and K. Yeung, *Properties of TiO_2 support and the performance of Au/TiO_2 Catalyst for CO oxidation reaction.* Gold Bulletin, 2007. **40**(1): p. 15-30.

78. Yang, J.B., et al., *Growth and magnetic properties of MnO_2−δ nanowire microspheres.* Applied Physics Letters, 2004. **85**(15): p. 3160-3162.

79. Wang, L.-C., et al., *MnO_2 Nanorod Supported Gold Nanoparticles with Enhanced Activity for Solvent-free Aerobic Alcohol Oxidation.* The Journal of Physical Chemistry C, 2008. **112**(17): p. 6981-6987.

80. Guliants, V.V. and M.A. Carreon, *Vanadium-Phosphorus-Oxides: from Fundamentals of n-Butane Oxidation to Synthesis of New Phases.* Catalysis, 2005. **18**: p. 1-45.

81. Hutchings, G.J., et al., *High temperature preparation of vanadium phosphate catalysts using water as solvent.* Phys. Chem. Chem. Phys., 2003. **5**: p. 3525-3533.

82. Bartley, J.K., J.A. Lopez-Sanchez, and G.J. Hutchings, *Preparation of vanadium phosphate catalysts using water as solvent.* Catalysis Today, 2003. **81**(2): p. 197-203.

83. Taufiq-Yap, Y.H., et al., *Effects of mechanochemical treatment to the vanadium phosphate catalysts derived from $VOPO_4{\cdot}2H_2O$.* Journal of Molecular Catalysis A: Chemical, 2006. **260**(1–2): p. 24-31.

84. Bordes, E., *Crystallochemistry of V-P-O phases and application to catalysis.* Catalysis Today, 1987. **1**(5): p. 499-526.

85. Hutchings, G.J., et al., *Comments on the nature of the active site of vanadium phosphate catalysts for butane oxidation.* Catalysis Today, 1998. **40**(2–3): p. 273-286.

86. Griesel, L., et al., *Preparation of vanadium phosphate catalyst precursors using a high pressure method.* Catalysis Today, 2005. **99**(1–2): p. 131-136.

87. Centi, G., G. Fornasari, and F. Trifirò, *On the mechanism of n-butane oxidation to maleic anhydride: Oxidation in oxygen-stoichiometry-controlled conditions.* Journal of Catalysis, 1984. **89**(1): p. 44-51.

88. Batis, N.H., et al., *Synthesis and characterization of new VPO catalysts for partial n-Butane oxidation to maleic anhydride.* Journal of Catalysis, 1991. **128**(1): p. 248-263.

89. Hutchings, G.J., *Heterogeneous catalysts-discovery and design.* J. Mater. Chem., 2008. **19**: p. 1222-1235.

90. Poli, G., et al., *The chemistry of catalysts based on vanadium-phosphorous oxides: Note II The role of the method of preparation.* Applied Catalysis, 1981. **1**(6): p. 395-404.

91. Hutchings, G.J. and R. Higgins, *Selective oxidation of n-butane to maleic anhydride with vanadium phosphorus catalysts prepared by comminution in the presence of dispersants.* Applied Catalysis A: General, 1997. **154**(1–2): p. 103-115.

92. Hutchings, G.J., et al., *Improved method of preparation of vanadium phosphate catalysts.* Catalysis Today, 1997. **33**(1–3): p. 161-171.

93. Bartley, J.K., R.P.K. Wells, and G.J. Hutchings, *The Unexpected Role of Aldehydes and Ketones in the Standard Preparation Method for Vanadium Phosphate Catalysts.* Journal of Catalysis, 2000. **195**(2): p. 423-427.

94. Lopez-Sanchez, J.A., et al., *High temperature preparation of vanadium phosphate catalysts using water as solvent.* Physical Chemistry Chemical Physics, 2003. **5**(16): p. 3525-3533.

95. Griesel, L., et al., *Preparation of vanadium phosphate catalysts from $VOPO_4{\cdot}2H_2O$: effect of $VOPO_4{\cdot}2H_2O$ preparation on catalyst performance.* Journal of Molecular Catalysis A: Chemical, 2004. **220**(1): p. 113-119.

96. Kamiya, Y., et al., *Microstructures of V-P-O catalysts derived from $VOHPO_4{\cdot}0.5H_2O$ of different crystallite sizes.* Journal of Molecular Catalysis A: Chemical, 2004. **220**(1): p. 103-112.

97. Lin, Z., et al., *The synthesis of highly crystalline vanadium phosphate catalysts using a diblock copolymer as a structure directing agent.* Catalysis Today, 2010. **157**(1–4): p. 211-216.

98. Pepera, M.A., et al., *Fundamental study of the oxidation of butane over vanadyl pyrophosphate.* Journal of the American Chemical Society, 1985. **107**(17): p. 4883-4892.

99. Centi, G., et al., *Mechanistic aspects of maleic anhydride synthesis from C4 hydrocarbons over phosphorus vanadium oxide.* Chemical Reviews, 1988. **88**(1): p. 55-80.

100. Schiøtt, B. and K.A. Jørgensen, *The oxidative species on a vanadyl pyrophosphate surface: A model for some steps in the maleic anhydride synthesis.* Catalysis Today, 1993. **16**(1): p. 79-90.

101. Schioett, B., K.A. Joergensen, and R. Hoffmann, *Formation of maleic anhydride on a vanadyl pyrophosphate surface: a theoretical study of the mechanism.* The Journal of Physical Chemistry, 1991. **95**(6): p. 2297-2307.

102. Jenkins, R. and R. Snyder, *Introduction to X-Ray Powder Diffractometry*. 1st ed. 1996: Wiley-Interscience. 432.

103. Atkins, P.W., *The Elements of Physical Chemistry*. 3rd Revised ed. 2000: Oxford University Press. 562.

104. Andrews, D.L. and A.A. Demidov, *An Introduction to Laser Spectroscopy*. 2nd ed. 2002: Springer. 386.

Chapter 2

Experimental

2. Experimental

2.1 Preparation of supports

2.1.1 Preparation of CeO_2 foams

CeO_2 foams were synthesised according to the method of Shen *et al* [1]. L-Asparagine (3.96 g, Aldrich) was dissolved in water (120 ml) while stirring at 45 °C for 5 min. $CeCl_3.7H_2O$ (0.932 g, Aldrich) was added and the solution was stirred for a further 10 min. The solution was then placed in a sealed autoclave (Baskerville, 250 ml) and heated (160 °C) for a range of times (2-48 h). Following the reaction the precursor material was recovered by filtration, washed with water (100 ml) and ethanol (50 ml) and dried (110 °C, 4 h). The oxide foam was formed by calcination in static air at 350 °C for 2 h. The resultant ceria foams were denoted foamCeO_2-*x*h, where *x* is the crystallisation time in hours.

2.1.2 Preparation of MnO_2 nanowire microspheres

MnO_2 materials were synthesised according to the method of Yang *et al* [2] who prepared MnO_2 material hydrothermally at 120 °C for a certain reaction time (12 hr). However, their preparation method was extended to investigate the effect of reaction time on the morphology and the phase of the support. In a typical preparation, Hydrated manganese sulfate $MnSO_4.H_2O$ (14.198 g, Aldrich) was dissolved in water (165 ml) while stirring at room temperature for 15 min. Ammonium persulfate $(NH_4)_2S_2O_8$ (19.169 g, Aldrich) was added and the solution was stirred to form a clear solution. The solution was then placed in a sealed autoclave (Baskerville, 250 ml) and heated (120

°C) for a range of times (6-240 h). Following the reaction the resulting black material was recovered by filtration, washed with water (1L) and dried (60 °C, 24h). The resultant MnO_2 nanowire microspheres were denoted MnO_2-*x*h, where *x* is the crystallisation time in hours.

2.2 Preparation of gold catalysts

2.2.1 Sol-immobilisation method

2.2.1.1 Sol-immobilisation using THPC stabiliser

An aqueous sodium hydroxide (1.5 ml, 0.2 M) was diluted with deionised water (46.7 mL) and tetrakis hydroxymethyl phosphonium chloride (THPC, 1 ml) was added with stirring. After 3 min, an aqueous solution of $HAuCl_4.3H_2O$ (0.82 ml, 0.062 M, equivalent to 10 mg of Au) was added and the solution was stirred for a further 30 min. The stirring was then stopped and the support (0.99 g) was added. After 2 min, H_2SO_4 (0.15 ml, 0.1 M) was added and the mixture was shaken gently for 1 h. The solid was recovered by filtration and washed with deionised water (800 ml) and dried in air (110 °C, 16 h).

2.2.1.2 Sol-immobilisation using PVA stabiliser

A 1 wt% solution of PVA (Aldrich, MW = 10 000, 80 % hydrolyzed) was added to an aqueous $HAuCl_4$ solution (0.062 M, equivalent to 10 mg of Au) with vigorous stirring (PVA/Au (w/w) = 1.2); a 0.1 M freshly prepared solution of $NaBH_4$ ($NaBH_4$/Au (mol/mol) = 5) was then added to form a metallic sol; the color of the sol was light-red

(Au). After 30 min of sol generation, the colloid was immobilized by adding the support (0.99 g) (acidified at pH 1, by sulfuric acid) under vigorous stirring. After 2 h the slurry was filtered, the solid washed thoroughly with distilled water and dried at 110 °C for 16 h.

2.2.1.3 Reflux Sol-immobilisation method

All sol-immobilised catalysts synthesised above by PVA method were refluxed according to the method of Hutchings and co-workers [3]. Typically, 0.4 g of catalyst was placed in a round bottom flask and water (100 ml) was added into the flask. The round bottom flask was connected to a reflux condenser and placed in an oil bath which was heated at 90 °C, under vigorous stirring; the solution was left to reflux for 1 h. After the reflux period, the slurry was filtered and washed thoroughly with distilled water (800 ml) and dried at 110 °C overnight.

2.2.2 Impregnation method

An aqueous solution of $HAuCl_4.3H_2O$ (0.062 M, equivalent to 10 mg of Au) was added to the support (0.99 g) under stirring. The paste formed was dried at 110 °C for 16 h and calcined in static air, typically at 400 °C for 3 h.

2.2.3 Deposition precipitation

0.99 g of the support was mixed with 150 ml distilled water and stirred at 60 ºC. To this, a solution of $HAuCl_4.3H_2O$ (0.062 M, equivalent to 10 mg of Au) was added;

subsequently a solution of NaOH was added drop-wise to the mixture to maintain an overall pH of 9. After 1.5 h the solution was filtered and washed with 1L distilled water. The catalyst was dried at 110 ºC for 16 h and calcined in static air at 400 ºC for 3 h.

2.3 Preparation of vanadium phosphate catalysts

The vanadium phosphate hemihydrate ($VOHPO_4 \cdot 0.5H_2O$) precursor was synthesised according to the literature [4] using two different methods denoted the VPO and VPD routes.

2.3.1 Preparation of $VOHPO_4.0.5H_2O$ precursor via VPO route

2.3.1.1 Standard procedure

V_2O_5 (2 g, Strem) and H_3PO_4 (1.66 ml, 85%, Aldrich) were added to isobutanol (2-methyl-1-propanol, 42.5 ml, Aldrich) and the mixture heated under reflux conditions for 16 h. The resultant pale blue solid was recovered by vacuum filtration, and washed with isobutanol (100 ml) and ethanol (100 ml), then dried in air at 110 °C. This material was denoted P-VPO0.

2.3.1.2 Copolymer modified procedure

For the copolymer modified materials, V_2O_5 and H_3PO_4 were reacted in isobutanol with different amounts of PAAMA (poly (acrylic acid-co-maleic acid) solution. In a typical preparation, PAAMA (50 %, average Mw=3,000, Aldrich) was added drop wise to a solution of H_3PO_4 (1.66 ml, 85 %, Aldrich) and isobutanol (42.3 ml, anhydrous, Aldrich) in a round bottom flask. The solution was stirred at room temperature until

homogeneous solution formed. Then, V_2O_5 (2 g, Aldrich) was added and stirred well, and the temperature was raised to 110 °C for 16 h. The resulting light blue solid was recovered by vacuum filtration, and washed with isobutanol (100 ml) and ethanol (100 ml), then dried in air at 110 °C. Three samples were prepared with different concentrations of PAAMA: 5 g/L (denoted P-VPO5), 15 g/L (denoted P-VPO15) and 25 g/L (denoted P-VPO25). The precursors P-VPO0, P-VPO5, P-VPO15 and P-VPO25 were activated at 400 °C in situ in a flow of 1.7 % butane in air until steady state observed to give their respective catalysts, denoted C-VPO0, C-VPO5, C-VPO15 and C-VPO25.

2.3.2 Preparation of $VOHPO_4.0.5H_2O$ precursor via VPD route

2.3.2.1 Preparation of $VOPO_4.2H_2O$

Vanadium phosphate dihydrate ($VOPO_4 \cdot 2H_2O$) was first synthesised by the standard method without any modification. In the typical preparation, V_2O_5 (10 g, Aldrich) was refluxed with H_3PO_4 (45 ml, 85%, Aldrich) in water (120 mL) for 24 h. The yellow $VOPO_4 \cdot 2H_2O$ was recovered by filtration, washed with water and acetone and dried in air (110 °C, 16 h).

2.3.2.2 Preparation of $VOHPO_4 \cdot 0.5H_2O$ via $VOPO_4.2H_2O$ using the standard procedure

To prepare the standard vanadium phosphate hemihydrate ($VOHPO_4 \cdot 0.5H_2O$) precursor, $VOPO_4 \cdot 2H_2O$ (2 g) was refluxed in isobutanol (40 mL) for 18 h. The

resultant blue solid was recovered by hot filtration, washed with isobutanol (25 ml) and ethanol (33 ml) and dried in air (110 °C, 16 h). This material was denoted P-VPD0.

2.3.2.3 Preparation of $VOHPO_4 \cdot 0.5H_2O$ via $VOPO_4.2H_2O$ using copolymer modified procedure

For the copolymer modified materials, the $VOPO_4 \cdot 2H_2O$ was refluxed in isobutanol with different amounts of PAAMA. In a typical preparation, PAAMA was added drop wise with stirring to isobutanol (40 ml, anhydrous, Aldrich) in a round bottom flask at room temperature until a homogeneous solution formed. $VOPO_4 \cdot 2H_2O$ (2 g) was added to this solution, which was stirred well and heated to the reflux temperature for 18 h. The pale blue solid was recovered by filtration and washed by isobutanol (25 ml) followed by ethanol (33 ml) and dried at 110 °C for 16 h. Three samples were prepared with different concentrations of PAAMA: 5 g/L (denoted P-VPD5), 15 g/L (denoted P-VPD15) and 25 g/L (denoted P-VPD25). The precursors P-VPD0, P-VPD5, P-VPD15 and P-VPD25 were activated at 400 °C in situ in a flow of 1.7 % butane in air until steady state observed to give their respective catalysts, denoted C-VPD0, C-VPD5, C-VPD15 and C-VPD25.

For gold catalysts, sol-immobilisation using THPC was used to deposit gold on ceria foam supports prepared above and the catalysts were tested for benzyl alcohol oxidation as will be shown in chapter 3. While Sol-immobilisation using PVA and its corresponding reflux method, impregnation and DP preparation methods were employed to deposit gold on MnO_2 nanowire microspheres prepared above and the

catalysts were tested for benzyl alcohol and CO oxidation and the results will be discussed in chapter 4.

Vanadium phosphate catalysts either the standard or the modified ones will be tested for n-butane oxidation and the results will be discussed in chapter 5.

2.4 Characterisation techniques

2.4.1 Powder X-ray diffraction (XRD)

Powder X-ray diffraction (XRD) is a rapid technique for the determination of the crystalline materials as it reveals useful information about the crystal structures of the material by its diffraction pattern. Therefore, it is used effectively to analyse suitable heterogeneous catalysts. The XRD technique was developed by Braggs, William and Lawrence and the basic equation used in XRD is called the Bragg Law (Equation 2.1):

Equation 2.1 $$n\lambda = 2d \sin\theta$$

Where n is an integral number, λ is the wavelength of x-ray, d is the difference between planes and θ is glancing angle.

The X-ray diffraction equipment comprises mainly of an X-ray source, sample holder and detector to detect the diffracted X-rays. The generated X-rays are aimed towards the sample, those that are reflected off the crystal plane with an angle that is equal to the glancing angle. The difference in length between the X-rays shown in Fig. 2.1 is AB + BC which, therefore, is equivalent to:

$$\mathbf{AB + BC = 2d \sin\theta}$$

When this difference is equivalent to an integral number of a wavelength (AB + BC = nλ), the reflected waves interfere constructively and thus the reflection can be observed and detected as it satisfies the Bragg law [5, 6].

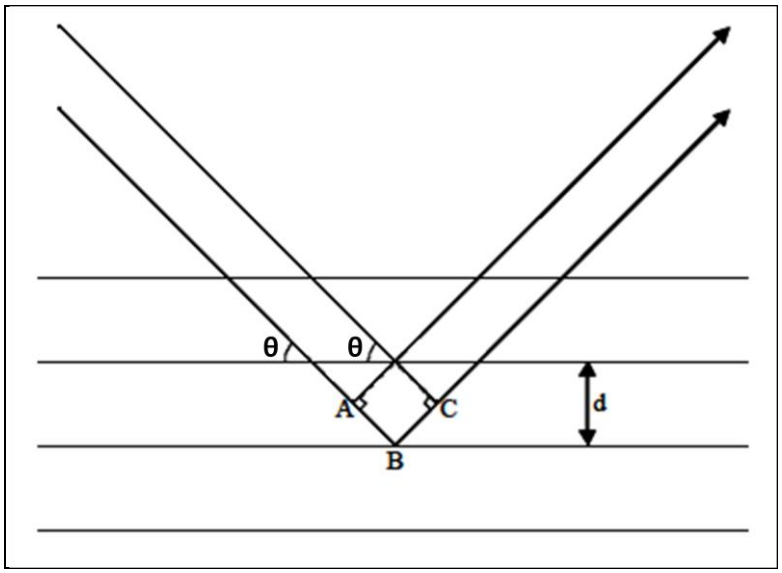

Fig. 2.1 A demonstration of Bragg equation

In this study, Powder X-ray diffraction (XRD) was performed using a PANalytical X'Pert Pro with a CuK_{α} X-ray source operated at 40 kV and 40 mA fitted with an X'Celerator detector. Each sample was scanned from 2θ = 10 to 80 at a certain time which was 30 minutes. All materials prepared in this thesis showed a very well determined diffraction patterns. The reflections of produced were compared with the references reported in the literature for each material.

Powder X-ray diffraction (XRD) provides detailed information about the structure of the material such as its phase and planes in details but one of its limitations is that lack of sensitivity. Some materials consist of very low concentrations of other phases that are undetectable by XRD. Therefore, other characterisation techniques such as Raman spectroscopy were employed to obtain a clear background of the material structure.

2.4.2 Laser Raman Spectroscopy

Laser Raman spectroscopy is a powerful characterization technique for heterogeneous catalyst materials. It was used in this study for the phase determination of vanadium phosphate catalysts (chapter 5) and for manganese dioxide (chapter 4).

The Raman effect arises when a sample is illuminated by a radiation of frequency ν and the scattered light can be detected and recorded. Typically, when the incoming light strikes the molecules in the sample it excites them and scatters the light as a result. Scattering can exist as elastic, Rayleigh scattering, or as inelastic, Raman scattering. In Rayleigh scattering, both emitted and incoming photons have a similar wavelength and the difference in energy between them is equal to zero. In Raman scattering, and due to the inelastic collision between the incoming photon and the molecule in the sample, the vibration energy changes by ΔE_m as shown in equation 2.2.

Equation 2.2 $$\mathbf{h\nu_i - h\nu_s = \Delta E_m}$$

Where $h\nu_i$ is the incoming photon energy, $h\nu_s$ is the emitted photon energy. $h\nu_i$ must be different from $h\nu_s$ and the difference in energy between them, ΔE_m, can have a positive

or negative value. If the molecule acquires energy, ΔE_m will be positive leading to Stoke Raman scattering. If the molecule loses energy, ΔE_m will be negative leading to anti-Stoke Raman scattering.

Fig. 2.2 shows the vibration energy levels of the molecule. In Raman scattering, if the incoming photons collided with the molecules, gave up some of their energy and emerged in a lower frequency, molecules will fall into a higher level leading to Raman Stoke scattering. On the contrary, some photons gain energy from the excited molecules and emerge as higher frequency and the molecules then fall into a lower level which is Raman Anti-Stoke scattering. Radiation that scattered without any difference in frequency is called Rayleigh scattering [7].

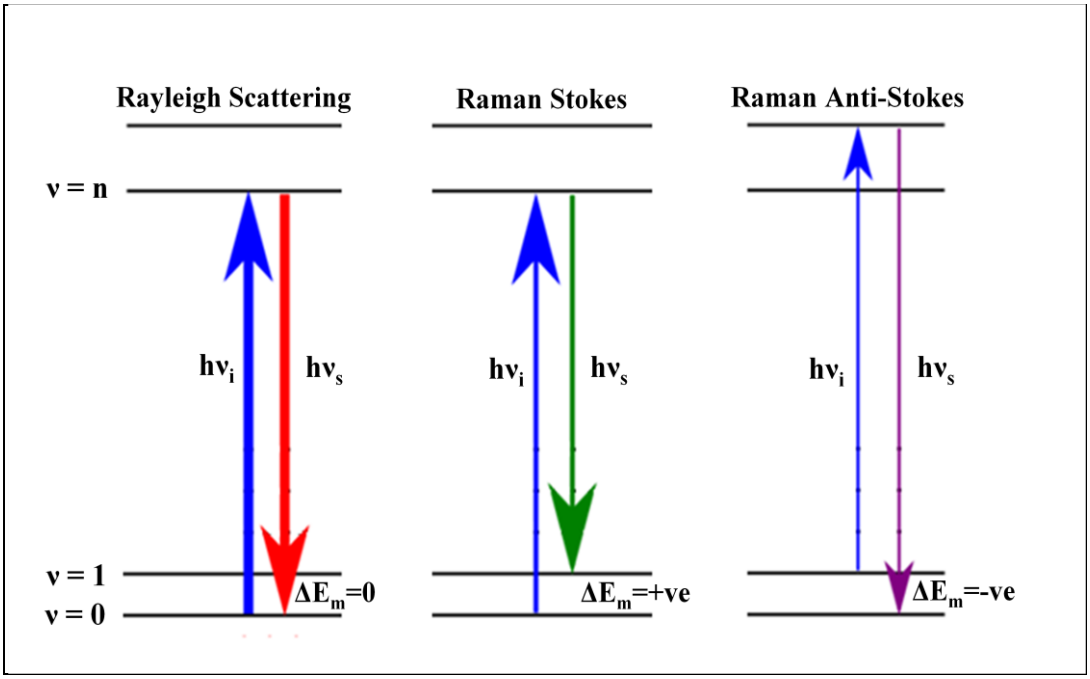

Figure 2.2 Raman and Rayleigh scattering

In this study, the Laser Raman spectroscopy (Renishaw in-via Ramascope) was employed (Fig. 2.3). Typically, all samples were used as a powder (approx 0.1 g) prior to placing them on a metal slide inside the spectrometer. The powder was analysed under an IR class laser 514.5 and 785 nm which will be shown in each chapter.

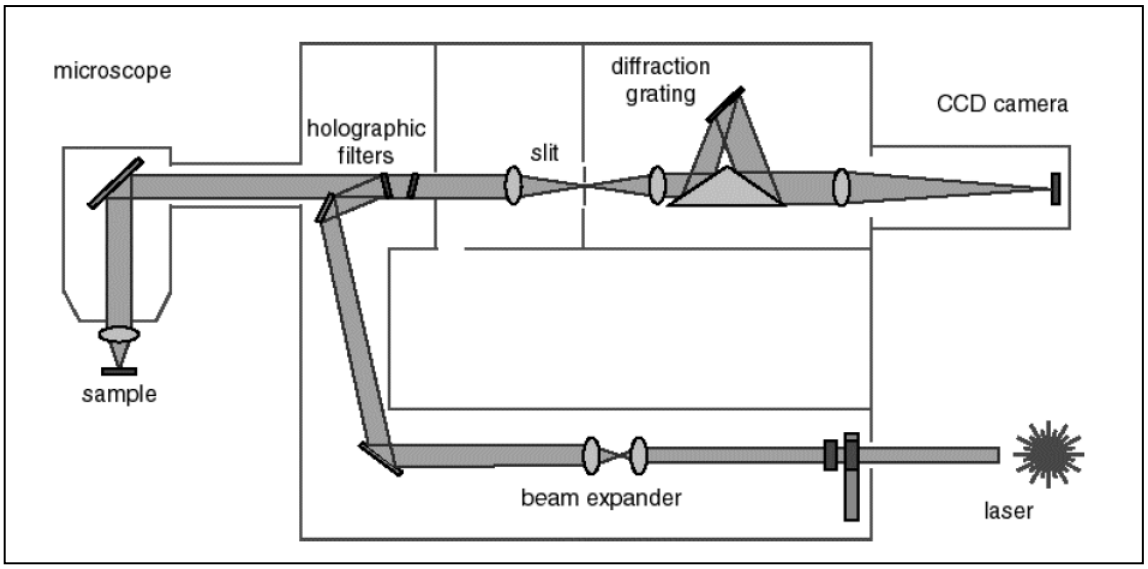

Figure 2.4 Schematic diagram of. Laser Raman spectroscopy (LRS)

2.4.3 Electron microscopy (SEM, TEM and STEM)

Scanning electron microscopy (SEM) is a very significant technique for catalysts characterisation. Electrons are used in SEM instead of light to produce images. Therefore, SEM can present high quality images with detailed information about the morphology because of the enormous depth of focus on the sample compared to optical microscopy [8].

In a typical process, an electrons beam is generated by a metallic filament cathode that is heated in vacuum by passing a voltage to it. Tungsten is usually used as a filament because of its high melting point and low vapour pressure. This electron beam is accelerated through the column of microscopy by a powerful force performed by the anode. The beam is condensed and focused by lenses and directed to the sample as a spot. The collision between the incoming electron primary beam and the sample causes electrons to be emitted from the sample surface because of elastic and inelastic collision. The electrons emitted from the sample atom's nucleus due to the elastic collision have high electron energy and are called backscatter electrons. These electrons are detected by a backscatter detector and are mainly used for showing the contrast in chemical components. Secondary electrons have low energy and are as a result of the inelastic collision of the primary beam with the sample nucleus where significant energy loss takes place. These electrons are collected by a secondary electrons detector to form an image of the surface. Both secondary and backscatter electrons are converted to a signal then sent to a viewing screen (Fig. 2. 5).

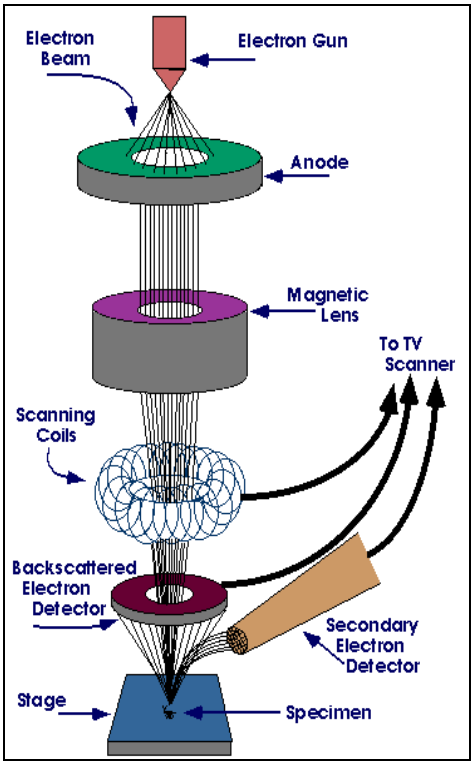

Fig.2.5 Schematic diagram of scanning electron microscope (SEM)

Transmission electron microscopy (TEM) is a powerful technique in heterogeneous catalysis and it is used for the determination of the size, shape and compositions of the materials [9]. When electrons emitted from a gun on the top of the unit they proceed through electromagnetic lenses and can be focused into a fine beam. This beam hits the sample and many types of electrons are reflected from the surface of the sample and disappeared as shown in Fig. 2.6.

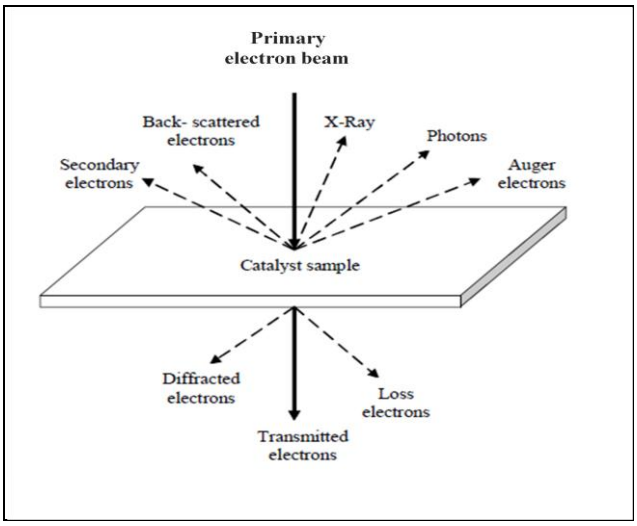

Figure 2.6 Interactions between electrons and the sample

The un-reflected electrons that transmit through the sample are magnified by electromagnetic lenses and then hit a fluorescent screen at the bottom of the microscope which generates the TEM image. The image can be studied and recorded by a camera (Fig. 2.7).

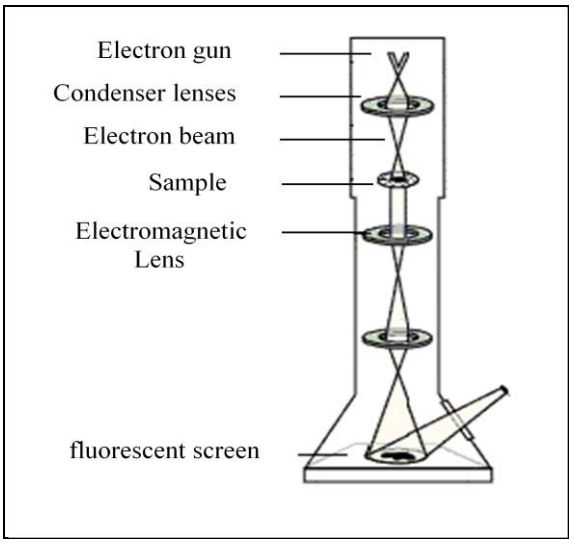

Figure 2.7 Schematic diagram of transmission scanning microscope (TEM)

The contrast observed on the TEM image reflections are the interaction between the transmitted electrons and different atoms in the sample. Based on the density of the atom (typically, metals has a higher electrons density than supports, therefore they appear darker in the TEM image.

Scanning transition electron microscopy (STEM) is another type of electron microscopy. In STEM, a very thin primary beam scans a film of a sample and then transmitted electron signal is detected to form an image using a detector like annular dark field (ADF). The chemical component can also be identified when other detectors are employed such as Energy Dispersive X-Ray (EDX) detector.

SEM, TEM and STEM are very important technique in many fields such as medical, biological, materials and heterogeneous catalysis [9]. They can present images with detailed information about the composition, morphology and size of the material.

In this study, Scanning electron microscopy (SEM) analyses were carried out on a Carl Zeiss EVO-40 SEM equipped with a backscatter detector and an Oxford Instruments silicon lithium energy dispersive X-ray detector. TEM images were obtained in a 200kV JEOL 2000FX electron microscope equipped with a thermionic LaB6 source. The samples were ground in high purity ethanol then a drop of the suspension was placed on a holey carbon film supported on a 300 mesh copper TEM grid. Samples for scanning transmission electron microscopy (STEM) were prepared for analysis by grinding the powders between clean glass slides and then dry dispersing them onto a holey carbon film supported on a Cu mesh TEM grid. The samples were then examined using high angle annular dark field (HAADF) imaging mode in an aberration corrected JEOL JEM-2200FS (S) TEM operating at 200 kV. TEM and STEM images were obtained by

Professor Christopher Kiely and his group in the material science department at the Lehigh University, USA.

2.4.4 Surface area measurements (BET)

BET surface area method is a common technique for the determination of surface area of the materials. It is extensively used in catalyst characterisation because it is most often the greater the surface area the more active catalyst. BET method was developed by Brunaure, Emmett, and Teller in 1938 [10]. In this method, the surface area of a material is based on the volume of the surface adsorbed gas at a certain temperature and pressure. Typically, the gas that is used in the BET method is N_2 and its concept relies on the BET equation (equation 2.3).

Equation 2.3

$$\frac{P}{V(P_o - P)} = \frac{1}{V_m C} + \frac{C - 1}{V_m C}\frac{P}{P_o}$$

Where V is the volume of the adsorbed gas at pressure P, Vm is the volume of the monolayer of gas adsorbed, Po is the saturation vapour pressure of adsorbates at the temperature of adsorption and C is a constant, related to the heat of adsorption and condensation of gas.

This equation gives a straight line when $P/V(P_o-P)$ is plotted against P/P_o so V_m and C can be calculated accordingly. Once V_m and C are calculated, the surface area can be calculated from equation 2.4 by assuming every molecule of adsorbed N^2 occupied σ = 0.162 nm^2.

Equation 2.4 $\mathbf{SA(m^2/g) = V_m N_a \sigma / M V_o}$

Where SA is the surface area, N_a is Avogadro number (6.023×10^{23}), σ is the area of adsorbate = 0.162 nm^2 at 77 K, M is sample weight and V_o is the molar volume of gas.

2.4.5 Temperature-Programmed Reduction (H_2-TPR)

Temperature programmed reduction is a characterisation technique that determines the reducibility of the metal oxides species in the material [11, 12]. Typically, a reducing gas mixture (usually hydrogen diluted in argon or nitrogen) flows over the sample which is heated gradually. During the gas flow over the sample, a thermal conductivity detector (TCD) measures the thermal conductivity changes of the consumed gas and records it as a signal. The TCD signal refers to the concentration of the hydrogen consumed (reacted with oxygen present in the material). The TPR profile can be obtained by plotting the TCD signal with the temperature. TPR is a useful technique in catalysis by which different catalysts can be compared by their reducibility profile in an effort to explain differences in activity and selectivity which may be related to the surface structure.

In this study, TPR analysis was performed on a Quantachrome ChemBET instrument. Samples (0.02 g) were pre-treated at 100 °C (ramp=20 °C min^{-1}) under He for 1 h prior to reaction to clean the surface. Analysis was performed under 10 % H_2/Ar (BOC 99.99 %, 25 ml min^{-1}) 30-850 °C, 20 °C min^{-1}.

2.4.6 Gas Chromatography (GC)

Gas chromatography is widely used in the academic and industrial laboratories. It is employed for separating and analysing a mixture of components. A GC comprises of an injector port, a carrier gas (mobile phase), columns (the stationary phase) and detectors (Fig. 2.8). The sample is injected and is vaporised immediately in the injection port, which is held at a high enough temperature to achieve this. The sample components are in the gas phase where they can be transported by a carrier gas e.g. argon, helium or nitrogen over the column to a suitable detector. The length, wall composition and hence the polarity separate the components accordingly and they elute thereafter (Fig. 2.8).

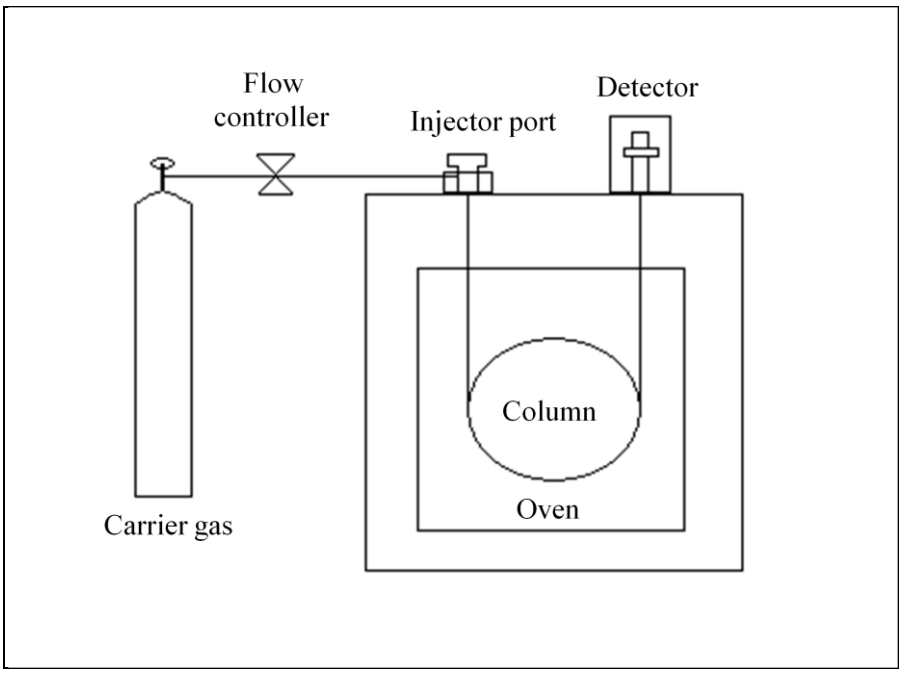

Figure 2.8 Schematic diagram of gas chromatography (GC)

The separation occurs because of the interaction between the sample components and the column which is packed with an inert surface that acts as a stationary phase. There are two kinds of columns which commonly used for separation in GC, packed and capillary. Packed columns consist of a fine inert solid material coated with liquid phase as a stationary phase. They typically possess 1.5-10 m in length with a 2-4 mm internal diameter. Capillary columns are made of a capillary tube and their inner walls are lined with a fine layer of material such as polyamide. The capillary tube diameter is typically 50-500 μm and has a length between 5-200 m. Capillary columns are more efficient and therefore are the most used columns in GC due to their high separation power. Once the sample components have been separated, they are analysed and registered by a detector and then quantified by the user. Two most common detectors used in GC, the flame ionization detector (FID) and the thermal conductivity detector (TCD).

The TCD theory is based on the detectable difference between the thermal conductivity of two streams, the first is a carrier gas as a reference and the second contains the carrier gas and the compound. The TCD comprises of tungsten-rhenium filaments configured as a Wheatstone bridge. These filaments are heated by applying an electric current through them. The carrier gas that has a very high thermal conductivity such as helium flows across the filaments to remove the heat. When the sample molecule with a lower thermal conductivity comes from the column to the sample filaments, the difference in thermal conductivity is detected as a change in voltage which can be displayed. The TCD detector is less sensitive than the FID but it is suitable for all compounds not only hydrocarbons. Therefore it is widely used for gas analysis such as for component streams containing O_2, CO, CO_2, N_2, NO, NO_2.

The FID contains a stainless steel chamber (jet) and the column is connected directly with it. When the carrier gas exits the column it enters the chamber, mixed with hydrogen and air and is combusted at the tip of the chamber. The molecules that ionise in the combustion process are attracted and recovered by a metal collector electrode which is located just to the side of the flame. The resulting electron current is converted by an amplifier to milli volts. The FID is very sensitive to the hydrocarbons but insensitive to molecules like O_2, CO, CO_2, N_2, NO, NO_2. In both TCD and FID, the peak area for each molecule is corrected with a response factor (RF) then it is divided by the relative response factor of the compound to obtain the true number of the count.

2.5 Catalyst evaluation

2.5.1 Oxidation of benzyl alcohol

The benzyl alcohol oxidation reactions were carried out in a glass reaction vessel (Colaver, 50 ml) at a constant pressure of oxygen (1 barg unless otherwise stated) (Fig. 2.8).

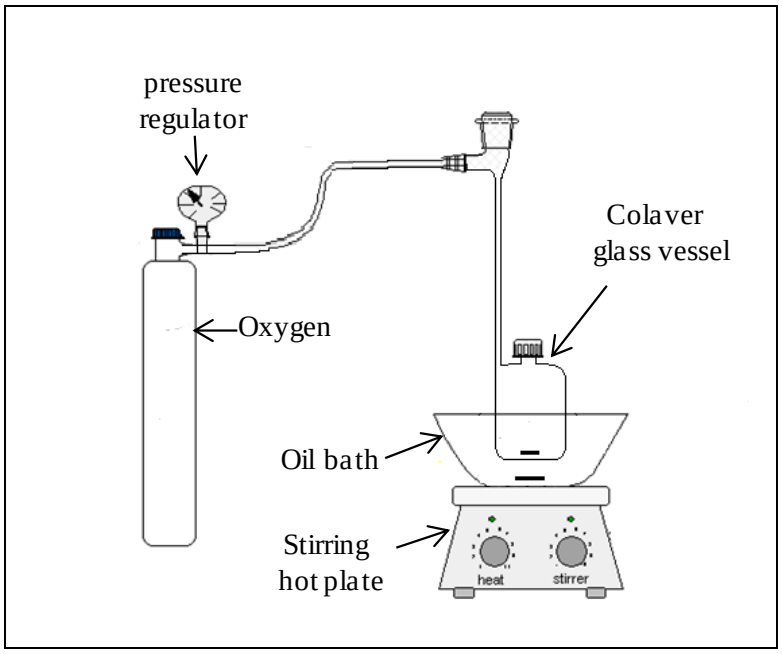

Figure 2.9 Schematic diagram of the glass Colaver reactor used for the oxidation of benzyl alcohol.

Typically, the vessel was charged with benzyl alcohol (2 g) and catalyst, Au/CeO_2 or Au/MnO_2 (20 mg, unless otherwise stated). The vessel was then purged with oxygen 5 times and was left under the desired pressure. The reaction suspension was heated/stirred to 120 °C for 4 h. For the analysis of the products, and GC (Varian Star 3400 CX with a 30 m CP-Wax 52 CB column) and FID detector were employed. For quantification of the reactants consumed and products generated, 0.5 ml of the reaction solution was added to 0.5 mL of mesitylene as an internal standard and 0.06 µL of this mixture was injected into the GC. The products were identified by comparison with authentic samples.

2.5.2 CO oxidation

Catalyst samples (Au/MnO_2) were evaluated for CO oxidation using a fixed-bed laboratory microreactor operated at atmospheric pressure (Fig. 2.10).

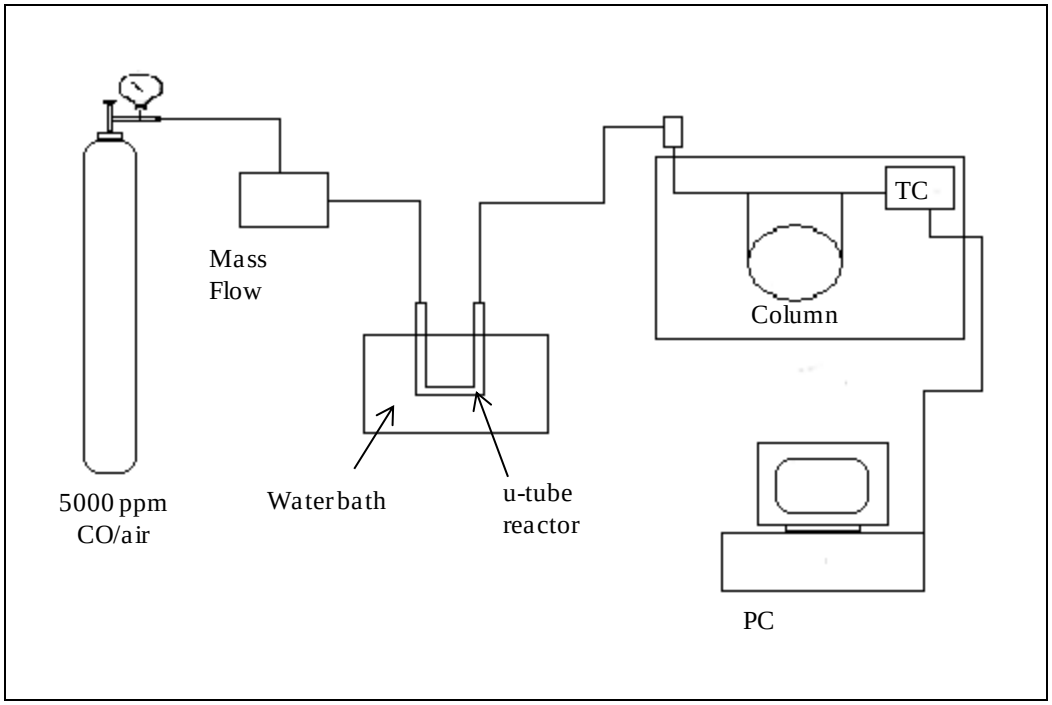

Figure 2.10 Schematic diagram of the micro reactor used for CO oxidation

Typically CO (5000 ppm in synthetic air) provided by BOC was fed to the reactor at a controlled rate of 20-40 ml/min using mass flow controllers and passed over the catalyst (25-100 mg). The catalyst temperature was maintained at 30 °C by immersing the quartz bed in a thermostatically controlled water bath. The products were analyzed using online gas chromatography (Varian 3800) with a 1.5 m packed carbosieve column. The GC injects the products every 4 minutes for 2 h. The column temperature

was kept at 195 °C to provide a good separation of CO/air and CO_2. A thermal conductivity detector was employed for products detection and analysis.

The GC was calibrated using a known concentration of CO_2 to find out the maximum area corresponding to a 100 % conversion (5000 ppm of CO should produce 5000 ppm of CO_2) and the calculation is displayed in equation 2.5.

Equation 2.5 $$\textbf{CO conversion} = (\textbf{CO}_2 \textbf{ counts/ Total CO}_2 \textbf{ counts}) \times 100$$

The CO conversion was calculated and plotted as a function of time on-line.

2.5.3 Oxidation of n-butane

The reactor used for the catalyst evaluation for the selective oxidation of n-butane to maleic anhydride is displayed in Fig. 2.11. In a typical procedure, 0.2 g of the hemi-hydrate precursor (approx. 0.3 ml) was placed inside a stainless steel tube reactor (1/5'' diameter) and was held in the centre of the tube with quartz wool. A mixture of 1.7 % n-butane (BOC, 99.95 %) in air (total flow was around 10 ml min^{-1}) that controlled by a mass flow controller was fed through a stainless steel tube into the catalyst reactor. The GHSV (gas hourly space velocity) which is the total gas flow divided by the catalyst volume used in the catalytic test was around 2000 h^{-1}. The reactor was placed inside a cylindrical furnace (LPC Elements) and was heated up to 400 °C with a temperature ramp of 3 °C min^{-1}. The temperature was maintained by Eurotherm controller that was positioned in contact with the catalyst bed. The products flow through a heated tube, to prevent any condensation, to the on-line gas chromatograph. The gas chromatography

used for the products on-line analysis is Varian 3400. The GC was set to inject the products every 34 minutes. Two columns were used in this GC for separation. Porapak Q (PQ, 2m x 2mm i.d.) column was used to separate CO_2, n-butane whereas O_2, N_2, and CO were separated by a molecular sieve 13X (MS13X, 2m x 2mm i.d.) column.

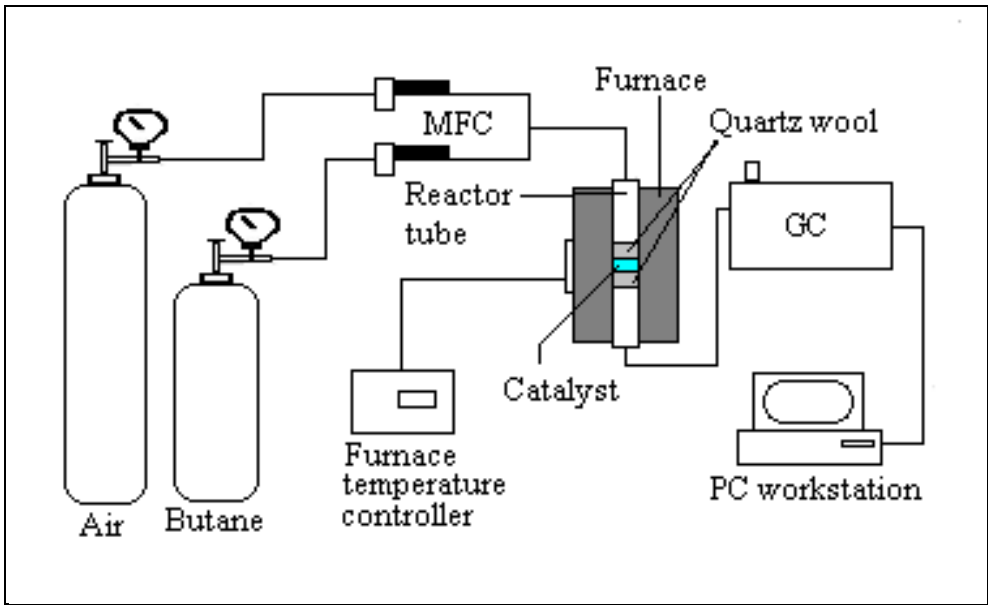

Figure 2.11 Schematic diagram of the reactor used for the oxidation of butane

In the method used for the analysis in this GC, the reactor effluent was injected using helium as acarrier gas into the Porpak Q column which is connected to the molecular sieve column. After 0.9 minutes, CO_2 was eluted from the porapak column to the detector. At this time O_2, N_2 and CO were parked in the molecular sieve column and after 9 minutes the flow was restored and these gases eluted. Once O_2, N_2 and CO (14 minutes) had eluted, the molecular sieve is bypassed again and the temperature of the

oven is heated up to 160 °C with a ramp of 50 °C min^{-1}. This is to allow a quick elution of the un-reacted butane and finally the elution of maleic anhydride from the Porapak Q. All eluted products were detected by a TCD detector for analysis and quantification. Each component was represented as a signal peak and the peaks were recognized according to their retention time observed. The peak area for every product was corrected using a response factor according to Dietz et al [13] then divided by the relative response factor of the compound to obtain the true number of the counts.

The conversion and selectivity were calculated and plotted as function of time on line (T.O.L). The conversion of butane at a specific time was obtained by equation 2.6.

Equation 2.6

$$\text{Conversion at specific time} = \frac{\text{the response value of the butane peak when no reaction} - \text{the response value of the butane peak at this time}}{\text{response value of the butane peak when no reaction}}$$

To find out the response value of butane when no reaction takes place (blank run), the reactor was cooled to 200 °C after each catalytic test and measurements taken for several runs. The selectivity was defined as the amount of product formed divided by the total amount of products formed and corrected for molar ratios.

2.6 References

1. Shen, Z., et al., *Macroporous Lanthanide-Organic Coordination Polymer Foams and Their Corresponding Lanthanide Oxides.* Advanced Materials, 2008. **20**(5): p. 984-988.

2. Yang, J.B., et al., *Growth and magnetic properties of $MnO_2{-}\delta$ nanowire microspheres.* Applied Physics Letters, 2004. **85**(15): p. 3160-3162.

3. Lopez-Sanchez, J.A., et al., *Facile removal of stabilizer-ligands from supported gold nanoparticles.* Nat Chem, 2011. **3**(7): p. 551-556.

4. Hutchings, G.J., et al., *Comments on the nature of the active site of vanadium phosphate catalysts for butane oxidation.* Catalysis Today, 1998. **40**(2–3): p. 273-286.

5. Atkins, P.W., *The Elements of Physical Chemistry*. 3rd Revised ed2000: Oxford University Press. 562.

6. Andrews, D.L. and A.A. Demidov, *An Introduction to Laser Spectroscopy*. 2nd ed2002: Springer. 386.

7. Brunauer, S., P.H. Emmett, and E. Teller, *Adsorption of Gases in Multimolecular Layers.* Journal of the American Chemical Society, 1938. **60**(2): p. 309-319.

8. Monti, D.A.M. and A. Baiker, *Temperature-programmed reduction. Parametric sensitivity and estimation of kinetic parameters.* Journal of Catalysis, 1983. **83**(2): p. 323-335.

9. Hurst, N.W., et al., *Temperature Programmed Reduction.* Catalysis Reviews, 1982. **24**(2): p. 233-309.

10. Jenkins, R. and R. Snyder, *Introduction to X-Ray Powder Diffractometry*. 1st ed1996: Wiley-Interscience. 432.

11. Goldstein, J., et al., *Scanning Electron Microscopy and X-ray Microanalysis*. 3rd ed2003: Springer. 689.

12. Flegler, S.L., J.W.H. Jr, and K.L. Klomparens, *Scanning and Transmission Electron Microscopy: An Introduction*. New Ed ed1997: OUP USA. 320.

13. Dietz, W.A., *Response Factors for Gas Chromatographic Analyses.* Journal of Chromatographic Science, 1967. **5**(2): p. 68-71.

Chapter 3

Oxidation of benzyl alcohol using gold nanoparticles supported on CeO_2 foam mental

3.1. Introduction

Alcohol oxidation is an important reaction in the fine chemicals industry, in particular for the synthesis of aldehydes which are valuable intermediates in the perfume industry [1-3]. There is a need to develop effective catalysts that can replace the stoichiometric oxygen donors, such as chromate or permanganate, which are still utilized in some processes today [4-7]. With the recent advent of green chemistry there is a need to identify atom-efficient oxidation reactions that can be carried out using molecular oxygen, rather than an activated form of oxygen, under mild solvent-free reaction conditions. In this respect the oxidation of alcohols to aldehydes represents a demanding target.

Supported gold nanoparticles have been found to be effective for the oxidation of CO [8] and more recently they have been applied to the oxidation of alcohols [9-12]. Rossi, Prati and co-workers [13-15] clearly demonstrated that supported gold nanoparticles were effective catalysts for the oxidation of alcohols. In these early studies, the presence of base, e.g. sodium hydroxide, was found to be essential for activity and consequently the sodium salts of the acids were formed. Subsequently, Corma and co-workers [16-19] demonstrated that Au/CeO_2 catalysts are active for the selective oxidation of alcohols to aldehydes and ketones and for the oxidation of aldehydes to acids in the absence of base under solvent-free conditions. This was a key observation that spurred further interest in this reaction.

It is known that the morphology and particle size of the gold nanoparticles is very important with respect to activity and hence a sol-immobilisation method was used in

this chapter to produce catalysts with a very narrow particle size distribution, typically 2-5 nm in diameter [20-23]. However, the interaction between the nanoparticles and the support is equally important. Recently, Shen and co-workers [24] have described the production of lanthanide polymer foams and subsequently oxide foams via hydrothermal reaction between the lanthanide cation and L-asparagine. In this chapter, the results for the oxidation of benzyl alcohol using gold supported on a CeO_2 foam prepared according to the method of Shen *et al.* will be discussed in details [24].

3.2 Experimental

3.2.1 Preparation of CeO_2 foams

CeO_2 foams were synthesised according to the method of Shen *et al* [24] described in details in Chapter 2 (section 2.1.1).

3.2.2 Preparation of the gold sol and the supported gold catalyst

The CeO_2 foam supported gold catalysts were synthesised by the sol-immobilisation method using THPC as a stabiliser described in Chapter 2 (section 2.2.1.1). For comparison Au/CeO_2 catalysts were freshly prepared using 2 different commercial CeO_2 supports (Aldrich). For all catalysts prepared the same starting sol formulation was utilized.

3.2.3 Oxidation of benzyl alcohol

The benzyl alcohol oxidation reactions were carried out in a glass Colaver reaction vessel (50 ml) at a constant pressure of oxygen (1 barg unless otherwise stated). In a typical experiment, the catalyst (20 mg) was suspended in benzyl alcohol (2 g) and heated to 120 °C for 4 h (unless otherwise stated).

3.2.4 Characterisation

The CeO_2 foam materials and CeO_2 supported gold catalysts were characterised with X-ray powder diffraction (XRD), scanning electron microscopy (SEM), nitrogen adsorption (BET surface area measurements) and laser Raman spectroscopy (LRS). For selected catalysts, temperature-programmed reduction (H_2-TPR) and scanning transition electron microscopy (STEM) were used for further investigation as will be clarified in the discussion.

3.3 Results and discussion

3.3.1 Preparation of CeO_2 foams and Au/CeO_2

A set of samples were prepared using L-asparagine to form a cerium coordination polymer foam precursor as described by Shen *et al* [24]. The crystallization time at 160 °C was varied from 2-48 h and the precursors calcined to form the oxide. Powder X-ray diffraction showed that after calcination all materials comprised crystalline CeO_2 (Fig. 3.1).

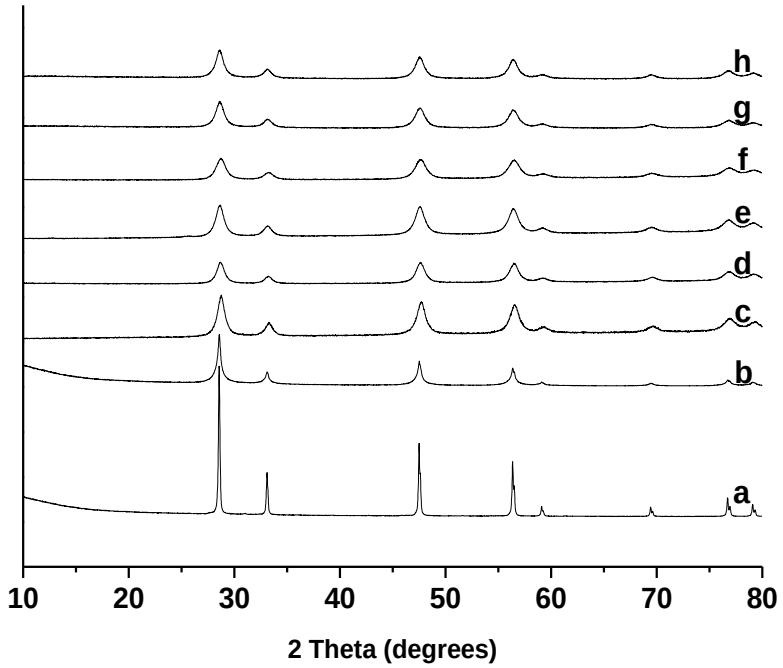

Figure 3.1 XRD patterns of the CeO_2 foams; **a** = commercial CeO_2 (Aldrich), b = commercial nano-CeO_2 (Aldrich) **c** = Au/foamCeO_2-2h, **d** = Au/foamCeO_2-4h, **e** = Au/foamCeO_2-8h, **f** = Au/foamCeO_2-12h, **g** = Au/foamCeO_2-24h and **h** = Au/foamCeO_2-48h.

However, the morphology of the oxide structures varied quite markedly with the crystallization time (Fig. 3.2). Crystallization for 2 h was insufficient to form a foam structure, and the precursor comprised hollow spheres (Fig. 3.2a). An open foam structure was formed after 4 h crystallisation which possesses microporosity along with the inherent macroporosity of the foam (Fig. 3.2b). The surface areas and average micropore diameters of the foams samples are shown in Table 3.1 and Fig. 3.3 and it is apparent that the sample obtained after 4 h crystallization has the highest surface area.

As the crystallization time was increased the foams became less open and eventually the macropore structure collapsed.

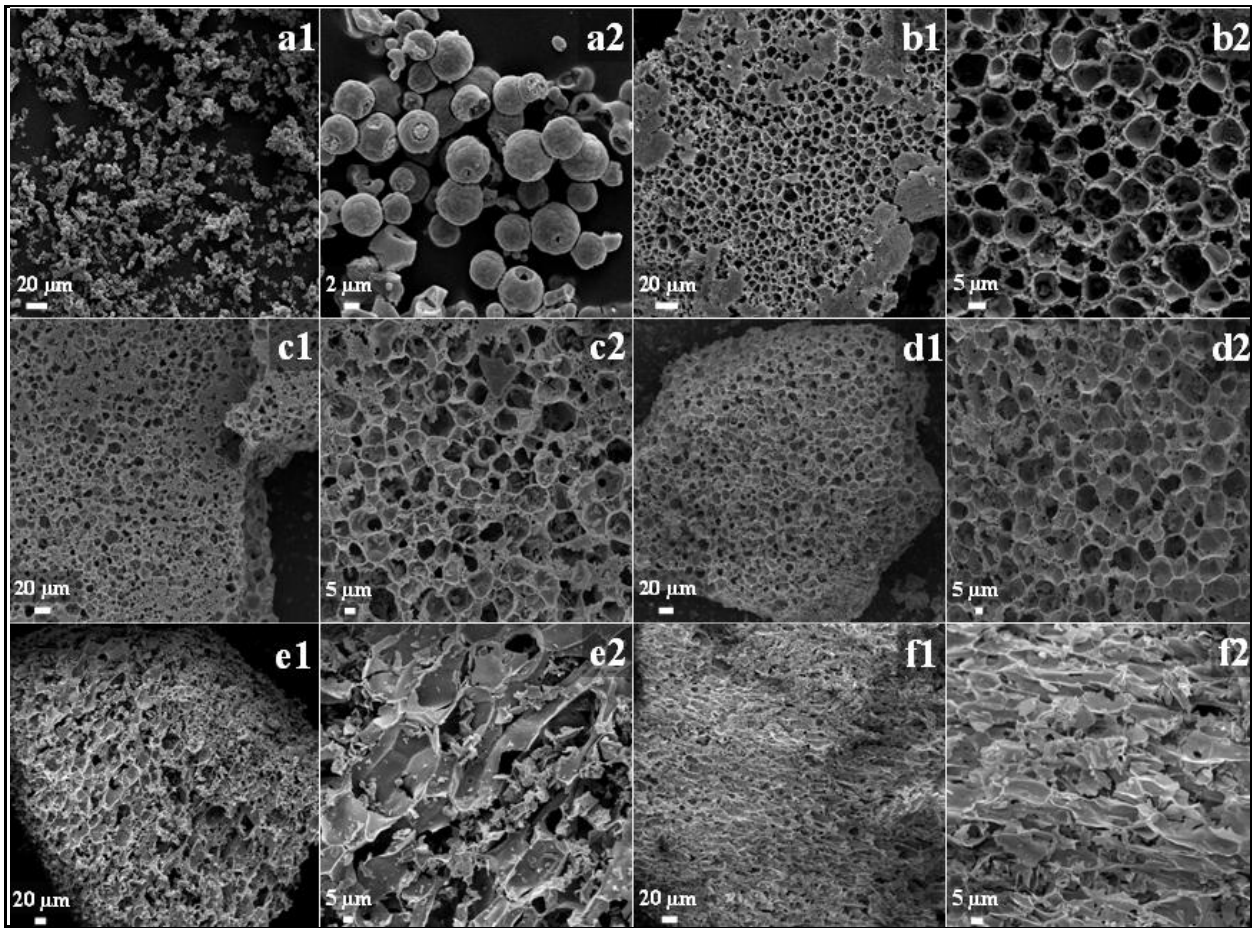

Figure 3.2 Effect of crystallisation time on the morphology of the CeO_2 foam, all samples calcined at 350 °C. **a** = Au/foamCeO_2-2h, **b** = Au/foamCeO_2-4h, **c** = Au/foamCeO_2-8h, **d** = Au/foamCeO_2-12h, **e** = Au/foamCeO_2-24h and **f** = Au/foamCeO_2-48h.

The data were contrasted with two commercial samples of CeO_2 and it is apparent that the foam samples have distinct narrow micropores which are not present in the commercial samples (Fig. 3.3).

Table 3.1 Surface area and average pore size for CeO_2 and 1% Au/CeO_2 materials

Sample	BET surface area of CeO_2 (m^2/g)	Average pore diameter (Å)	BET surface area of Au/CeO_2 (m^2g^{-1})
Au/CeO_2 (Aldrich)	5	280	5
Au/nano-CeO_2 (Aldrich)	101	310	95
Au/foamCeO_2-2h	41	86	39
Au/foamCeO_2-4h	57	88	50
Au/foamCeO_2-8h	50	64	49
Au/foamCeO_2-12h	53	62	50
Au/foamCeO_2-24h	54	55	52
Au/foamCeO_2-48h	51	68	50

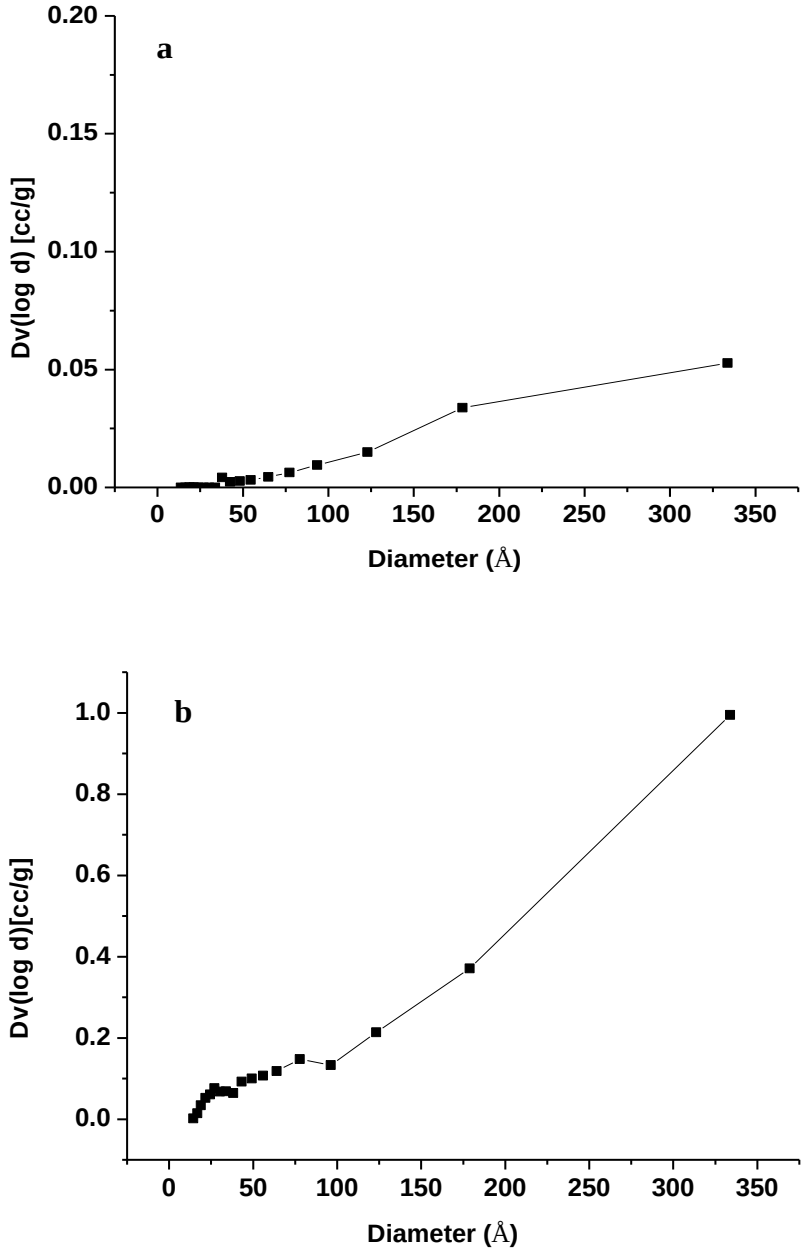

Figure 3.3 Pore diameter plots for CeO_2 foams; **a** = commercial CeO_2 (Aldrich) & **b** = commercial nano-CeO_2 (Aldrich)

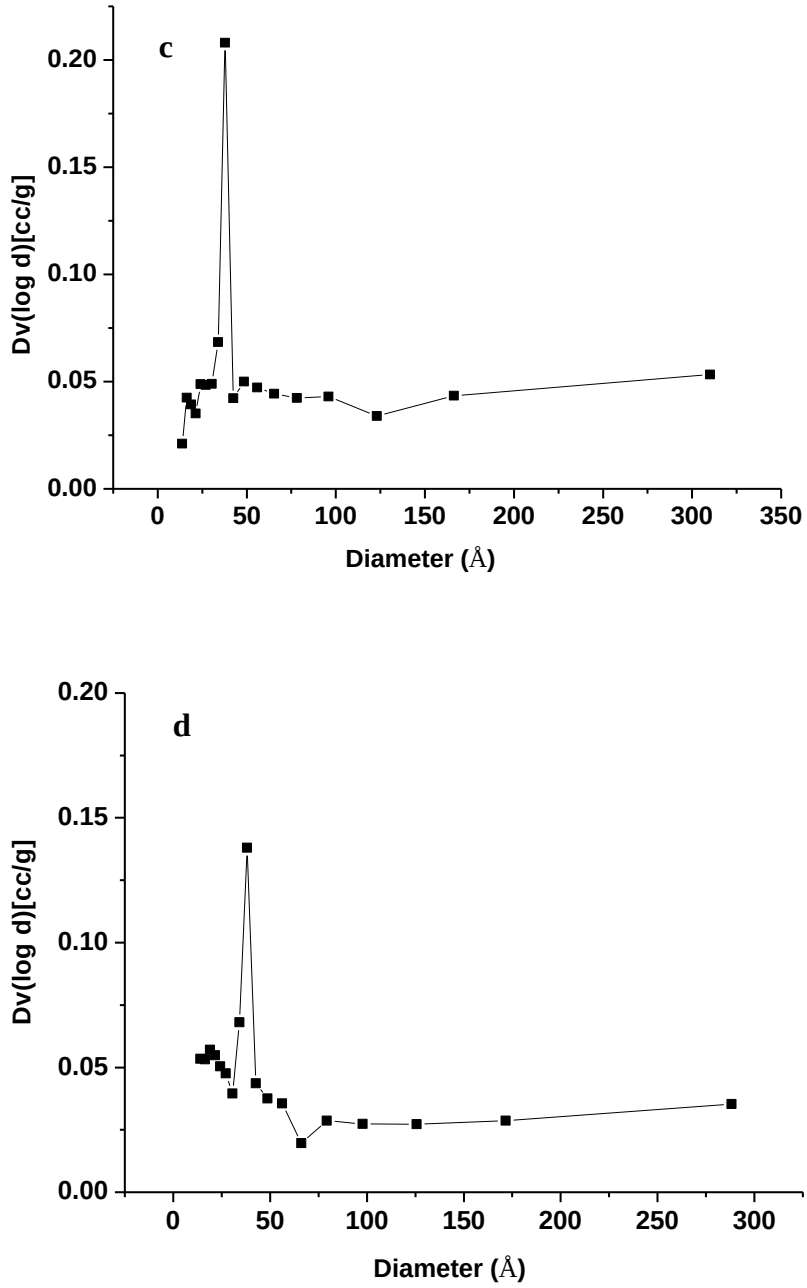

Figure 3.3 Pore diameter plots for CeO_2 foams; **c** = foamCeO_2-2h (Aldrich) & **d** = foamCeO_2-4h

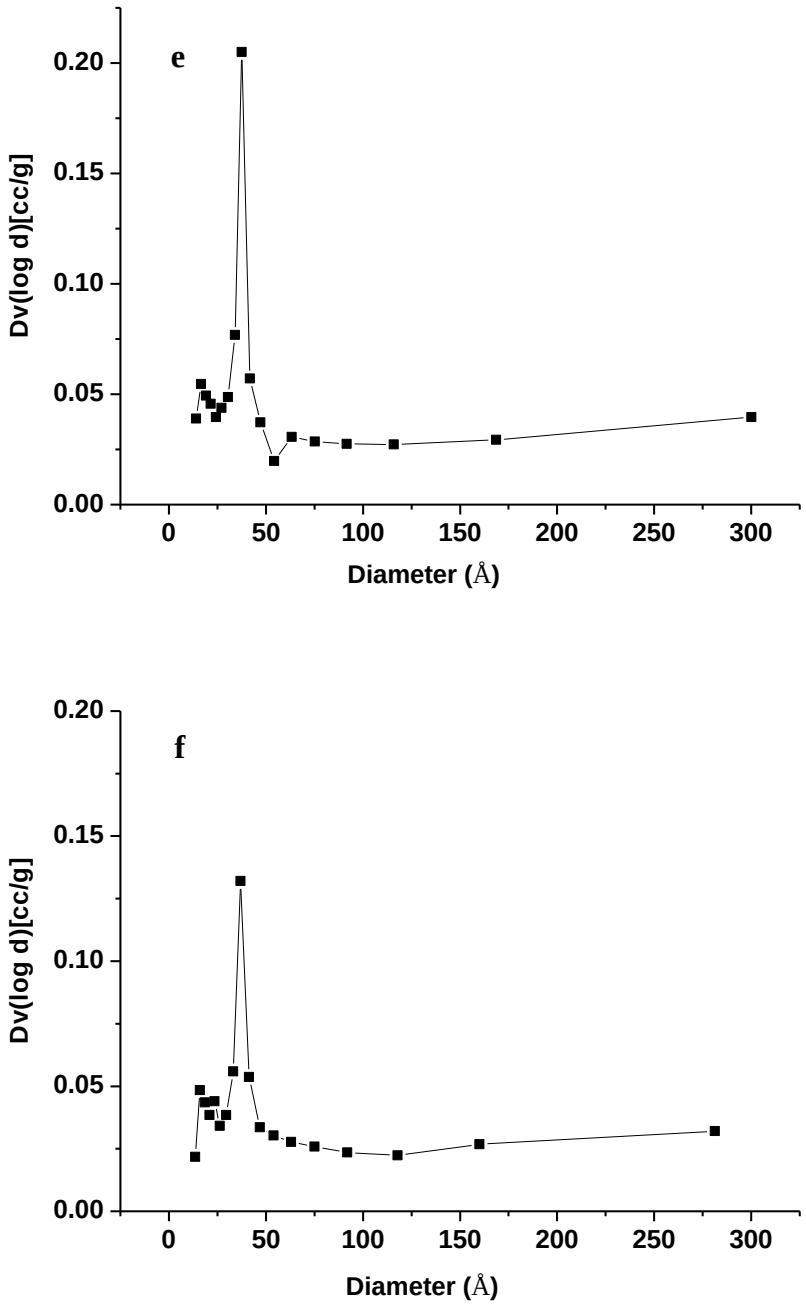

Figure 3.3 Pore diameter plots for CeO_2 foams; **e** = foamCeO_2-8h (Aldrich) & **f** = foamCeO_2-12h

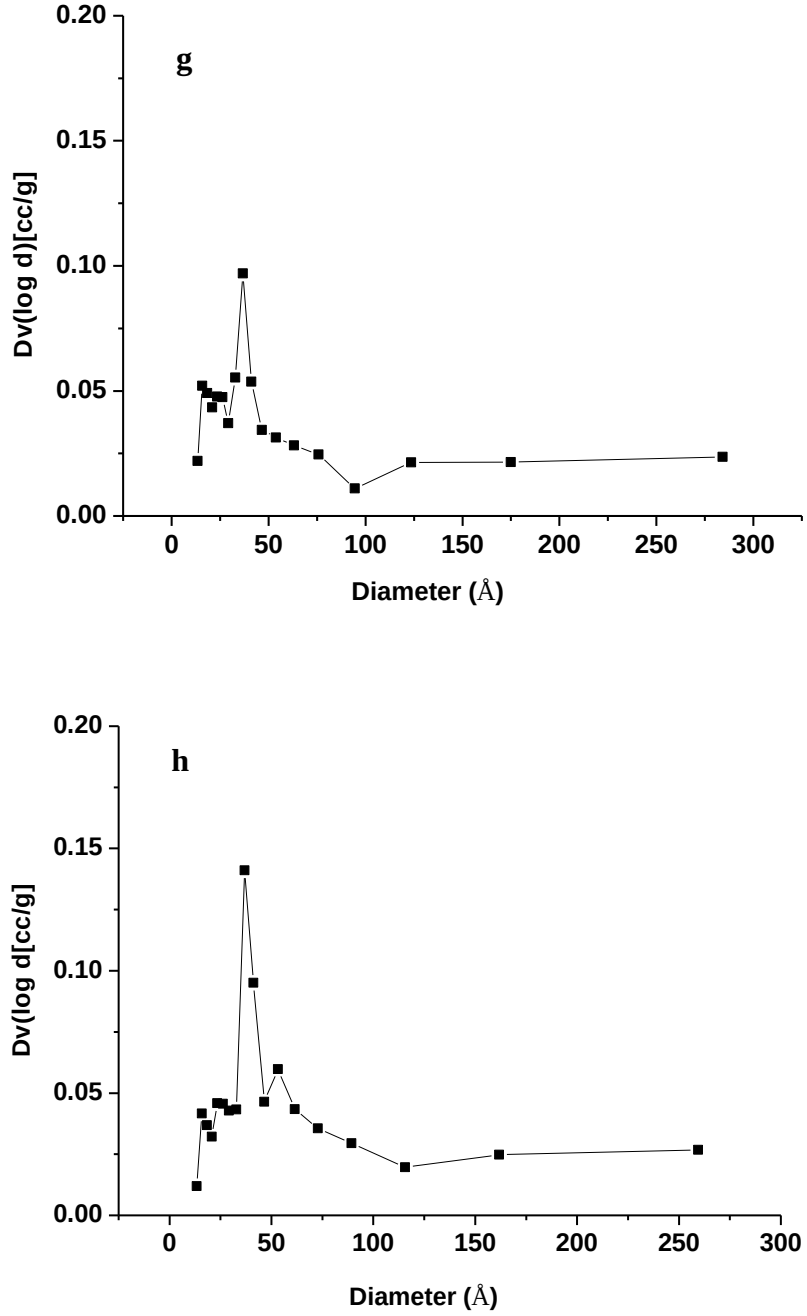

Figure 3.3 Pore diameter plots for CeO_2 foams; **g** = foamCeO_2-24h (Aldrich) & **h** = foamCeO_2-48h

1 wt% Au was added to the all the CeO_2 supports which had no discernable effect on the morphology of the foams (Fig. 3.4).

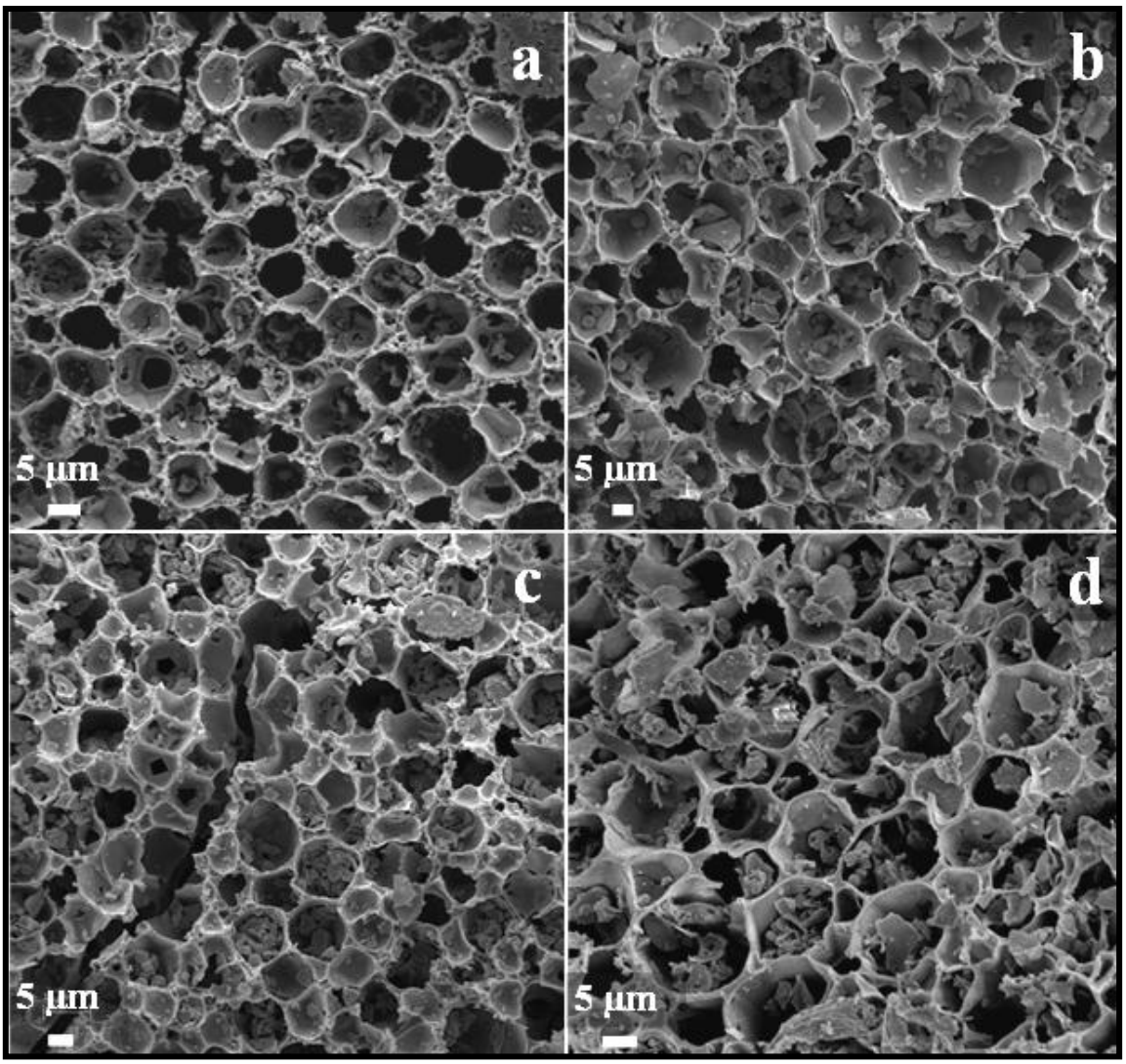

Figure 3.4 SEM images of **a** = foamCeO_2-4h, **b** = Au/foamCeO_2-4h (prior to testing), **c** = Au/foamCeO_2-4h (post-testing) and **d** = Au/foamCeO_2-4h (after 3rd re-use).

The Au was deposited from a gold sol formed by stabilization of the Au nanoparticles using THPC. Previous studies have shown that this methodology leads to Au nanoparticles with a very narrow particle size distribution [22, 23]. The Au nanoparticles were not observed by powder XRD (Fig. 3.5) which suggests that small gold nanoparticles have been formed which is consistent with the previous findings [25, 26].

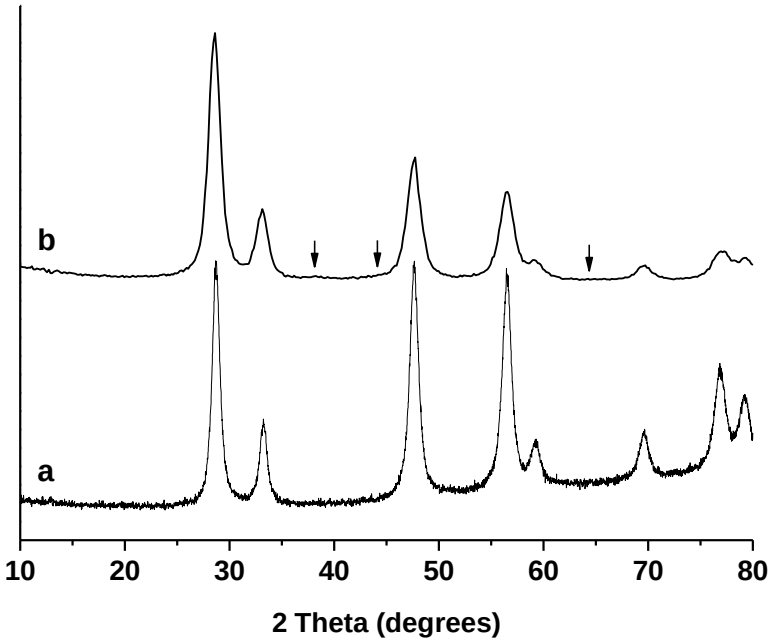

Figure 3.5 X-Ray diffraction pattern of (a) CeO_2-4h foam and (b) 1% Au/CeO_2-4h with the angles highlighted where Au diffraction peaks are expected: (2Θ = 38.1°, 44.2° and 64.6°).

3.3.2 Oxidation of benzyl alcohol using Au/CeO_2 catalysts

The oxidation of benzyl alcohol was investigated under conditions that gave low conversion, so that differences in reactivity could be readily discerned. Initially the experiments were carried out under the standard reaction conditions using stirring. However, the ceria foams were unstable under these conditions; therefore, the catalysts were tested without stirring.

Table 3.2 demonstrates the results of benzyl alcohol oxidation using all Au/CeO_2 catalysts. The CeO_2 foams in the absence of Au were found to have a low activity and representative data for the 4 h sample are shown in the same table. The Au/foamCeO_2 catalysts were more active than those prepared using the two commercial samples of CeO_2, while the Au/sphericalCeO_2 exhibited the lowest activity. The commercial samples were selected as they showed surface areas that were lower or higher than the foam samples used in this study. In addition to the surface area, the catalyst that has been reported to have the highest activity is the Au on nano-particulate ceria catalyst prepared by Corma and co workers [16-19]. This result influenced the choice of nano-CeO_2 (Aldrich) as a comparison support in this study.

The selectivity to the products (Table 3.2) was not greatly affected by the morphology of the support with benzaldehyde and minor amounts of benzoic acid and benzyl benzoate produced. Minor amounts of two disproportionation and dehydrogenation products, toluene and benzene, were also formed as the mechanism of this reaction has been previously discussed in Chapter 1 [21, 27].

Table 3.2 Oxidation of benzyl alcohol over the 1% Au/CeO_2 catalysts[a]

Catalyst	Conversion (%)	Selectivity (%)					
		Benzaldehyde	Toluene	Benzoic acid	Benzene	Benzyl benzoate	Dibenzyl ether
Au/CeO_2-Aldrich	1.6	96.3	1.5	0.6	0.9	0.5	0.3
$Au/nanoCeO_2$-Aldrich	2.4	96.5	1.5	0.2	1.2	0.5	0.2
$foamCeO_2$-4h (Blank)	0.6	98.0	0.0	0.7	0.0	1.3	0.0
$Au/foamCeO_2$-2h	1.4	94.5	2.0	0.0	3.0	0.0	0.5
$Au/foamCeO_2$-4h	3.7	95.0	1.2	0.0	3.0	0.8	0.0
$Au/foamCeO_2$-8h	3.4	94.8	1.1	0.0	3.0	1.1	0.0
$Au/foamCeO_2$-12h	3.3	94.0	1.2	0.0	4.0	0.6	0.3
$Au/foamCeO_2$-24h	2.7	95.0	1.2	0.0	2.5	1.0	0.3
$Au/foamCeO_2$-48h	2.2	96.0	1.7	0.7	0.5	1.0	0.0

[a] Benzyl alcohol (2 g), Catalyst (20 mg), O_2 1 barg, 120 °C, 4 h.

Among all Au/foam CeO_2 catalysts, the $Au/foamCeO_2$-4h is the most active, indicating that supporting the gold nanoparticles within and on the most macroporous foam structure gave the highest conversion. Fig. 3.6 illustrated that the catalyst performance was dependent on the crystallization time of the precursor foam. As the crystallisation

time of the foam increased the activity of the corresponding Au catalysts decreased. The catalyst Au/CeO_2-48h showed lower activity than even the Au/CeO_2-nano. This can be ascribed to the destruction of foam structure as the reaction time increased which affected the porosity of the synthesised ceria (See Fig. 3.2).

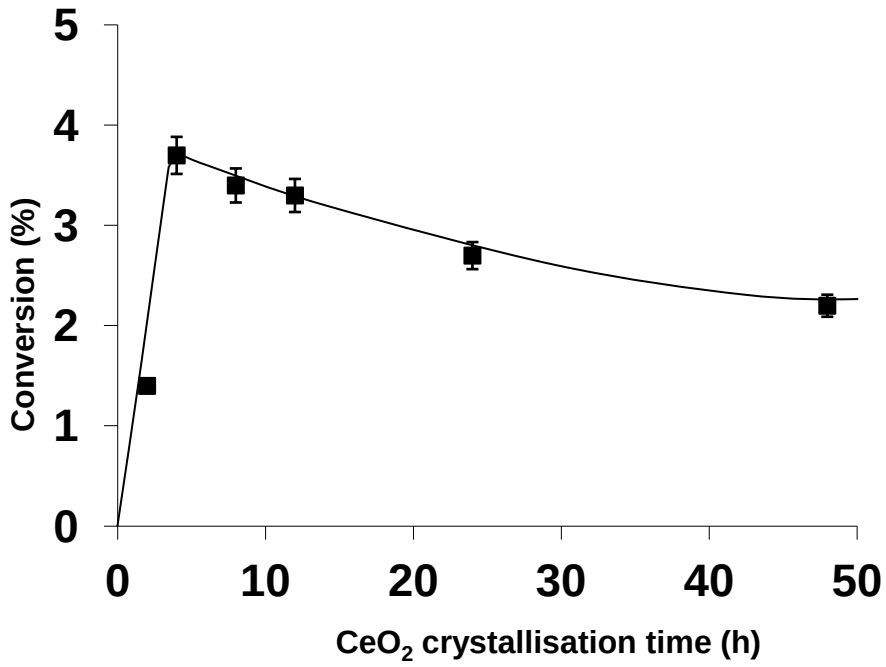

Figure 3.6 Oxidation of benzyl alcohol using Au/foamCeO_2 showing the effect of crystallization time on conversion as a function of foam crystallization time

Two representative catalyst samples (*i.e.* Au/CeO_2 (Aldrich) and Au/foamCeO_2-4h samples) were characterized by HAADF-STEM imaging to investigate the effect of different CeO_2 supports on the size distribution of the Au nanoparticles. Representative micrographs of both catalysts and their corresponding Au particle-size distributions are

shown in Fig. 3.7. It is clear that Au nanoparticles on both supports have reasonably narrow particle size distributions, but have quite different mean sizes. For the Au nanoparticles supported the commercial CeO_2 material, their diameters fall within the 1 to 4 nm range, with a mean value of 2.2 nm (Fig. 3.7a-b), which is consistent with previously reported results on such materials [22, 23]. In contrast, when supported on the CeO_2 foam, the Au particle sizes mainly fall within the 5 to 10 nm range, with a mean value of 8 nm (Fig. 3.7c-d). This is very interesting as the same Au sol was used as the precursor for the Au nanoparticles and hence it is apparent that the surface of the ceria can play a major role in determining the particle size distribution of the formed nanoparticles.

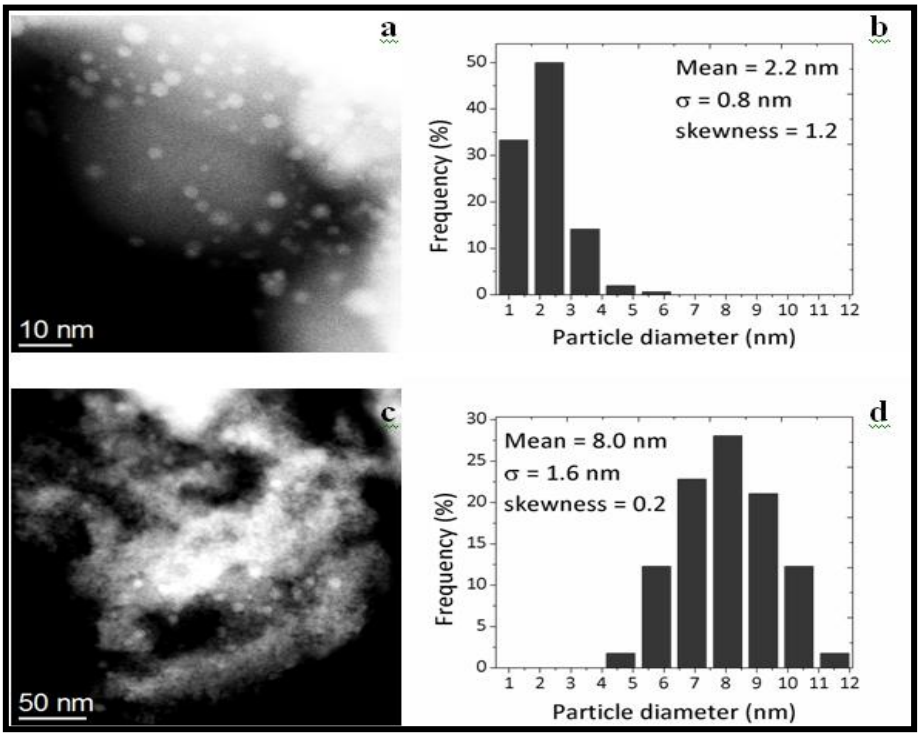

Figure 3.7 Representative HAADF-STEM micrographs and the corresponding Au particle size distributions for (**a, b**) Au/CeO_2 (Aldrich), and (**c, d**) $Au/foamCeO_2$-4h.

Surprisingly, the large Au nano-particles formed on the foam structures were found to have a higher activity than those on the particulate CeO_2 samples (Table 3.2). Haider *et al*. [28] showed that the size of the Au nano-particles had a pronounced effect on the activity of benzyl alcohol oxidation. They found that nano-particles with a size of < 2 nm and > 8 nm had a lower activity compared to those between *ca.* 2 and 7 nm. Abad *et al.* [18] also performed a systematic study on particle size versus activity for Au/CeO_2 catalysts prepared by deposition-precipitation. They found that there was a clear correlation between particle size and activity, although the catalysts studied did not have mean particle diameters <5 nm.

All the catalysts in this study were synthesized by sol deposition and using this methodology all of the colloidal gold nano-particles formed during the initial step are 1-3 nm with a small particle size distribution. The size of the gold particles does not typically change when they are deposited on the support and as expected the Au/nano-CeO_2 material was found to have a mean particle size of 2.2 nm. However, the CeO_2 foam has caused the Au nano-particles to coalesce on the surface leading to an average particle size of ~8 nm. According to these previous studies [18, 28] the CeO_2 foam supported catalysts with large Au particles should have a poor activity. However, the activity was found to be higher for this catalyst, which could be due to the large percentage of particles in the 5-7 nm range (Fig. 3.7a). The reason for the sintering of the colloidal particles when they are deposited onto the foam supports is not clear, although it could be related to the crystallinity of the support. Hutchings and co-workers have previously shown that a nano-crystalline CeO_2, prepared using supercritical

antisolvent precipitation, formed a highly dispersed Au catalyst [29]. This was attributed to the nano-crystalline nature of the support which prevented sintering of Au particles across the grain boundaries.

In addition to the Au particle size, the surface area of Au/foamCeO_2 catalysts (~ 50 m^2g^{-1}) was significantly less than this of the CeO_2 Nano one (95 m^2g^{-1}). Although the Au/foamCeO_2 catalysts had larger Au particle size (Fig 3.7) and lower surface area (Table 3.1), the Au/foamCeO_2 catalysts exhibited higher activity towards the oxidation of benzyl alcohol. Fig. 3.8 summarises the Au particle size, surface area and the activity of the commercial and foam Au/CeO_2 catalysts.

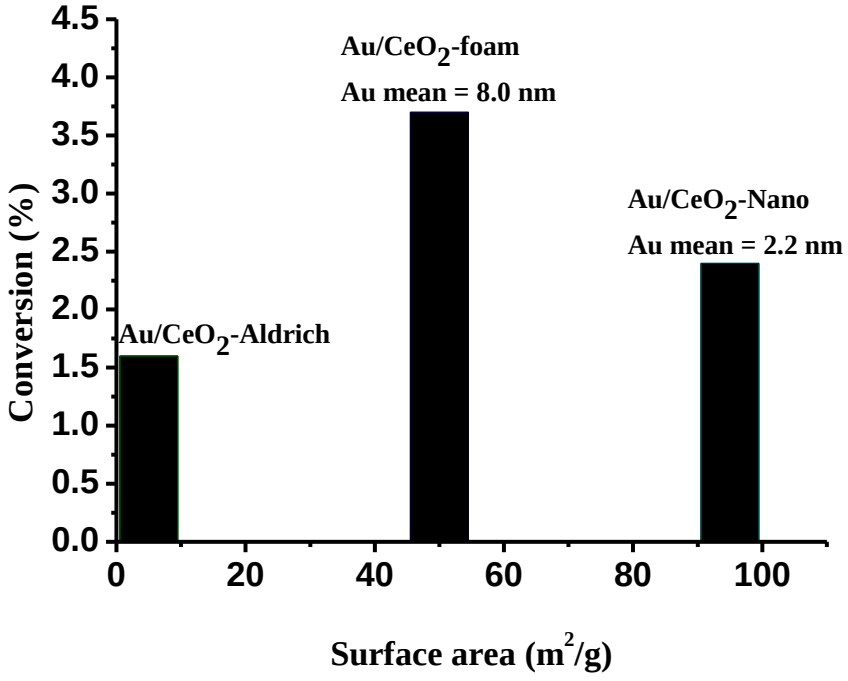

Figure 3.8 The surface area and Au particle size of the Au/CeO_2 catalysts versus the conversion of benzyl alcohol.

The Au particle size distribution and the surface area of the catalysts led to conclude that the enhancement in activity found for the Au/foamCeO_2 materials must be related to a support effect, and is despite the large Au particle size, rather than because of it. To investigate the reactivity of the ceria TPR analysis was performed on the foamCeO_2-4h and the commercial standard (Aldrich) along with the corresponding Au/CeO_2 materials (Fig. 3.9).

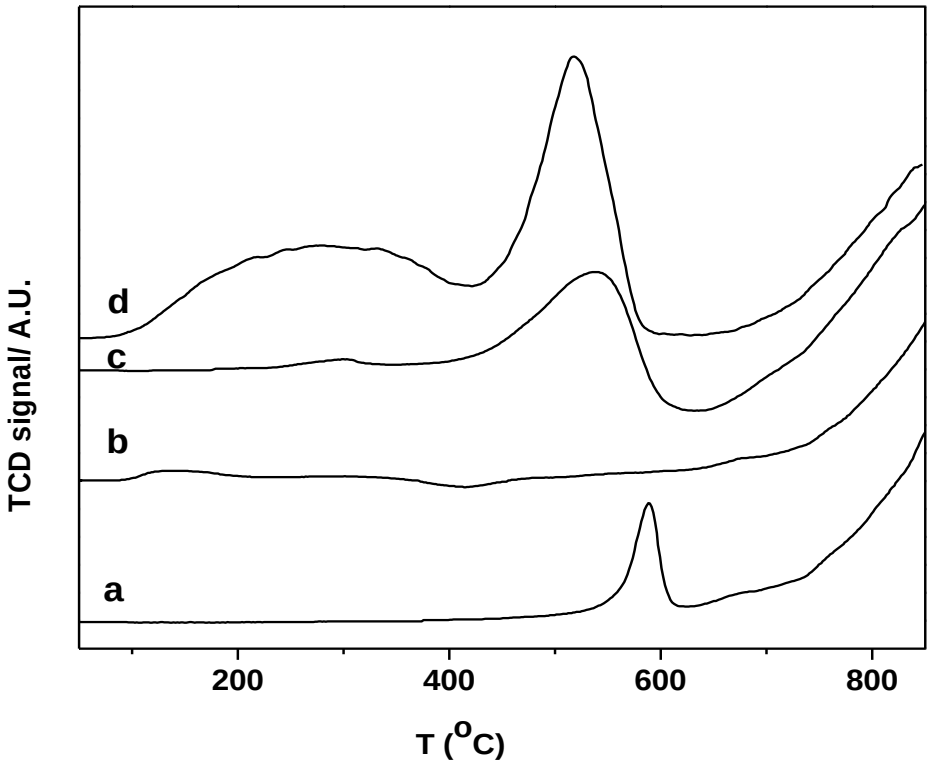

Figure 3.9 TPR measurements of the (**a**) CeO_2 (Aldrich), (**b**) Au/CeO_2 (Aldrich), (**c**) foamCeO_2-4h and (**d**) Au/foamCeO_2-4h.

The commercial CeO_2 showed two reduction peaks at 590 °C and 700 °C, which is comparable to previous studies [30, 31]. The reduction altered little with the addition of the metal and it was found to decrease with the addition of gold which can be seen in the trace for 1%Au/CeO_2 (Aldrich) (Fig. 3.8b). Interestingly, the CeO_2 foam samples exhibited a greater degree of surface reduction, indicated by the presence of two reduction features (at *ca.* 300 and 500 °C), and the addition of Au increased the surface reducibility further, while still retaining the original reduction peak. The presence of the two reduction features indicates there is a greater amount of potentially more labile surface oxygen species for the foam samples than the commercial sample. This increased H_2 uptake indicates that the Au/foamCeO_2 catalysts should exhibit greater activity for oxygenation reactions.

As mentioned above the support can play an important role in dispersing the active metal, but it can also play a crucial role in the oxidation activity. CeO_2 is commonly found to be the best support for Au oxidation catalysts. Corma and co-workers attributed this to the defects on the CeO_2 surface acting as an oxygen pump to supply O to the metal [16-19], and can be used as a stoichiometric oxidant in the absence of O_2. The TPR results on the CeO_2 foam catalysts show that the surface is more easily reduced than the catalysts prepared using commercial CeO_2, and have more surface oxygen available for reaction. These features make it an ideal support based on the mechanism proposed by Corma for Au/CeO_2 catalysts [16-19].

There have been a number of studies carried out using Au/CeO_2 catalysts for the oxidation of benzyl alcohol [16-19, 28, 32]. Table 3.3 contains some comparisons between the TOF achieved in this study with those reported in the literature.

Table 3.3 A comparison between the TOF values in this study with those in the literature.

Catalyst	Catalyst mass & Au loading	Reaction Temperature (°C)	Reaction time (h)	O_2 pressure (bar)	Stirring	TOF (h^{-1})	Reference
Au/CeO_2-Aldrich	0.02g cat. (Au=1%)	120	4	1	No	72.8	This work
$Au/nanoCeO_2$-Aldrich	0.02g cat. (Au=1%)	120	4	1	No	109.3	
$Au/foamCeO_2$-2h	0.02g cat. (Au=1%)	120	4	1	No	63.7	
$Au/foamCeO_2$-4h	0.02g cat. (Au=1%)	120	4	1	No	168.5	
$Au/foamCeO_2$-8h	0.02g cat. (Au=1%)	120	4	1	No	154.8	
$Au/foamCeO_2$-12h	0.02g cat. (Au=1%)	120	4	1	No	150.3	
$Au/foamCeO_2$-24h	0.02g cat. (Au=1%)	120	4	1	No	122.9	
$Au/foamCeO_2$-48h	0.02g cat. (Au=1%)	120	4	1	No	100.2	
Au/CeO_2	0.20g cat. (Au=2.5%)	130	5	5	Yes	250	Su *et al.* [32]
Au/CeO_2	0.10g cat.	100	3	atm	Yes	99	Haider *et al.* [28]
$Au/supercriticalCeO_2$	0.025g cat. (Au=2.5%)	140	4	10	Yes	552	Miedziak *et al.* [29]

Direct comparisons with the previous studies are difficult as the reaction conditions used vary considerably. Although the catalysts were tested without stirring in this study, the TOF obtained in this study for the Au/foamCeO_2 catalysts were of a higher or similar magnitude to those calculated from other studies. The Au/foamCeO_2 catalysts especially Au/foamCeO_2 one exhibited higher TOF than that reported by Haider *et al.* [28]. The TOF values of this study were less than those produced by Miedziak *et al.*[29] and Haider *et al.* [32]. However, the reaction conditions used in these studies were much harsher than those used in this study. In these studies the reaction was carried out at ≥130 °C, ≥ 5 bar O_2 and with stirring whereas the reaction in this study was carried out without stirring at 120 °C and 1 bar O_2.

3.3.2.1 The effect of catalyst mass

The effect of increasing the mass of catalyst on activity was carried out to check for mass transport limitations and the results are shown in Fig. 3.10 for Au/foamCeO_2-4h and this catalyst was selected as it exhibited the best activity. The catalyst mass was varied, 5, 10, 20 and 40 mg and the amount of catalyst had no significant effect on reaction selectivity and benzaldehyde was formed as the major product (94-95 %) with minor amounts of toluene, benzene and benzyl benzoate also observed as the only by-products as it has been observed previously for this reaction [21, 22]. However, the conversion was found to increase as the amount of catalyst increased which indicates that there was no mass transport limitation problem under these conditions.

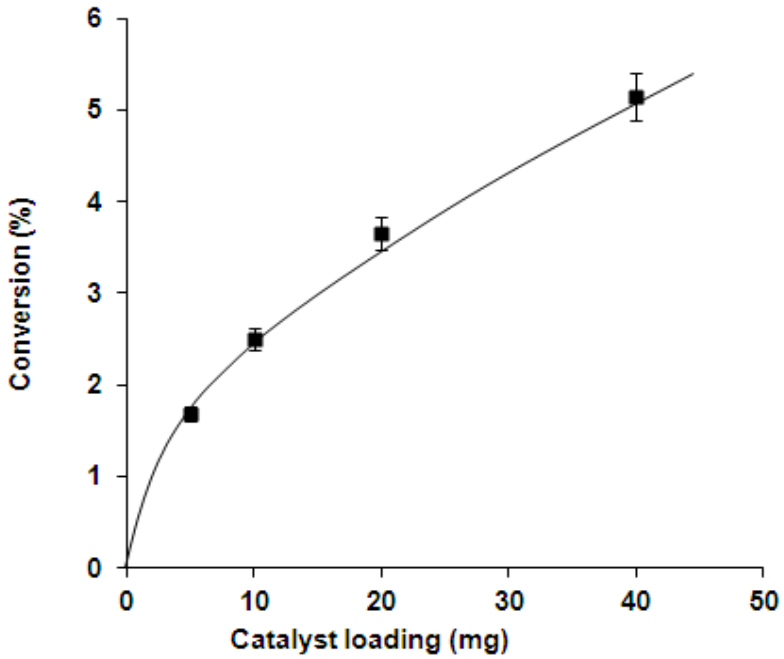

Figure 3.10 Effect of catalyst mass on conversion. (Benzyl alcohol (2 g), Catalyst: Au/foamCeO_2-4h, O_2 1 barg, 120 °C, 4 h.

3.3.2.2 Time on-line analysis of Au/foamCeO_2-4h

The effect of the reaction time on conversion and selectivity is shown in Fig. 3.11a-b. For Au/foamCeO_2-4h, as the conversion steadily increases the selectivity to toluene also increases very slightly after 4 h of reaction. However, this increase in conversion with the time was not linear indicating that the catalysts deactivated slightly as the reaction time increased. Generally, the deactivation of the catalyst can occur due to many reasons such as the sintering of Au particles, the depletion of the oxygen provided by the support or the blockage of the active sites by byproducts.

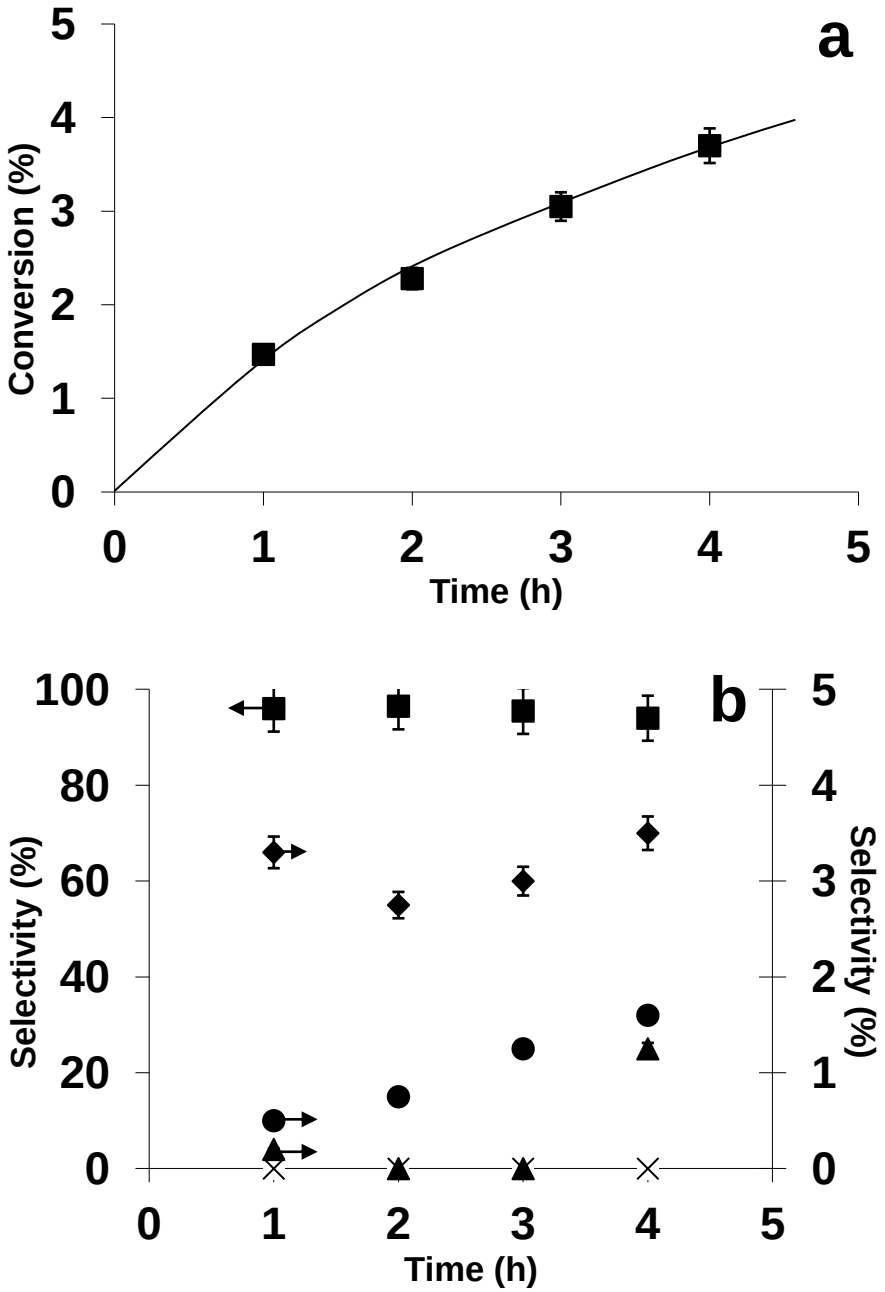

Figure 3.11 Oxidation of benzyl alcohol using Au/foamCeO_2 showing the effect of (a) conversion as a function of time-on-line for Au/foamCeO_2-4h and (b) selectivity as function of time-on-line for Au/foamCeO_2-4h; ■ = benzaldehyde, ♦ = benzene, ● = toluene, ▲ = benzyl benzoate and x = benzoic acid.

3.3.2.3 The effect of oxygen pressure

The effect of oxygen pressure on the oxidation of benzyl alcohol was determined for the most active foam catalyst (Au/foamCeO_2-4h). The reaction was carried out under the same conditions used for the catalysts evaluation except the oxygen pressure. The results shown in Table 3.4 show that as the oxygen pressure decreases (from 1 barg to 0.2 barg) the conversion slightly decreases and the selectivity to benzaldehyde increases so that it becomes the only observed product. It is therefore apparent that oxygen is involved with the formation of the observed by-products as described in detail in Chapter 1 [21, 27].

Table 3.4 Effect of oxygen pressure on the oxidation of benzyl alcohol using Au/foamCeO_2-4h as catalyst[a].

O_2 Pressure (barg)	Conversion (%)	Selectivity (%)					
		Benzaldehyde	Toluene	Benzoic acid	Benzene	Benzyl benzoate	Dibenzyl ether
1	3.7	94	1.6	0	3.5	1.3	0.2
0.6	3.5	98	0.8	0	0.3	0.2	0.2
0.2	3.3	100	0	0	0	0	0

[a] Benzyl alcohol (2 g), Catalyst (20 mg), 120 °C, 4 h.

3.3.2.4 The reaction in the absence of oxygen

To further study the effect of oxygen on the reaction a test was performed in the absence of oxygen. The same reaction conditions were used except the oxygen was replaced with 1 bar helium.

The conversion of benzyl alcohol (Table 3.5) decreased remarkably compared to the same reaction carried out with O_2. Furthermore, the selectivity towards toluene enhanced considerably and it was 24 %. This confirms that the oxygen is involved in the oxidation reaction to form benzaldehyde as a major product. It is well known that the absence of oxygen or a very low pressure of it increase the possibility of the disproportionation reaction to take place and hence the formation of toluene as mentioned earlier in chapter 1 [27].

Table 3.5 Effect of oxygen pressure on the oxidation of benzyl alcohol using Au/foamCeO_2-4h as catalyst[a]

Gas	Conversion (%)	Selectivity (%)					
		Benzaldehyde	Toluene	Benzoic acid	Benzene	Benzyl benzoate	Dibenzyl ether
Oxygen	3.7	94.0	1.6	0.0	3.5	1.3	0.2
Helium	1.1	73.0	24.0	2.0	0.6	0.2	0.2

[a] Benzyl alcohol (2 g), Catalyst (20 mg), 120 °C, 4 h.

3.3.2.5 Reusability of Au/foamCeO_2-4h

One of the advantages of heterogeneous catalysts is the ease of their recovery and reusability. The successful recovery and re-use thereafter is crucial feature of green chemistry.

Re-use of catalysts was investigated for Au/foamCeO_2-4h (Table 3.6) as it was shown to be the best catalyst. Following the reaction of benzyl alcohol under the addressed conditions, the catalyst was left to stand in air until it settled in the bottom of a vial followed by pouring the liquid and the catalyst was washed with acetone. This procedure was repeated three times before the catalyst was dried at 110 °C for 1 h. In the re-use experiments larger amounts of the catalyst were used in the initial experiments so that the correct catalyst mass (20 mg) could be used in subsequent reactions. It is clear that the catalysts are fully reusable although Fig. 3.11 in page 103 displayed a slight deactivation as the reaction time increased until 4 h. This is thought that washing the used catalyst with acetone removes all products that might block the active sites in the catalyst especially when the reaction is curried out without stirring and hence improve its reusability. Examination of the morphology of the foams after use as a catalyst also confirms that the structures are stable under these conditions (Fig. 3.4 in page 96).

Table 3.6 Reusability of Au/foamCeO_2-4h[a]

Catalyst	Conversion (%)	Selectivity (%)					
		Benzaldehyde	Toluene	Benzoic acid	Benzene	Benzyl benzoate	Dibenzyl ether
Fresh Catalyst	3.7	94.0	1.6	0	3.5	1.2	0
1st reuse	4.0	96.0	0.9	0	1.7	1.4	0
2nd reuse	3.8	95.0	1.0	0	2.0	2.0	0
3rd reuse	3.6	96.5	0.8	0	1.8	0.9	0

[a] Benzyl alcohol (2 g), Catalyst (20 mg), O_2 1 barg, 120 °C, 4 h.

3.4 Conclusions

Different morphologies namely foam and spheres, of ceria were prepared hydrothermally at different reaction times. When Au nanoparticles were supported on the CeO_2 foams using a sol-immobilization method the activity of them for solvent-free benzyl alcohol oxidation was superior to Au/commercialCeO_2 catalysts although they had larger Au particles and less surface area. The high activity of Au/foamCeO_2 catalysts is attributed to the greater liability of surface oxygen in the support compared with commercial CeO_2 materials as confirmed by TPR analysis. The activity was found to be dependent on the crystallization time of the precursor foam. A crystallization time

of 4 h was found to produce the most active catalyst, which retained activity and a high selectivity to benzaldehyde (ca. 96 %) when re-used and this is related to the structure of the material. The TOF value of the Au/foamCeO_2 catalyst was higher or similar to those reported in the literature [28, 29, 32] although the catalysts were tested without stirring in this study.

3.5 References

1. Sheldon, R.A. and J.K. Kochi, *Metal-catalyzed oxidations of organic compounds*. 1981, New York: Academic Press. 424.

2. Pillai, U.R. and E. Sahle-Demessie, *Oxidation of alcohols over Fe^{3+}/montmorillonite-K10 using hydrogen peroxide.* Applied Catalysis A: General, 2003. **245**(1): p. 103-109.

3. Hudlický, M., *Oxidations in organic chemistry*. 1990, Washington DC: ACS. 433.

4. Griffith, W.P. and J.M. Joliffe, *Dioxygen Activation and Homogenuous Catalytic Oxidation*. 1991, Amsterdam: Elsevier.

5. Cainelli, G. and G. Cardillo, *Chromium oxidations in organic chemistry*. 1984, Berlin: Springer.

6. Lee, D.G. and U.A. Spitzer, *Aqueous dichromate oxidation of primary alcohols.* The Journal of Organic Chemistry, 1970. **35**(10): p. 3589-3590.

7. Menger, F.M. and C. Lee, *Synthetically useful oxidations at solid sodium permanganate surfaces.* Tetrahedron Letters, 1981. **22**(18): p. 1655-1656.

8. Haruta, M., et al., *Novel Gold Catalysts for the Oxidation of Carbon Monoxide at a Temperature far Below 0.deg.C.* Chemistry Letters, 1987. **16**(2): p. 405-408.

9. Meenakshisundaram, S., et al., *Oxidation of alcohols using supported gold and gold-palladium nanoparticles.* Faraday Discussions, 2010. **145**: p. 341-356.

10. Miedziak, P., et al., *Oxidation of benzyl alcohol using supported gold–palladium nanoparticles.* Catalysis Today, 2011. **164**(1): p. 315-319.

11. Boronat, M., et al., *Mechanism of selective alcohol oxidation to aldehydes on gold catalysts: Influence of surface roughness on reactivity.* Journal of Catalysis, 2011. **278**(1): p. 50-58.

12. Gutiérrez, O.Y., et al., *Deep HDS over NiMo/Zr-SBA-15 catalysts with varying MoO_3 loading.* Catalysis Today, 2008. **130**(2–4): p. 292-301.

13. Prati, L. and M. Rossi, *Gold on Carbon as a New Catalyst for Selective Liquid Phase Oxidation of Diols.* Journal of Catalysis, 1998. **176**(2): p. 552-560.

14. Porta, F., et al., *Metal sols as a useful tool for heterogeneous gold catalyst preparation: reinvestigation of a liquid phase oxidation.* Catalysis Today, 2000. **61**(1–4): p. 165-172.

15. Prati, L. and G. Martra, *New gold catalysts for liquid phase oxidation.* Gold Bulletin, 1999. **32**(3): p. 96-101.

16. Corma, A. and M.E. Domine, *Gold supported on a mesoporous CeO_2 matrix as an efficient catalyst in the selective aerobic oxidation of aldehydes in the liquid phase.* Chemical Communications, 2005(32): p. 4042-4044.

17. Abad, A., et al., *A Collaborative Effect between Gold and a Support Induces the Selective Oxidation of Alcohols.* Angewandte Chemie International Edition, 2005. **44**(26): p. 4066-4069.

18. Abad, A., A. Corma, and H. García, *Catalyst Parameters Determining Activity and Selectivity of Supported Gold Nanoparticles for the Aerobic Oxidation of Alcohols: The Molecular Reaction Mechanism.* Chemistry – A European Journal, 2008. **14**(1): p. 212-222.

19. Abad, A., et al., *Efficient chemoselective alcohol oxidation using oxygen as oxidant. Superior performance of gold over palladium catalysts.* Tetrahedron, 2006. **62**(28): p. 6666-6672.

20. Dimitratos, N., et al., *Solvent free liquid phase oxidation of benzyl alcohol using Au supported catalysts prepared using a sol immobilization technique.* Catalysis Today, 2007. **122**(3–4): p. 317-324.

21. Lopez-Sanchez, J.A., et al., *Au-Pd supported nanocrystals prepared by a sol immobilisation technique as catalysts for selective chemical synthesis.* Physical Chemistry Chemical Physics, 2008. **10**(14): p. 1921-1930.

22. Villa, A., C.E. Chan-Thaw, and L. Prati, *Au NPs on anionic-exchange resin as catalyst for polyols oxidation in batch and fixed bed reactor.* Applied Catalysis B: Environmental, 2010. **96**(3–4): p. 541-547.

23. Villa, A., et al., *Gold Sols as Catalysts for Glycerol Oxidation: The Role of Stabilizer.* ChemCatChem, 2009. **1**(4): p. 510-514.

24. Shen, Z., et al., *Macroporous Lanthanide-Organic Coordination Polymer Foams and Their Corresponding Lanthanide Oxides.* Advanced Materials, 2008. **20**(5): p. 984-988.

25. Grunwaldt, J.-D., et al., *Preparation of Supported Gold Catalysts for Low-Temperature CO Oxidation via "Size-Controlled" Gold Colloids.* Journal of Catalysis, 1999. **181**(2): p. 223-232.

26. Luciani, S., et al., *The mechanism of surface doping in vanadyl pyrophosphate, catalyst for n-butane oxidation to maleic anhydride: The role of Au promoter.* Catalysis Today, 2011. **169**(1): p. 200-206.

27. Li, G., et al., *Solvent-free oxidation of benzyl alcohol with oxygen using zeolite-supported Au and Au–Pd catalysts.* Catalysis Letters, 2006. **110**(1): p. 7-13.

28. Haider, P., et al., *Gold-Catalyzed Aerobic Oxidation of Benzyl Alcohol: Effect of Gold Particle Size on Activity and Selectivity in Different Solvents.* Catalysis Letters, 2008. **125**(3): p. 169-176.

29. Miedziak, P.J., et al., *Ceria prepared using supercritical antisolvent precipitation: a green support for gold-palladium nanoparticles for the selective catalytic oxidation of alcohols.* Journal of Materials Chemistry, 2009. **19**(45): p. 8619-8627.

30. Andreeva, D., et al., *Gold catalysts supported on ceria and ceria–alumina for water-gas shift reaction.* Applied Catalysis A: General, 2006. **302**(1): p. 127-132.

31. Carabineiro, S.A.C., et al., *Exotemplated ceria catalysts with gold for CO oxidation.* Applied Catalysis A: General, 2010. **381**(1–2): p. 150-160.

32. Su, F.-Z., et al., *Aerobic oxidation of alcohols catalyzed by gold nanoparticles supported on gallia polymorphs.* Catalysis Communications, 2008. **9**(6): p. 1027-1032.

Chapter 4

Oxidation of benzyl alcohol and CO using gold nanoparticles supported on MnO_2 nanowire micro spheres

4.1. Introduction

It has been reported in Chapter 1 and Chapter 3 that the oxidation of alcohols to their corresponding aldehydes is an important process in chemical synthesis as well as in the perfumery industry [1-3]. It was also reported in these chapters that supported gold nanoparticles can perform well for many chemical reactions such as CO oxidation [4], the direct synthesis of hydrogen peroxide from oxygen and hydrogen [5-8], the water gas shift reaction (WGSR) [9], epoxidation of olefins [10, 11], selective oxidation of alcohols [12-15] and total oxidation of hydrocarbons [16]. The performance of gold catalysts essentially relies on the size of the gold particles. Nevertheless, there are some factors that could inherently affect the catalyst activity such as gold oxidation state, the preparation method and the choice of support. With supported gold catalysts, the structure and the morphology of the support can play a major role in the catalyst performance [17]. The support structure and morphology can influence the catalyst activity as they can affect some properties such as the gold particle size [18-21], the metal-support interaction [19-24], the exposure of more reactive planes that are rich in oxygen [25-27] and the dispersion and reducibility of gold catalysts [28-30]. In Chapter 3 it has been established that gold is more active for solvent free oxidation of benzyl alcohol when supported on ceria foam due to the facile reduction of its surface compared to the conventional ceria [31].

In this work, MnO_2 supports were hydrothermally synthesised according to the method of Yang *et al.* [32] who oxidized the hydrated manganese sulfate $MnSO_4.H_2O$ with ammonium persulfate $(NH_4)_2S_2O_8$ at 120 °C. However, the previous work was extended and the effect of reaction time on the morphology was investigated. Subramanian *et al.*

[33] hydrothermally reacted aqueous solutions of $MnSO_4.H_2O$ with $KMnO_4$ at 140 °C for different times (1-18 h) and found that the morphology changed from plate like to nanorods as the reaction time increased. This was the inspiration to apply this logic to the method of Yang *et al*. The synthesised MnO_2 materials were then evaluated as a support for Au and the catalyst activity investigated for the solvent-free oxidation of benzyl alcohol and gas phase CO oxidation.

4.2 Experimental

4.2.1 Preparation of MnO_2 nanowire microspheres

MnO_2 supports were synthesised according to the method of Yang *et al.* [32] described in details in Chapter 2 (Section 2.1.2).

4.2.2 Preparation of gold catalysts

4.2.2.1 Sol-immobilisation method (SI)

The MnO_2 supported gold catalysts were synthesised by the sol-immobilisation method using PVA as a stabiliser described in Chapter 2 (Section 2.2.1.2). The same starting sol formulation was utilized for all catalysts prepared.

4.2.2.2 Reflux Sol-immobilisation method (RSI)

All sol-immobilised catalysts prepared above were refluxed according to the method of Hutchings *et al.* [34] described in Chapter 2 (Section 2.2.1.3).

4.2.2.3 Impregnation method (IM)

The MnO_2 gold supported catalysts were synthesised by the impregnation method described in Chapter 2 (Section 2.2.2).

4.2.2.4 Deposition precipitation method (DP)

The MnO_2 gold supported catalysts were synthesised by the deposition precipitation method described in Chapter 2 (Section 2.2.3).

4.2.3 Oxidation of benzyl alcohol

The reactions were carried out in a glass Colaver reaction vessel (50 mL) as described in Chapter 2 (Section 2.5.1). Typically, the vessel was charged with benzyl alcohol (2 g) and catalyst (20 mg) and purged 5 times with oxygen, leaving the vessel at constant pressure (1 barg unless otherwise stated). The mixture was stirred at 120 °C for 4 h (unless otherwise stated).

4.2.4 Oxidation of CO

CO oxidation reaction was carried out using a fixed-bed laboratory microreactor as described in Chapter 2 (Section 2.5.2).

4.2.5 Characterisation

The MnO_2 materials and MnO_2 supported gold catalysts were characterised using X-ray powder diffraction (XRD), scanning electron microscopy (SEM), nitrogen adsorption

(BET surface area measurements) and laser Raman spectroscopy (LRS). For selected catalysts, temperature-programmed reduction (H_2-TPR) was used for further investigation.

4.3 Results and discussion

4.3.1 Preparation of MnO_2 and Au/MnO_2

A set of MnO_2 samples were synthesised according to the method of Yang *et al.* [32] with a crystallization time of 6-240 h at 120 °C. X-ray diffraction showed that although all materials comprised crystalline MnO_2, two different phases were present (Fig. 4.1). For MnO_2 samples prepared for 6-24 h, α-MnO_2 phase was mainly formed with an impurity of γ phase [32, 35, 36], However, when the crystallization time was increased, above 24 h, β-MnO_2 phase [35, 36] was formed and it remained stable for the longer crystallization times (72-240 h). The α-MnO_2 phase can be identified by the major XRD peaks at 12.78°, 17.92°, 28.68°, 37.46°, 42.30°, 49.80°, 56.30°, 59.90°, 65.30° and 69.15°. The β-MnO_2 phase can be identified by the major peaks at 28.88°, 37.32°, 42.62°, 56.65°, 59.10°, 64.96°, 67.15° and 72.30°. Although there is an overlap of the XRD reflections for the two phases, the α-MnO_2 phase can be detected by the reflections at $2\Theta < 20°$ as well as the reflection at 69.15° which do not present in β-MnO_2 phase, while the presence of the β-MnO_2 phase is clear at $2\Theta = 28.88°$.

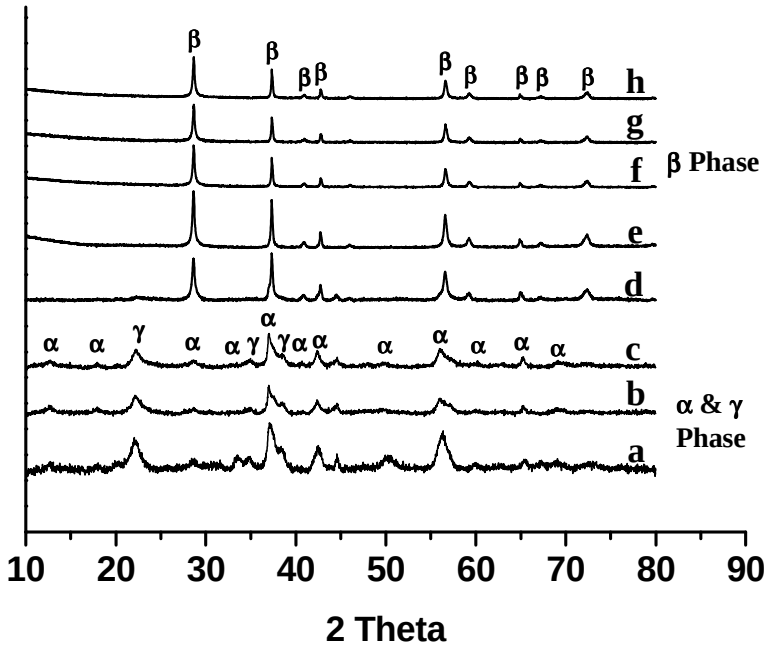

Figure 4.1 XRD patterns of the MnO_2 samples. **a** = MnO_2-6h, **b** = MnO_2-12h, **c** = MnO_2-24h, **d** = MnO_2-48h, **e** = MnO_2-72h, **f** = MnO_2-96h, **g** = MnO_2-120h and **h** = MnO_2-240h.

The morphology of the prepared MnO_2 samples changed remarkably with the crystallization time (Fig. 4.2).

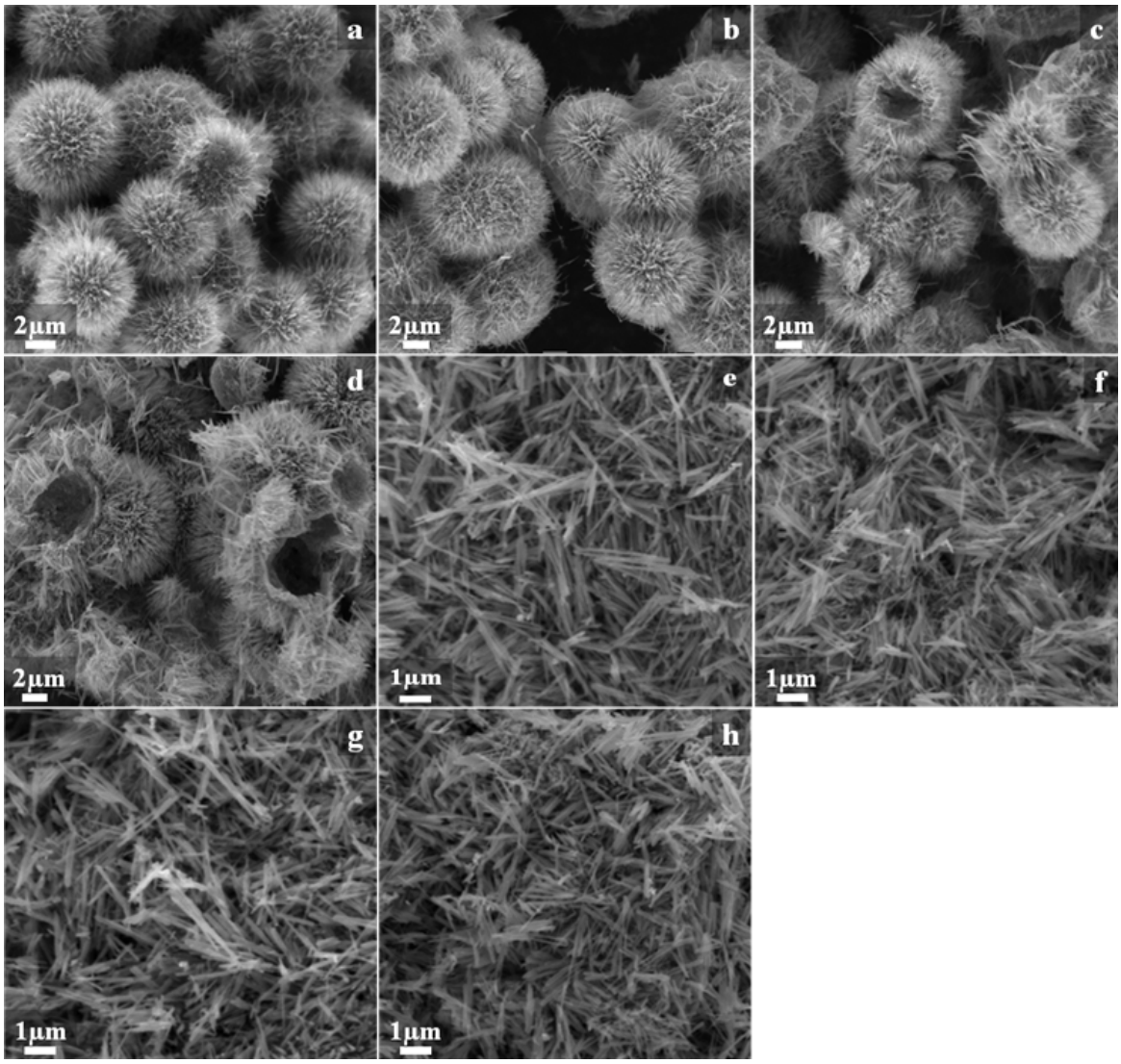

Figure 4.2 Effect of crystallisation time on the morphology of the MnO_2, **a** = MnO_2-6h, **b** = MnO_2-12h, **c** = MnO_2-24h, **d** = MnO_2-48h, **e** = MnO_2-72h, **f** = MnO_2-96h, **g** = MnO_2-120h, **h** = MnO_2-240h.

For the reactions carried out for 6 to 12 h the predominant morphology was found to be microspheres, however, for reactions at 24 and 48 h the spheres started to collapsed showing cracked shells evolved to a nanowire structure for crystallization times from 72

to 240 h. In other words, the phase transformed from α- to β-MnO_2 and the morphology changed from microspheres to nanowires as the crystallization time increased.

The surface areas and average micropore diameters of the samples are shown in Table 4.1 for all prepared MnO_2 supports and their corresponding Au catalysts. It is apparent that the samples obtained after 6 & 12 h crystallization have the highest surface areas and the surface area remarkably decreased as the crystallization time increased for both the prepared MnO_2 samples and the Au/MnO_2 catalysts. However, the crystallization time had no discernable effect on the average pore diameter. Furthermore, the surface areas increased after adding Au on the samples prepared at 12 and 24 h (microspheres), whereas the addition of Au had no effect on those prepared from 48 to 240 h (nanowires).

Table 4.1 Surface area and average pore diameter for MnO_2 and SI 1% Au/MnO_2 materials.

	Support			Catalyst		
	Area (m^2g^{-1})	Average pore diameter (Å)	Total pore volume (ccg^{-1})	Area (m^2g^{-1})	Average pore diameter (Å)	Total pore volume (ccg^{-1})
MnO_2-6h	71	33	0.06	72	33	0.06
MnO_2-12h	54	35	0.05	61	33	0.05
MnO_2-24h	41	35	0.04	52	33	0.04
MnO_2-48h	19	34	0.02	18	34	0.02
MnO_2-72h	12	34	0.01	11	34	0.01
MnO_2-96h	11	34	0.01	10	34	0.01
MnO_2-120h	11	34	0.009	10	35	0.009
MnO_2-240h	10	34	0.008	9	35	0.008

1 wt% Au was added to the all the MnO_2 supports by SI, IM and DP methods. It is apparent from Fig. 4.3 that adding gold had no discernable effect on the morphology and the catalysts prepared by SI method show that the morphology of the catalysts was robust under stirring conditions.

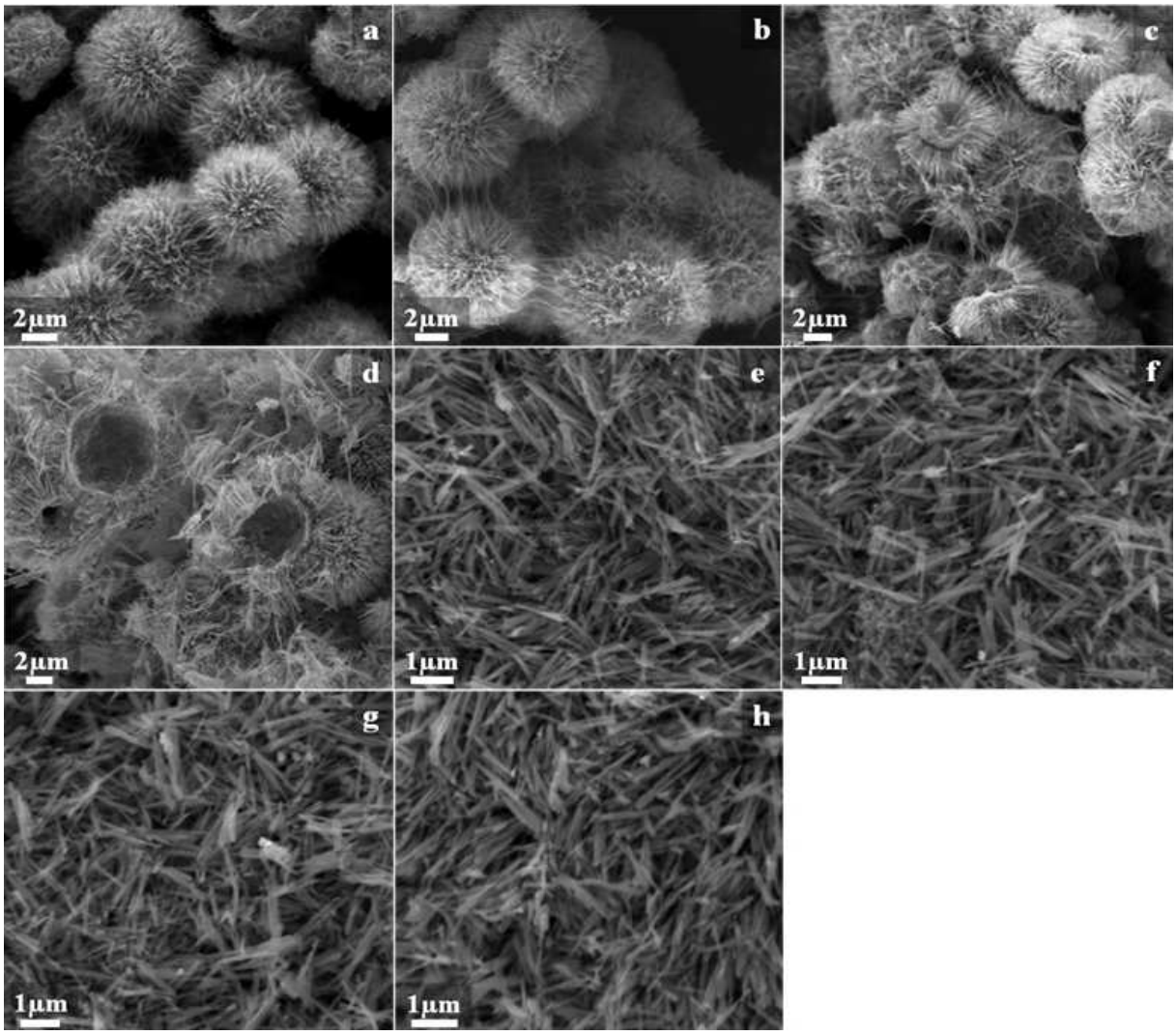

Figure 4.3 SEM images of the SI catalysts (after adding Au to MnO_2 supports) **a** = 1%Au/MnO_2-6h, **b** = 1%Au/MnO_2-12h, **c** = 1%Au/MnO_2-24h, **d** = 1%Au/MnO_2-48h, **e** = 1%Au/MnO_2-72h, **f** = 1%Au/MnO_2-96h, **g** = 1%Au/MnO_2-120h, **h** = 1%Au/MnO_2-240h.

4.3.2 Catalyst testing

4.3.2.1 Oxidation of benzyl alcohol using Au/MnO_2 catalysts

4.3.2.1.1 The effect of the preparation method

The first experiments were to determine the effect of the catalyst preparation method on the activity of benzyl alcohol. Initially, a sample was prepared with 12 h crystallisation time (MnO_2-12h) according to the method of Yang *et al.* [32]. Then, the corresponding Au/MnO_2-12h material was prepared by three different methods, IM, SI and DP. It is apparent from Table 4.2 that under the same conditions, SI method demonstrated the best catalytic performance for the oxidation of benzyl alcohol whereas the IM method catalysts had a very poor performance. Therefore, SI was used as the method of preparation for catalysts tested for benzyl alcohol oxidation.

Table 4.2 Oxidation of benzyl alcohol over 1% Au/MnO_2-12h catalyst prepared by different methods [a].

Preparation Method	Temp. (°C)	Conversion (%)	Selectivity (%)				
			B.Aldehyde	Toluene	Benzoic acid	Benzyl benzoate	Benzene
Sol-immobilisation (SI)	80	2.6	100	-	-	-	-
	100	4.3	98.0	-	-	2.0	-
	120	8.8	98.5	-	-	1.5	-
Impregnation (IM)	80	0.5	100	-	-	-	-
	100	1.0	100	-	-	-	-
	120	1.9	99	-	1.0	-	-
Deposition precipitation (DP)	80	2.2	99	-	1.0	-	-
	100	3.9	100	-	-	-	-
	120	7.5	99	-	1.0	-	-

[a] Benzyl alcohol (2 g), Catalyst (20 mg), O_2 1 barg, 4 h.

4.3.2.1.2 The effect of the catalyst structure and morphology

The results of the oxidation of benzyl alcohol using all MnO_2 materials and their corresponding Au catalysts prepared by SI and RSI are illustrated in Table 4.3. MnO_2 materials without Au were found to be quite active, and their activity increased as the preparation time increased. Particularly, α-MnO_2 prepared at 6-24 h which have a microspherical structure showed lower activity than β-MnO_2 prepared at 48-240 h which have a nanowire structure. The conversion increased from 2.5 % for MnO_2-12h to 5 % for MnO_2-72h.

However, upon Au addition, the activity of the catalysts that have microsphere structure was more active and it is apparent that the activity of the catalysts decreased as the preparation time of the MnO_2 supports increased. The conversion decreased from 8.8 % for the 1% Au/MnO_2-12h catalyst to 5.35 % for the 1% Au/MnO_2-240h catalyst. The addition of Au to the β-MnO_2 nanowires improved the activity slightly, for example: MnO_2-72h achieved 5 % conversion and it increased to 7 % when the Au was added while the conversion increased from 2.4 % to 8.8 % when the Au was added to MnO_2-12h. However, the Au/β-MnO_2 catalysts nanowire structure (72-96 h) achieved a100 % selectivity to benzaldehyde.

Table 4.3 Oxidation of benzyl alcohol over the sol-immobilised 1% Au/MnO_2 catalysts[a]

Support	catalyst	Conversion (%)	Selectivity (%)				
			B.Aldehyde	Toluene	Benzoic acid	Benzyl benzoate	Benzene
Prepared at 6h	MnO_2 (Blank)	2.4	99.5	-	0.5	-	-
	SI1% Au/MnO_2	8.6	99.0	-	-	1.0	-
	RSI 1% Au/MnO_2	8.1	100.0	-	-	-	-
Prepared at 12h	MnO_2 (Blank)	2.5	99.3	-	0.7	-	-
	SI 1% Au/MnO_2	8.8	98.5	-	-	1.5	-
	RSI 1% Au/MnO_2	8.3	99.0	-	-	1.0	-
Prepared at 24h	MnO_2 (Blank)	2.8	100.0	-	-	-	-
	SI 1% Au/MnO_2	8.5	97.5	-	-	2.5	-
	RSI 1% Au/MnO_2	8.4	99.5	-	-	0.5	-
Prepared at 48h	MnO_2 (Blank)	3.0	100	-	-	-	-
	SI 1% Au/MnO_2	8.2	98.0	-	0.7	1.3	-
	RSI 1% Au/MnO_2	7.0	99.7	-	-	0.3	-
Prepared at 72h	MnO_2 (Blank)	5.0	100.0	-	-	-	-
	SI 1% Au/MnO_2	7.0	99.7	-	-	0.2	-
	RSI 1% Au/MnO_2	6.8	99.8	-	-	0.2	-
Prepared at 96h	MnO_2 (Blank)	4.0	100.0	-	-	-	-
	SI 1% Au/MnO_2	5.6	100.0	-	-	-	-
	RSI 1% Au/MnO_2	5.5	100.0	-	-	-	-
Prepared at 120h	MnO_2 (Blank)	3.9	100.0	-	-	-	-
	SI 1% Au/MnO_2	5.5	100.0	-	-	-	-
	RSI 1% Au/MnO_2	5.6	100.0	-	-	-	-
Prepared at 240h	MnO_2 (Blank)	3.75	100.0	-	-	-	-
	SI 1% Au/MnO_2	5.35	100.0	-	-	-	-
	RSI 1% Au/MnO_2	5.4	100.0	-	-	-	-

[a] Benzyl alcohol (2 g), Catalyst (20 mg), O_2 1 barg, 120 °C, 4 h.

Two representative catalyst samples, namely Au/MnO_2-12h (microspheres) and Au/MnO_2-96h (nanowires), that illustrated different catalytic performance towards benzyl alcohol oxidation were characterised by TEM imaging to investigate the effect of the morphology on the gold particle size (Fig. 4.4). The images in Fig. 4.4 show that although the same Au sol was used as the precursor for all catalysts the particle size of Au varied remarkably in the resultant catalysts. For the Au supported on MnO_2-12h material, the Au particles were bigger than those supported on MnO_2-96h. Furthermore, the Au particles were better dispersed on the MnO_2-96h material. This suggests that the nanowire β-MnO_2 is much more suitable for Au deposition, and the resultant Au-MnO_2 interaction is stronger, therefore imparting a greater stability against sintering. As mentioned in the introduction, the morphology of the support can determine the particle size of the formed Au catalysts [18-21] and in Chapter 3, it was found that although the same Au sol was used throughout the Au particles were bigger when supported on the ceria foam compared to commercial ceria [31].

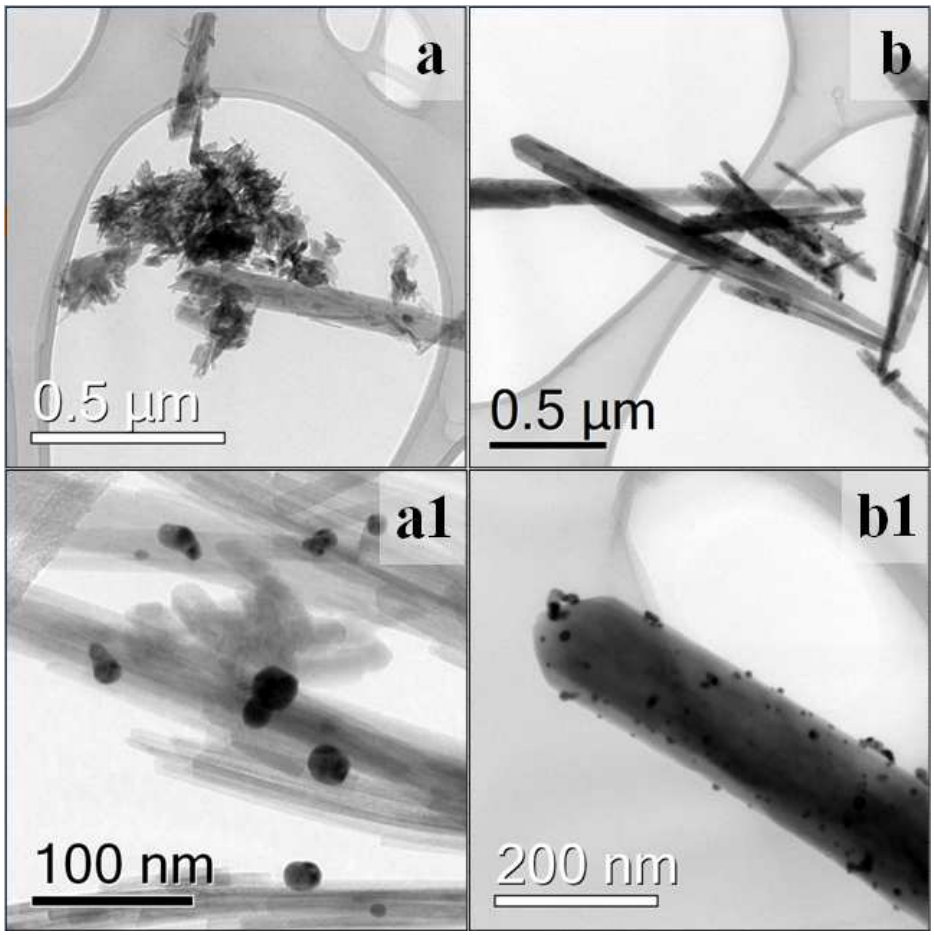

Figure 4.4 Bright field TEM micrographs of SI catalysts for (**a, a1**) Au/MnO_2-12h, and (**b, b1**) Au/MnO_2-96h.

Surprisingly, Au/MnO_2-12h which had bigger Au nanoparticles exhibited higher activity for the oxidation of benzyl alcohol than Au/MnO_2-96h. It is well known that gold catalysis relies essentially on the particle size of the Au, however, the other factors such as the preparation method and the choice of support [17] and even the support structure and morphology can play a major role in determining the performance of Au supported catalysts [18-21]. Although the reason of the higher activity of the Au/MnO_2-12h catalyst is not clear as it had bigger Au particles, it could be attributed to a

combination of Au particle size along with the surface area, crystal phase and morphology of MnO_2. The catalysts prepared by RSI did not show any improvement in the activity over the SI catalysts. The RSI method which includes an additional reflux step to the SI one so the SI catalysts were refluxed in water, recovered and dried so they were called RSI catalysts. This additional reflux step in the RSI preparation method is to remove PVA that covers the gold nanoparticles. During the benzyl alcohol oxidation the facile removal of PVA ligands from supported gold nanoparticles is achieved by benzyl alcohol itself under reaction conditions used in the experiments. PVA is soluble in benzyl alcohol at 120 °C under stirring. To confirm this, 1% Au/MnO_2-12h was refluxed in water and then in benzyl alcohol, PVA, the MnO_2 support and a set of PVA impregnated MnO_2 samples were analysed by laser Raman spectroscopy (Fig. 4.5a). It is apparent, by expanding the area between 500 and 750 cm^{-1} that the peak which appears at 567 cm^{-1} for the support, which is attributed to the Mn-O lattice vibration in MnO_2, is present in both refluxed catalysts while it has disappeared in the un-refluxed catalyst and PVA sample (Fig 4.5b). Furthermore, this peak is visible for the low concentrations of PVA on MnO_2 but decreases as the concentration of PVA increased (Fig 4.5b). Both 1% Au/MnO_2-12h catalysts refluxed in water and in benzyl alcohol were tested for CO oxidation and they illustrated very similar performance (Fig. 4.6). This indicates that the presence of PVA ligands on the catalyst blocks this peak, whereas with the reflux method this is removed.

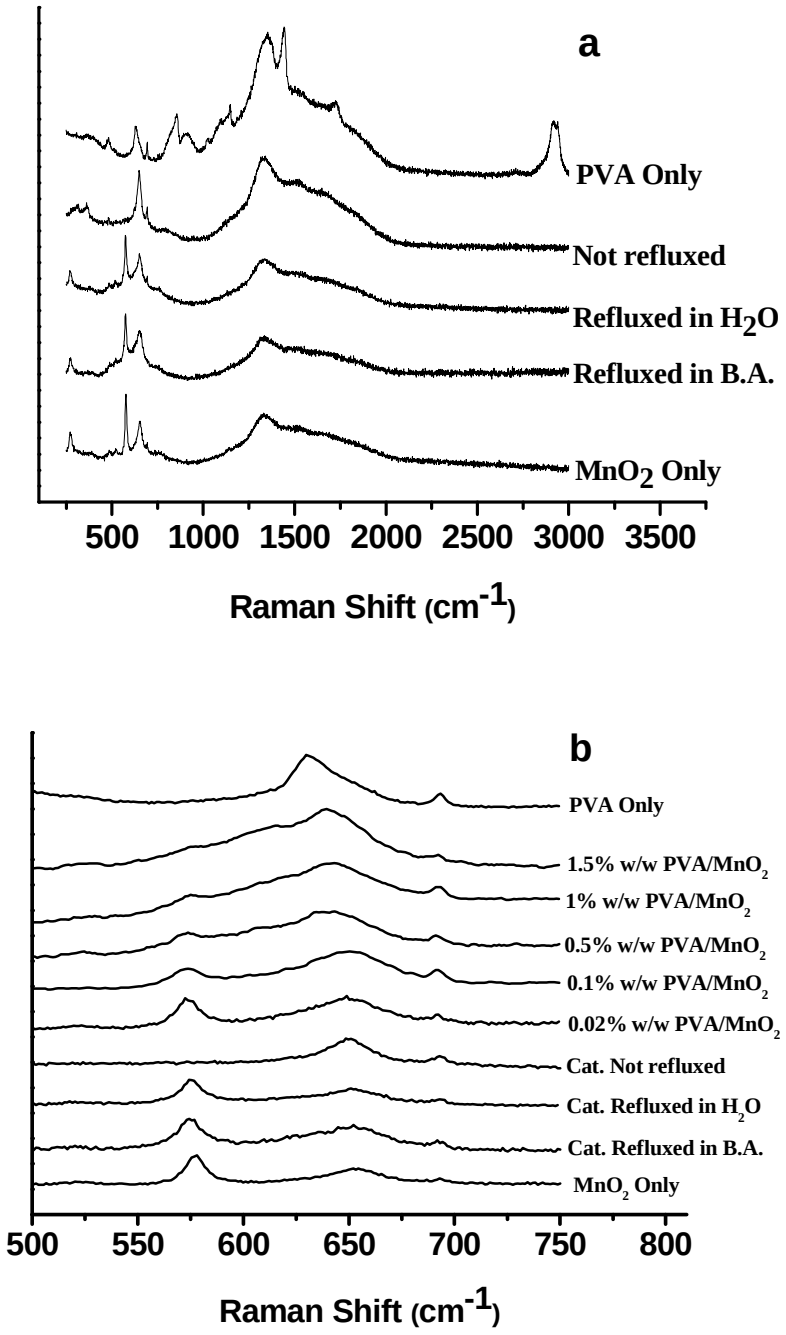

Figure 4.5 Laser Raman spectroscopy analysis of SI catalysts and reference materials (a & b) and CO oxidation by un-refluxed and refluxed 1% Au/MnO_2-12h (c).

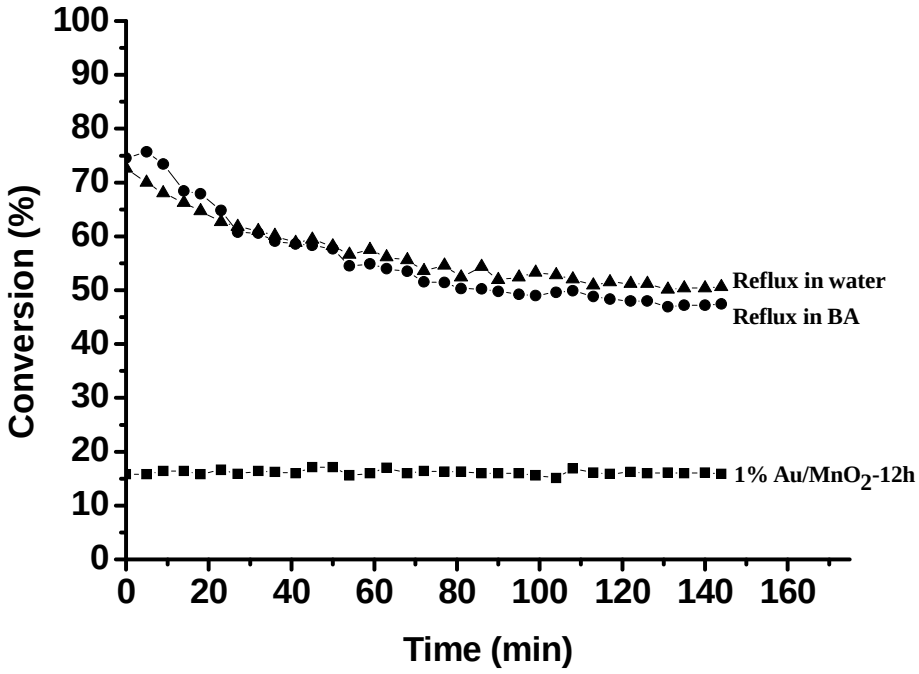

Figure 4.6 CO oxidation by of un-refluxed and refluxed 1% Au/MnO_2-12h

The morphology of the supports also had a slight effect on the selectivity of the products obtained (Table 4.3). In general, benzaldehyde was the major product with minor amounts of benzyl benzoate and benzoic acid for the microsphere catalysts while benzaldehyde became the only product observed in case of the nanowire structure catalysts. Producing benzaldehyde, benzyl benzoate and benzoic acid confirms that only the oxidation reaction of benzyl alcohol occurred [37, 38].

Many studies have been reported regarding the oxidation of benzyl alcohol by Au supported catalysts. Table 4.4 displays a comparison between the activities of the Au/MnO_2 catalysts with those in the literature.

Table 4.4 A comparison between the TOF values of the catalyst used in this study with those in the literature for the oxidation of benzyl alcohol.

Catalyst	Conversion (%)	Selectivity to benzaldehyde (%)	Benzaldehyde yield (%)	TOF ($molPhCHOg^{-1}_{Au}h^{-1}$)	Reference
MnO_2-12h (blank)	2.5	99.3	2.48	0.57	This work
Au/MnO_2-12h	8.8	98.5	8.67	2.01	
MnO_2-72h (blank)	5.0	100	5.0	1.16	
Au/MnO_2-72h	7.0	99.7	6.98	1.62	
Au/foamCeO_2-4h	3.7	95	3.52	0.83	Chapter 3 p100
Au/MnO_2	39.7	88.8	34.5	0.49	Choudhary *et al.* [39]
Au/ZrO_2	50.7	87.0	44.1	0.85	Choudhary *et al.* [39]
Au/TiO_2	6.0	93.2	5.6	0.82	Su *et al.* [40]
Au/Fe_2O_3	2.1	89.9	1.9	0.1	Su *et al.* [40]
Au/TiO_2	15.3	63.9	9.7	0.96	Enache *et al.* [41]

Table 4.4 shows that the Au/MnO_2 catalysts, especially the Au/MnO_2-12 catalyst, exhibited higher activity than some of those reported in the literature when the activity is calculated in molPhCHO/g_{Au}/h. Some other studies [12, 13, 42] illustrated a higher activity than the Au/MnO_2 ones in this work. However, the reaction in these studies was carried out at much higher O_2 pressure and temperatures.

4.3.2.1.3 The effect of catalyst mass

The effect of the catalyst mass on activity was studied to check for mass transport limitations. The catalyst mass was varied, 5, 10, 20 and 40 mg of Au/MnO_2-12h catalyst were tested and the results are shown in Fig. 4.6. The conversion increased as the amount of catalyst increased from 5 to 40 mg with no significant effect on reaction selectivity and benzaldehyde was the major product (98.5-100 %) with minor amount of benzyl benzoate as the only by-products [43] (Fig 4.7). This suggests that there was no mass transport limitation problem under these conditions.

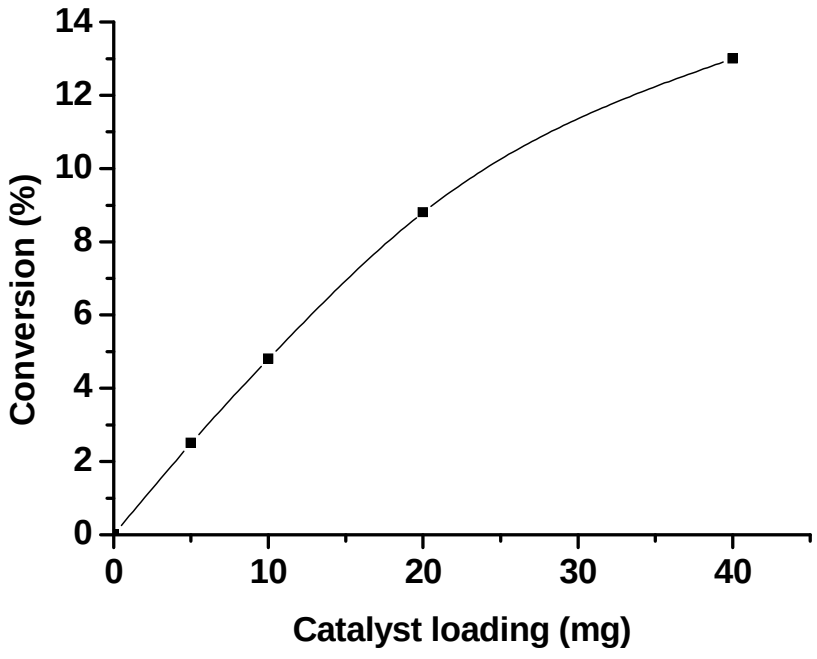

Figure 4.7 Effect of catalyst mass on conversion. Benzyl alcohol (2 g), Catalyst SI Au/MnO_2-12h, O_2 (1 barg), 120 °C & 4 h.

4.3.2.1.4 Time on-line analysis of Au/MnO_2-12h

The effect of the reaction time on the conversion and selectivity is shown in Table 4.5. For SI Au/MnO_2-12h, the conversion increased with the reaction time and only benzaldehyde was observed in the beginning of the reaction. However, a minor amount of benzyl benzoate was produced after 4 h of reaction time. This indicates that the partial oxidation of benzyl alcohol is stable at shorter reaction times. However, after 4 h further oxidation reaction to the produced benzaldehyde started to take place and it was explained in Chapter 1 the possible byproducts of benzyl alcohol oxidation [44].

Table 4.5 Time-online of Au/MnO_2-12h[a]

Time (h)	Conversion (%)	Selectivity (%)				
		B.Aldehyde	Toluene	Benzoic acid	Benzyl benzoate	Benzene
1	4.1	100	-	-	-	-
2	6.0	100	-	-	-	-
3	7.2	100	-	-	-	-
4	8.8	98.5	-	-	1.5	-

[a] Benzyl alcohol (2 g), Catalyst (20 mg), O_2 1 barg, 120 °C, 4 h.

4.3.2.1.5 Reusability of Au/MnO_2-12h

Re-use of the catalysts has also been investigated for SI Au/MnO_2-12h (Table 4.6). Following the reaction under standard conditions for 4 h the catalyst was recovered by centrifugation followed by two procedures of treatment. In the first procedure, the centrifuged catalyst was washed with 20 ml of a solvent (ethanol or acetone) and then dried at 110 °C for 1 h. In the second one, the centrifuged catalyst was not washed by any solvent and was dried at 110 °C for 1 h. In all re-use experiments larger amounts of the catalyst were used in the initial experiment so that the correct catalyst mass (20 mg) could be used in subsequent reactions. Table 4.6 illustrates the effect of washing procedure on the catalyst reusability.

The solvent used to wash the centrifuged catalyst prior to drying had a significant effect. When ethanol was used there was a dramatic drop in conversion and the selectivity was 100 % in all reuse experiments compared to 98.5 % for the fresh catalyst. Washing with acetone improved the reusability of the recovered catalyst slightly compared to ethanol solvent but the conversion decreased remarkably compared to the fresh catalyst. However, when no solvent used to wash the recovered catalyst there was a significant enhancement in the catalyst activity compared to the washed catalyst and the conversion decreased slightly in the first and third reuse with 100 % selectivity to benzaldehyde in all reuse experiments. It was found in Chapter 3 that washing the Au/foamCeO_2 catalyst with acetone in the reuse experiments removes the byproducts that might block the active sites of the catalyst. Interestingly, washing with solvents here had a negative effect on the catalyst reusability. This is thought to be due to the stirring effect during the reaction. In case of Au/foamCeO_2 catalyst the reaction was carried out without

stirring so washing the catalyst with acetone after the reaction could remove any byproducts that block the active sites whereas in case of Au/MnO_2 catalyst these byproducts could be removed by the stirring during the reaction. Therefore, washing with solvents afterwards might cause the active sites to be blocked by the solvent.

Table 4.6 Reusability of SI Au/MnO_2-12h[a]

Catalyst test	Washing solvent	Conversion (%)	Selectivity (%)				
			B.Aldehyde	Toluene	Benzoic acid	Benzyl benzoate	Benzene
1st test	Ethanol	8.8	98.5	0.0	0.0	1.50	0.0
1st Reuse		3.9	100	0.0	0.0	0.0	0.0
2nd Reuse		2.6	100	0.0	0.0	0.0	0.0
3rd Reuse		2.3	100	0.0	0.0	0.0	0.0
1st test	Acetone	8.8	98.5	0.0	0.0	1.50	0.0
1st Reuse		5.0	100	0.0	0.0	0.0	0.0
2nd Reuse		3.5	100	0.0	0.0	0.0	0.0
3rd Reuse		3.0	100	0.0	0.0	0.0	0.0
1st test	No washing	8.8	98.5	0.0	0.0	1.50	0.0
1st Reuse		8.45	100	0.0	0.0	0.0	0.0
2nd Reuse		8.40	100	0.0	0.0	0.0	0.0
3rd Reuse		7.9	100	0.0	0.0	0.0	0.0

[a] Benzyl alcohol (2 g), Catalyst (20 mg), O_2 1 barg, 120 °C, 4 h.

The results in Table 4.6 clearly illustrate the sensitivity of the catalyst to solvent used in the washing step and the best results were achieved when no solvent used in the washing step. Bawaked *et al*. [11] reported some factors that had a great effect on the catalyst reusability used for the Solvent-free selective epoxidation of cyclooctene using supported gold catalysts such as the drying method, drying atmosphere and the solvents used for washing the recovered catalyst.

Examination of the morphology of the microspheres after use as a catalyst also confirmed that the structures are stable under these conditions (Fig. 4.8).

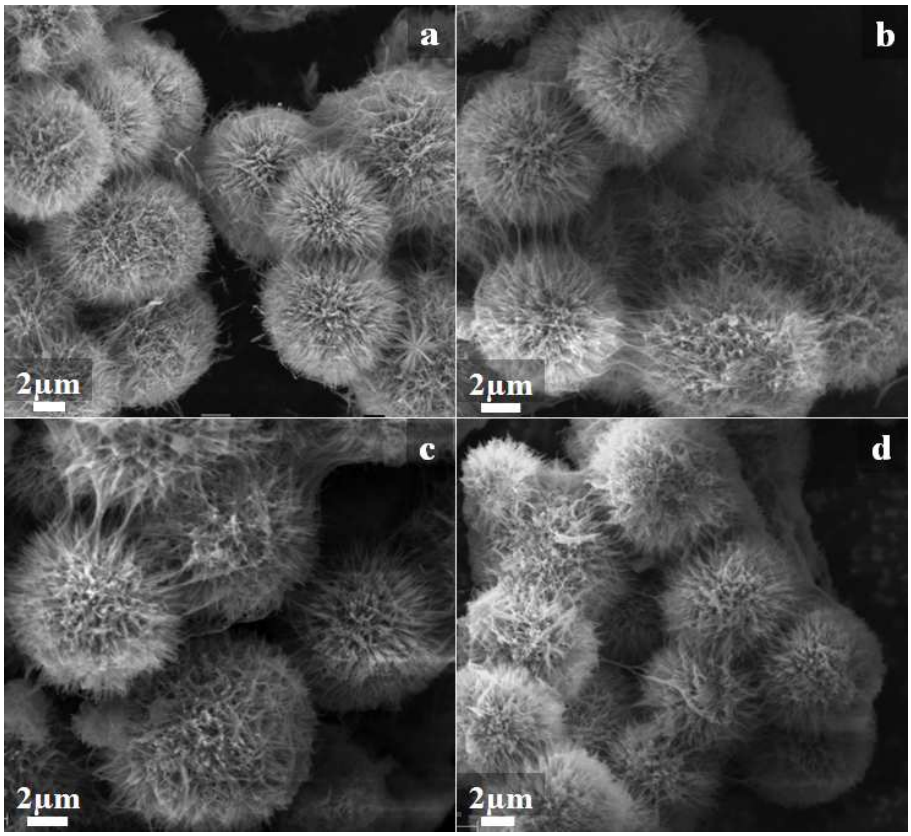

Figure 4.8 SEM images of **a** = MnO_2-12h, **b** = Au/MnO_2-12h (prior to testing), **c** = Au/MnO_2-12h (post-testing) and **d** = Au/MnO_2-12h (after 3rd re-use).

4.3.2.2 Oxidation of CO using Au/MnO_2 catalysts

4.3.2.2.1 The effect of the preparation method

The effect of the catalyst preparation method on the activity of CO oxidation was investigated. Initially, the Au/MnO_2-12h catalyst was prepared by four different methods, IM, SI, RSI and DP. Fig. 4.9 shows that under the same conditions, the DP and RSI were best for CO oxidation. It is clear that the IM method illustrated very low performance in comparison to the other methods. SI method exhibited better performance than IM. Therefore, DP, RSI and SI were used as methods to prepare catalysts for subsequent CO oxidation experiments.

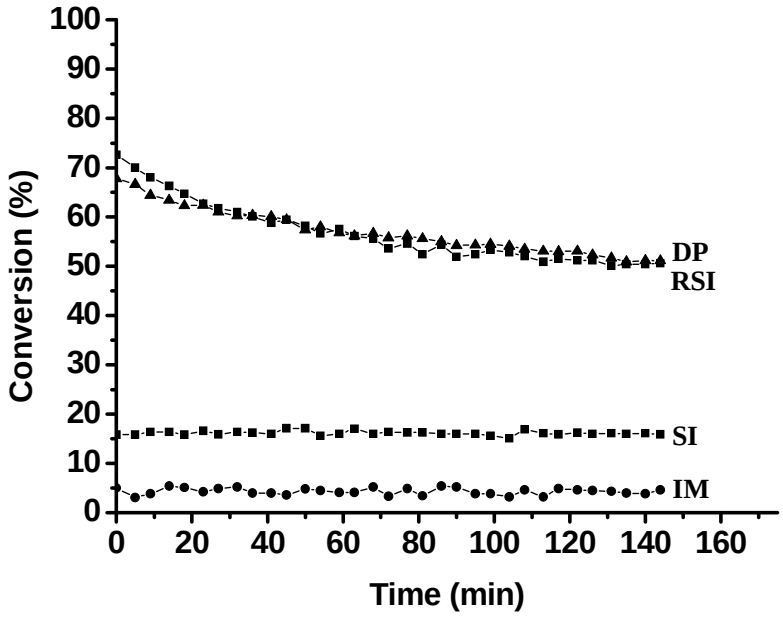

Figure 4.9 Oxidation of CO over 1% Au/MnO_2-12h catalyst prepared by different methods [a].
[a] CO flow rate (20 ml min^{-1}), Catalyst (100 mg), Temperature (30 °C), Time (140 min)

Fig. 4.10 illustrates the results of CO oxidation using the Au/MnO_2 catalysts prepared by SI and RSI and Fig. 4.11 shows the CO oxidation results for the DP catalysts. DP was the method that showed the best performance for CO oxidation. It is well known that the preparation method is one of the most important factors that can affect the catalyst activity of gold catalysis [17]. DP was found to be slightly better than the RSI method and both of them displayed much higher activity than SI method.

The SI catalysts were tested in the first experiments using 100 mg of the catalyst, 20 ml min^{-1} flow rate and 30 ºC. The results in Fig. 4.10a show that these catalysts were not very active and the best catalyst achieved less than 40 % conversion. However, following the water reflux according to the methodology described previously [34] these catalysts became very active for CO oxidation under these conditions. Refluxed 1% Au supported on MnO_2 prepared at 48, 72, 96, 120 and 240 h showed 100 % conversion and thus the flow rate was increased to 40 ml min^{-1} (Fig. 4.10b) and still Au/MnO_2-72, Au/MnO_2-96 and Au/MnO_2-120 showed 100 % conversion. The conversion of these catalysts decreased to lower than a 100 % when the amount of the catalysts decreased to 50 mg instead of 100 mg and it was apparent that the refluxed 1% Au/MnO_2-96h was the best catalyst for CO oxidation. The increased activity of the refluxed catalysts is due to the removal of the stabilizer (PVA) from the catalysts as explained previously in this Chapter in Section 4.3.2.1.2 [34]. The removal of PVA ligands that cover the Au nanoparticles is effective in the gas phase reactions such as CO oxidation because the gaseous reactants directly contact the Au nanoparticles. However, in benzyl alcohol oxidation these ligands are already removed during the

oxidation reaction and hence the reflux method of the catalyst prior to reaction has no effect on the catalysts activity.

The same experiments were repeated for DP catalysts (Fig. 4.11) and they showed similar results, albeit with a higher catalytic performance of the DP catalysts in comparison to the refluxed catalysts when the catalyst mass was reduced. The representative results are shown in Fig. 4.11a-b and it is clear that 1% Au/MnO_2-96h displayed the best performance of them. The catalyst 1% Au/MnO_2-96h prepared by DP exhibited 100 % conversion even when the flow rate decreased to 40 ml min^{-1} and the catalyst mass to 50 mg (Fig. 4.11b) compared to around 90 % conversion for the same catalyst prepared by RSI. The conversion of the DP catalyst only decreased to around 70 % when the catalyst mass decreased to 25 mg (Fig. 4.11b) which clearly shows that the DP preparation method was best for CO oxidation.

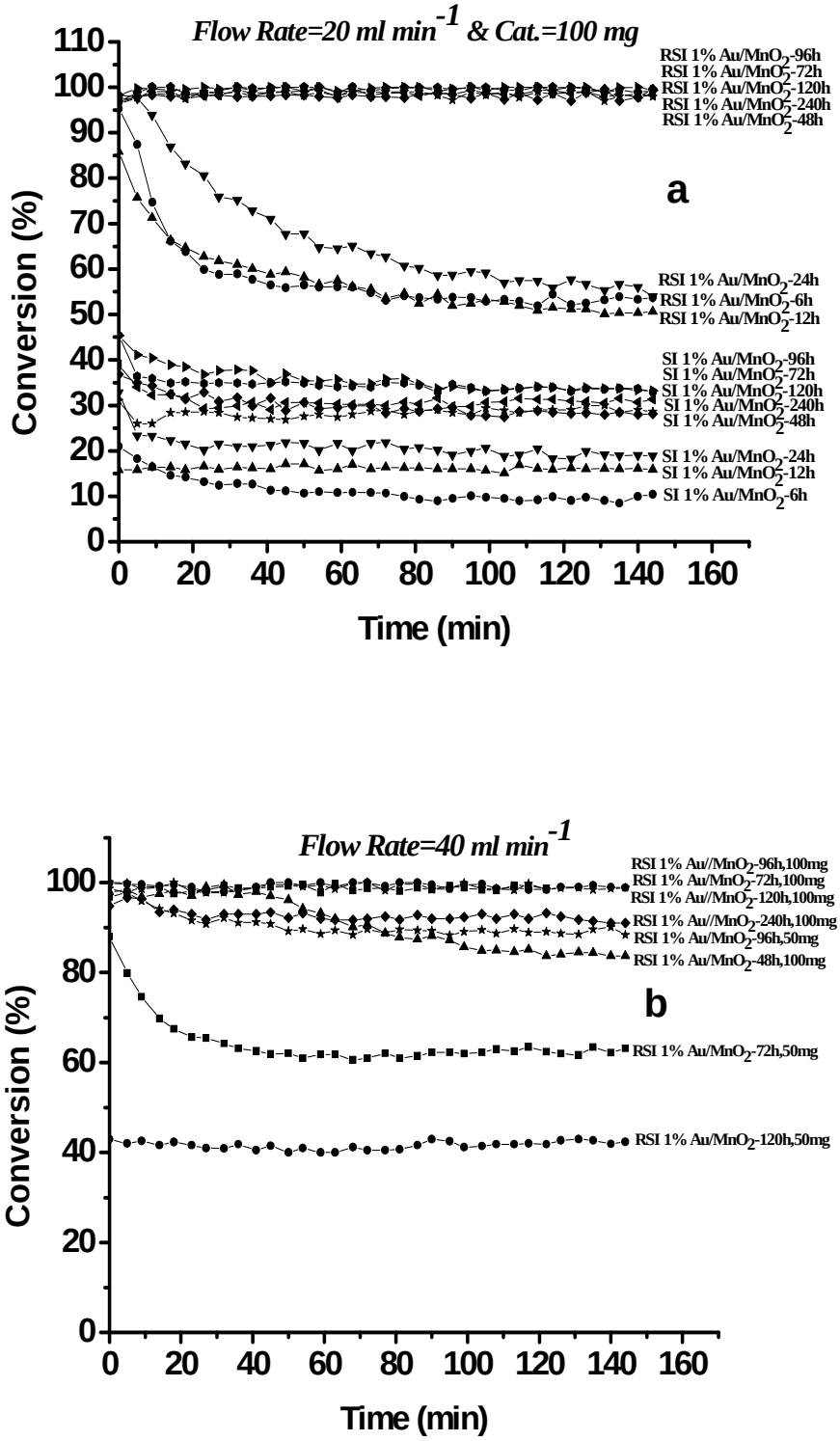

Figure 4.10 CO oxidation by SI and RSI catalysts.

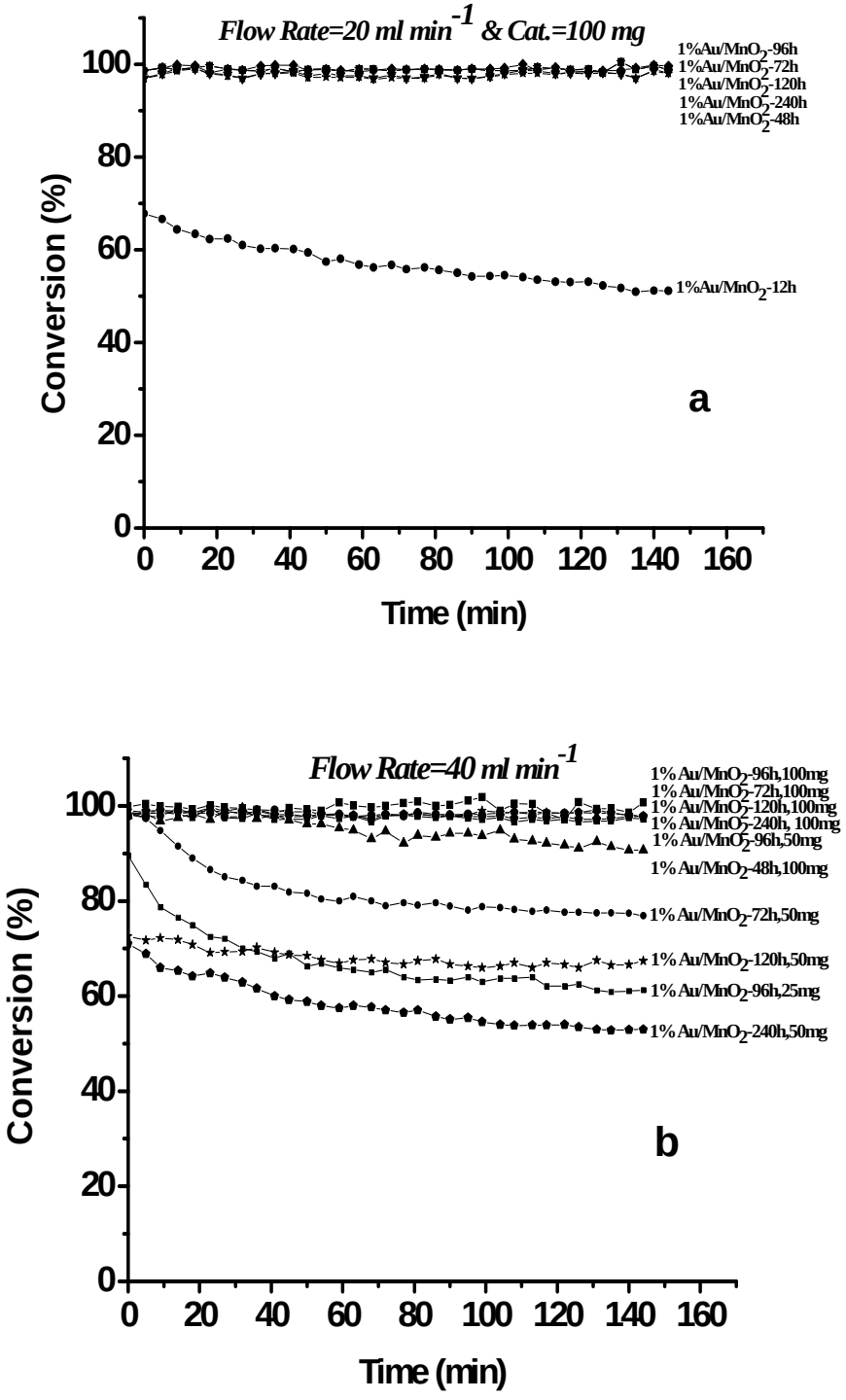

Figure 4.11 CO oxidation by DP catalysts.

TEM was used to examine the effect of the preparation method on the Au particle size distribution. Two catalyst samples (*i.e.* Au/MnO_2-96h) that have the same support morphology and phase (nanowires and β phase) but prepared by different methods, namely SI and DP were characterised by TEM. Representative micrographs of both catalysts and their corresponding Au particle-size distributions are shown in Fig. 4.12.

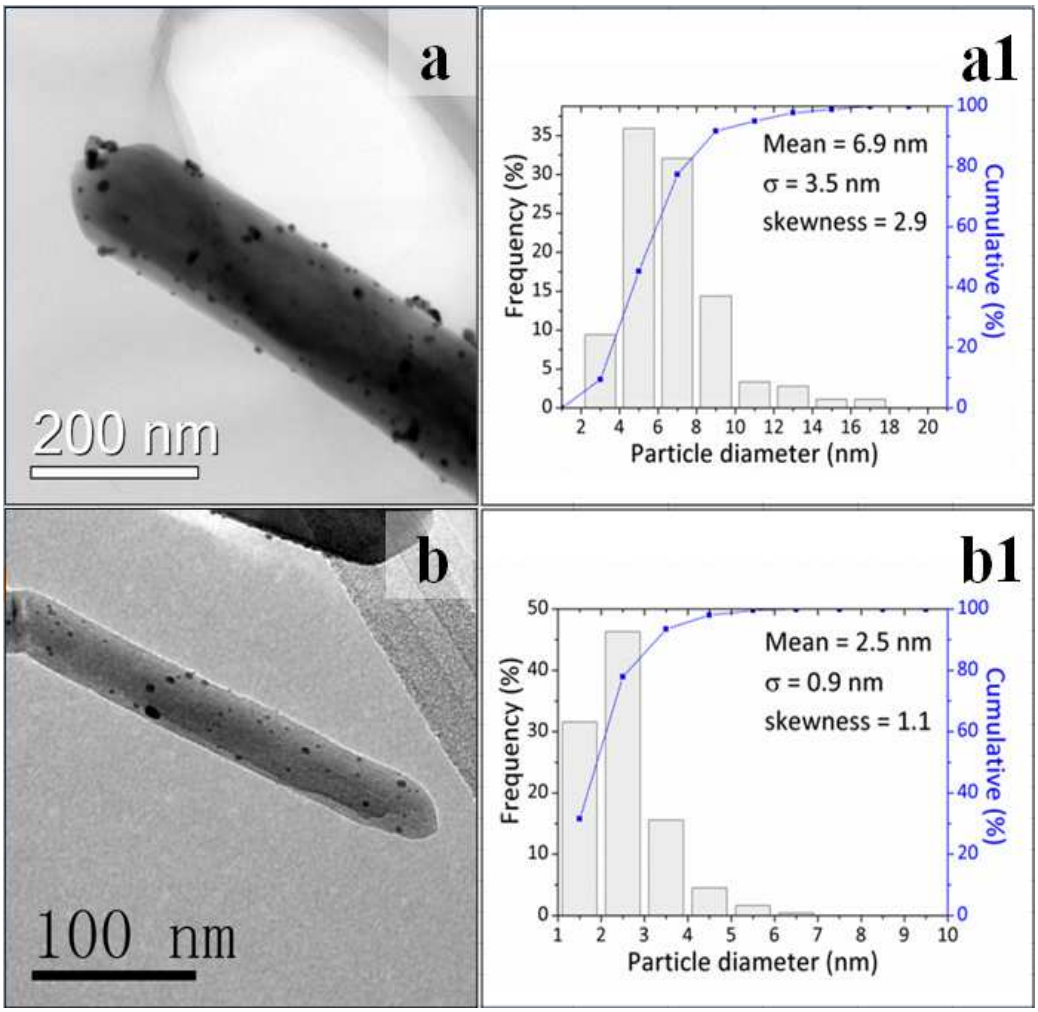

Figure 4.12 Representative TEM micrographs and the corresponding Au particle size distributions for (**a, a1**) SI Au/MnO_2-96h, and (**b, b1**) DP Au/MnO_2-96h.

Fig. 4.12 shows that both methods produced small particles and a high dispersion of Au on the supports. However, it is apparent that Au nanoparticles have a narrower particle size distribution with a mean value of 2.5 nm when deposited by the DP method (Fig. 4.12b-b1). The Au nanoparticles have quite a narrow particle size distribution with a mean size of 6.9 nm when deposited by the SI method (Fig. 4.12a-a1). The larger mean size exhibited by the SI material is a reflection of the initial size of the gold colloid before immobilization, while the DP material is not affected by such limitations, allowing access to smaller Au particles. The PVA used in the SI method that covers the gold nanoparticles seemed to have the major effect in this difference in the activity between the SI and DP catalysts because when the SI catalysts were refluxed to remove the PVA and prepare the RSI catalysts the activity was enhanced dramatically. However, the DP catalysts still showed better activity compared to the RSI ones as explained when the results of the Au/MnO_2-96h catalyst prepared by both RSI and DP were compared. This could be due to the smaller Au nanoparticles presented by the DP method. It is well documented in the literature that CO oxidation reaction is essentially very sensitive to the particle size of Au nanoparticles [45, 46].

4.3.2.2.2 The effect of the support structure and morphology

For all the catalysts, regardless of their preparation method, it was found that the catalyst activity increased as the support reaction time increased up to 96 h and then the activity decreased slightly for catalysts synthesized > 96 h, but was still higher than those catalysts supports which were prepared at shorter times (Fig. 4.10 and Fig. 4.11).

Generally, the preferred phase and morphology for CO oxidation was β-MnO_2 nanowires, which is the converse of the benzyl alcohol that preferred α-MnO_2 microspheres (Table 4.1).

TEM was employed to investigate the effect of the morphology of the support on the size of the Au nanoparticles. The SI catalysts Au/MnO_2-12h (α phase and microspheres) and Au/MnO_2-96h (β phase and nanowires) were investigated as well as their DP catalysts Au/MnO_2-12h and Au/MnO_2-96h (Fig. 4.13). It apparent from Fig. 4.13 that both SI and DP methods produced large Au nanoparticles when deposited on the alpha microsphere structure (MnO_2-12h) however, when deposited on the beta nanowire morphology (MnO_2-96h) the Au nanoparticles were much smaller and more homogeneously distributed. This suggests that the nanowire β-MnO_2 phase is much more suitable for Au deposition, and the resultant Au-MnO_2 interaction is stronger producing a greater stability against sintering and therefore better catalyst activity towards CO oxidation. This result is consistent with previous studies by Haruta *et al.* [45] and Tana *et al.* [46]. Haruta *et al.* [45] stated that the CO conversion decreases as the gold particles increase. They suggested that the smaller Au particles facilitate the interface between Au and support and therefore provide effective adsorption of CO and fast surface reduction with oxygen species provided by the support.

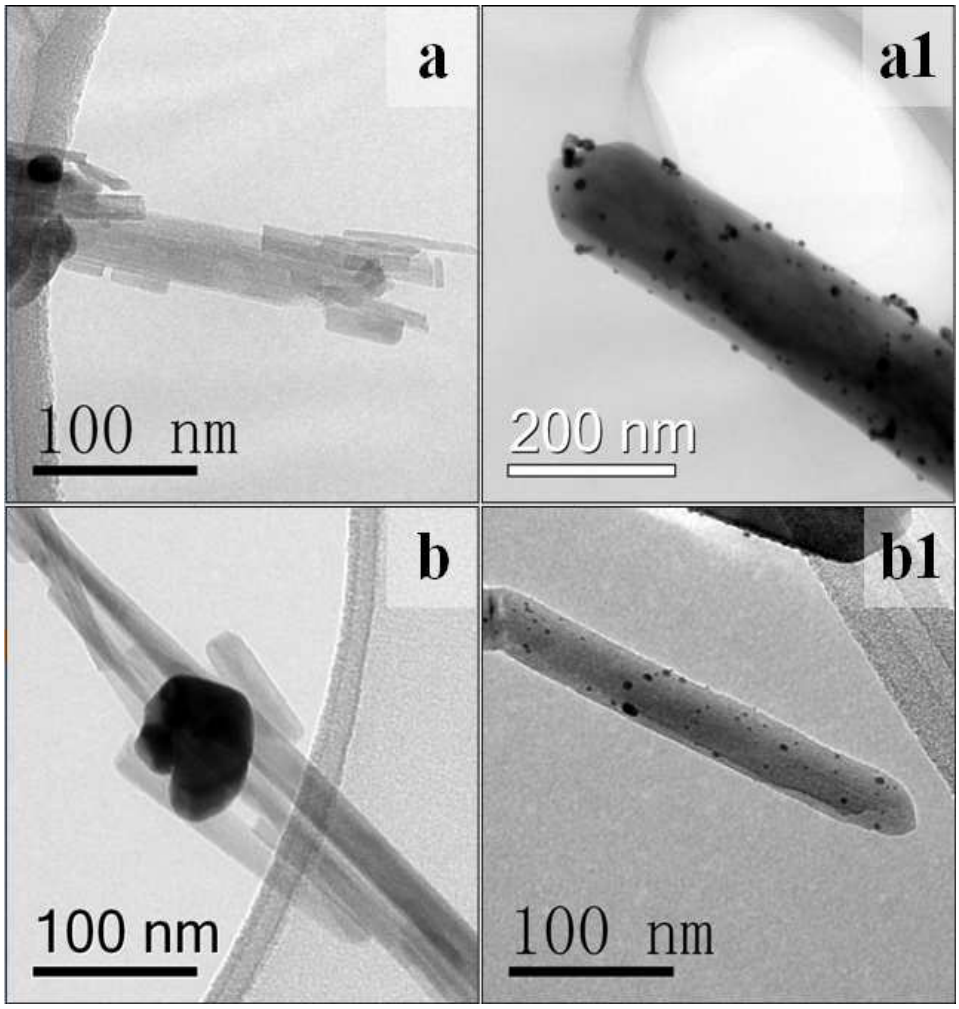

Figure 4.13 Bright field TEM of (a) SI Au/MnO_2-12h, (a1) SI Au/MnO_2-96h, (b) DP Au/MnO_2-12h and (b1) DP Au/MnO_2-96h.

However, it should be considered that in case of the reducible supports (TiO_2, CeO_2, Fe_2O_3, SnO_2, MnO_2, Co_3O_4, etc.) the reducibility of the support plays an important role in the CO oxidation. In this case, the Au particles interact with O_2 provided by the support and O_2 is adsorbed in a molecular form and this facilitates the oxidation of CO when it adsorbed on the metal-support interface. While in the case of irreducible supports (SiO_2, Al_2O_3, MgO, etc.) the activity depends mainly on the size of Au

particles as the adsorption of O_2 occurs on the gold particles [47]. MnO_2 is reported to be active for the CO oxidation at a relatively high temperature (> 120 ^{o}C) [48]. In this paper they reported that the α-MnO_2 and the β-MnO_2 both had a significantly different reactivity, with the alpha being active at about 130 ^{o}C and the beta at 170 ^{o}C, when both were prepared in nanorods. Nevertheless, if these phases were doped with silver, it was actually the Ag/β-MnO_2 to be more active than the Ag/α-MnO_2 [48]. These data demonstrate that not only the morphology but the crystal structure of the support is an important role for this reaction. The authors attributed the higher activity of Ag/β-MnO_2 to the stronger interaction between Ag and MnO_2 support as proved by TPR analysis. They stated that this interaction decreased the reduction temperature of β-MnO_2 and therefore promoted the activity to CO oxidation [48].

It is likely that a similar effect took place in this work, and therefore TPR analysis was employed on two samples of MnO_2 that have different morphologies and phases with different Au particle size to investigate the reactivity of them, namely microsphere α-MnO_2-12h and nanowire β-MnO_2-96h along with the corresponding sol-immobilised Au/MnO_2 materials (Fig. 4.14).

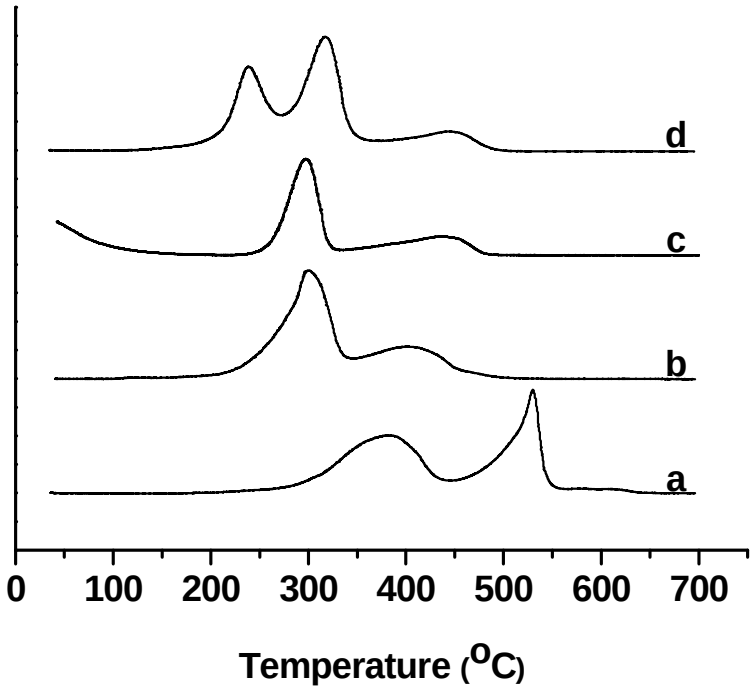

Figure 4.14 TPR measurements of the (**a**) MnO_2-12h, (**b**) SI Au/MnO_2-12h, (**c**) MnO_2-96h and (**d**) SI Au/MnO_2-96h.

Microsphere α-MnO_2-12h showed reduction peaks at 380 °C and 530 °C (Fig. 4.14a). It is thought that reduction which took place at lower temperature is ascribed to the reduction of MnO_2 to Mn_3O_4 whereas the high-temperature peak can be ascribed to the reduction of Mn_3O_4 to MnO [48, 49]. However, the reduction was shifted to lower temperature, namely 300 °C and 405 °C with the addition of gold which can be seen in Fig. 4.14b. Similar effects was found for nanowire β-MnO_2-96h but here the sample displayed a greater degree of reduction indicated by the presence of two reduction features at 295 and 440 °C (Fig 4.14c). The addition of Au increased the reduction further and although the reduction peak at 440 °C was retained, two reduction features

were present at 240 and 315 °C (Fig. 4.14d). The reduction of MnO_2 with higher crystallinity occurs through three steps corresponding to the reduction of MnO_2 to Mn_2O_3 (the lowest temperature peak), Mn_2O_3 to Mn_3O_4 and Mn_3O_4 to MnO (the highest temperature peak) [48]. The suggested reduction steps of MnO_2 material is illustrated in Scheme 4.1.

$$2MnO_2 + H_2 \longrightarrow Mn_2O_3 + H_2O$$

$$3Mn_2O_3 + H_2 \longrightarrow 2Mn_3O_4 + H_2O$$

$$Mn_3O_4 + H_2 \longrightarrow 3MnO + H_2O$$

Scheme 4.1 Reduction reactions of MnO_2 material

The surface of β-MnO_2 nanowires catalysts that contain much smaller Au nanoparticles was more easily reduced compared to the α-MnO_2 microspheres catalysts and this indicates stronger interaction between Au and MnO_2 support as this interaction decreased the reduction temperature. This confirmed the previous findings that smaller Au particles produce stronger Au-support interaction because they facilitate the interface between Au and support, provide effective adsorption of CO on them and fast surface reduction with oxygen species provided by the support [45, 46].

4.4 Conclusions

MnO_2 with different morphologies and phases, namely α-microspheres and β-nanowires were hydrothermally prepared by reacting $MnSO_4.H_2O$ and $(NH_4)_2S_2O_8$ at 120 °C for different reaction times. Au nanoparticles were supported on the MnO_2 supports using SI, DP and IM methods and were tested for CO oxidation and benzyl alcohol oxidation. For benzyl alcohol oxidation the SI exhibited the best catalytic performance compared to the other methods and the activity of SI catalysts were found to be dependent on the crystallization time of the support prepared. The Au/α-MnO_2 microspheres catalysts exhibited higher surface areas and therefore were the most active for benzyl alcohol oxidation compared to the Au/β-MnO_2 nanowires catalysts. They exhibited higher TOFs compared to the literature at under comparable reaction conditions. For CO oxidation, the DP method displayed the best activity. DP was found to be better than the RSI method and both of them were much better than the SI. This was ascribed to size of gold nanoparticles provided by the DP which was smaller compared to the other methods. The RSI catalysts showed much better performance than the SI ones due the removal of the PVA that covers Au particles in the SI catalysts. The effect of the morphology and structure of the support on the activity towards CO oxidation was investigated. It was found for all catalysts, regardless of their preparation method, the Au/β-MnO_2 nanowires catalysts were the preferred one for CO oxidation although they showed lower surface areas than the Au/α-MnO_2 microspheres catalysts. This was due to the small Au nanoparticles deposited on them which are essential for this reaction in particular as they provide a strong Au-MnO_2 interaction and therefore better

performance towards CO oxidation. Furthermore, the surface of β-MnO_2 nanowires catalysts was easily reduced as confirmed by the H_2-TPR due to the strong Au-MnO_2 interaction that facilitated the adsorption of CO and the surface reduction with oxygen species provided by the support. In general, the oxidation of benzyl alcohol preferred the SI methods and the microsphere α-MnO_2 catalysts whereas the CO oxidation preferred the DP method and the nanowire β-MnO_2catalysts.

4.5 References

1. Sheldon, R.A. and J.K. Kochi, *Metal-catalyzed oxidations of organic compounds*. 1981, New York: Academic Press. 424.

2. Pillai, U.R. and E. Sahle-Demessie, *Oxidation of alcohols over Fe^{3+}/montmorillonite-K10 using hydrogen peroxide.* Applied Catalysis A: General, 2003. **245**(1): p. 103-109.

3. Hudlický, M., *Oxidations in organic chemistry*. 1990, Washington DC: ACS. 433.

4. Haruta, M., et al., *Gold catalysts prepared by coprecipitation for low-temperature oxidation of hydrogen and of carbon monoxide.* Journal of Catalysis, 1989. **115**(2): p. 301-309.

5. Landon, P., et al., *Direct formation of hydrogen peroxide from H_2/O_2 using a gold catalyst.* Chemical Communications, 2002(18): p. 2058-2059.

6. Ntainjua, E.N., et al., *Direct synthesis of hydrogen peroxide using Au-Pd-exchanged and supported heteropolyacid catalysts at ambient temperature using water as solvent.* Green Chemistry, 2012. **14**(1): p. 170-181.

7. Edwards, J.K., et al., *Direct Synthesis of H_2O_2 from H_2 and O_2 over Gold, Palladium, and Gold–Palladium Catalysts Supported on Acid-Pretreated TiO_2.* Angewandte Chemie International Edition, 2009. **48**(45): p. 8512-8515.

8. Li, G., et al., *Direct synthesis of hydrogen peroxide from H_2 and O_2 using zeolite-supported Au-Pd catalysts.* Catalysis Today, 2007. **122**(3–4): p. 361-364.

9. Fu, Q., H. Saltsburg, and M. Flytzani-Stephanopoulos, *Active Nonmetallic Au and Pt Species on Ceria-Based Water-Gas Shift catalysts.* Science, 2003. **301**: p. 935-938.

10. Hayashi, T., K. Tanaka, and M. Haruta, *Selective Vapor-Phase Epoxidation of Propylene over Au/TiO_2 Catalysts in the Presence of Oxygen and Hydrogen.* Journal of Catalysis, 1998. **178**(2): p. 566-575.

11. Bawaked, S., et al., *Solvent-free selective epoxidation of cyclooctene using supported gold catalysts: an investigation of catalyst re-use.* Green Chemistry, 2011. **13**(1): p. 127-134.

12. Dimitratos, N., et al., *Solvent free liquid phase oxidation of benzyl alcohol using Au supported catalysts prepared using a sol immobilization technique.* Catalysis Today, 2007. **122**(3–4): p. 317-324.

13. Enache, D.I., et al., *Solvent-free oxidation of benzyl alcohol using titania-supported gold–palladium catalysts: Effect of Au–Pd ratio on catalytic performance.* Catalysis Today, 2007. **122**(3–4): p. 407-411.

14. Boronat, M., et al., *Mechanism of selective alcohol oxidation to aldehydes on gold catalysts: Influence of surface roughness on reactivity.* Journal of Catalysis, 2011. **278**(1): p. 50-58.

15. Demirel, S., et al., *Oxidation of mono- and polyalcohols with gold: Comparison of carbon and ceria supported catalysts.* Catalysis Today, 2007. **122**(3–4): p. 292-300.

16. Solsona, B.E., et al., *Supported gold catalysts for the total oxidation of alkanes and carbon monoxide.* Applied Catalysis A: General, 2006. **312**(0): p. 67-76.

17. Huang, J., W.-L. Dai, and K. Fan, *Remarkable support crystal phase effect in Au/FeO_x catalyzed oxidation of 1,4-butanediol to γ-butyrolactone.* Journal of Catalysis, 2009. **266**(2): p. 228-235.

18. Zhang, X., H. Wang, and B.-Q. Xu, *Remarkable Nanosize Effect of Zirconia in Au/ZrO_2 Catalyst for CO Oxidation†.* The Journal of Physical Chemistry B, 2005. **109**(19): p. 9678-9683.

19. Ho, K. and K. Yeung, *Properties of TiO_2 support and the performance of Au/TiO_2 Catalyst for CO oxidation reaction.* Gold Bulletin, 2007. **40**(1): p. 15-30.

20. Yan, W., et al., *Preparation and Comparison of Supported Gold Nanocatalysts on Anatase, Brookite, Rutile, and P25 Polymorphs of TiO_2 for Catalytic Oxidation of CO.* The Journal of Physical Chemistry B, 2005. **109**(21): p. 10676-10685.

21. Yan, W., et al., *Brookite-supported highly stable gold catalytic system for CO oxidation.* Chemical Communications, 2004(17): p. 1918-1919.

22. Carrettin, S., et al., *Nanocrystalline CeO_2 Increases the Activity of Au for CO Oxidation by Two Orders of Magnitude.* Angewandte Chemie International Edition, 2004. **43**(19): p. 2538-2540.

23. Abad, A., et al., *A Collaborative Effect between Gold and a Support Induces the Selective Oxidation of Alcohols.* Angewandte Chemie International Edition, 2005. **44**(26): p. 4066-4069.

24. Li, J., et al., *Influence of zirconia crystal phase on the catalytic performance of Au/ZrO_2 catalysts for low-temperature water gas shift reaction.* Applied Catalysis A: General, 2008. **334**(1–2): p. 321-329.

25. Mai, H.-X., et al., *Shape-Selective Synthesis and Oxygen Storage Behavior of Ceria Nanopolyhedra, Nanorods, and Nanocubes.* The Journal of Physical Chemistry B, 2005. **109**(51): p. 24380-24385.

26. Tana, et al., *Morphology-dependent redox and catalytic properties of CeO_2 nanostructures: Nanowires, nanorods and nanoparticles.* Catalysis Today, 2009. **148**(1–2): p. 179-183.

27. Si, R. and M. Flytzani-Stephanopoulos, *Shape and Crystal-Plane Effects of Nanoscale Ceria on the Activity of Au-CeO_2 Catalysts for the Water–Gas Shift Reaction.* Angewandte Chemie International Edition, 2008. **47**(15): p. 2884-2887.

28. Huang, X.-S., et al., *Morphology effects of nanoscale ceria on the activity of Au/CeO_2 catalysts for low-temperature CO oxidation.* Applied Catalysis B: Environmental, 2009. **90**(1–2): p. 224-232.

29. Idakiev, V., et al., *Gold catalysts supported on mesoporous zirconia for low-temperature water–gas shift reaction.* Applied Catalysis B: Environmental, 2006. **63**(3–4): p. 178-186.

30. Wang, L.-C., et al., *MnO2 Nanorod Supported Gold Nanoparticles with Enhanced Activity for Solvent-free Aerobic Alcohol Oxidation.* The Journal of Physical Chemistry C, 2008. **112**(17): p. 6981-6987.

31. Alhumaimess, M., et al., *Oxidation of Benzyl Alcohol by using Gold Nanoparticles Supported on Ceria Foam.* ChemSusChem, 2012. **5**(1): p. 125-131.

32. Yang, J.B., et al., *Growth and magnetic properties of $MnO_2{-}\delta$ nanowire microspheres.* Applied Physics Letters, 2004. **85**(15): p. 3160-3162.

33. Subramanian, V., et al., *Hydrothermal Synthesis and Pseudocapacitance Properties of MnO_2 Nanostructures.* The Journal of Physical Chemistry B, 2005. **109**(43): p. 20207-20214.

34. Lopez-Sanchez, J.A., et al., *Facile removal of stabilizer-ligands from supported gold nanoparticles.* Nat Chem, 2011. **3**(7): p. 551-556.

35. Liang, S., et al., *Effect of Phase Structure of MnO_2 Nanorod Catalyst on the Activity for CO Oxidation.* The Journal of Physical Chemistry C, 2008. **112**(14): p. 5307-5315.

36. Kim, H., et al., *Synthesis, structure and magnetic properties ofbeta-MnO2nanorods.* Nanoscale Research Letters, 2007. **2**(2): p. 81 - 86.

37. Jayamani, M. and C.N. Pillai, *Hydride transfer reactions: VIII. Reactions of benzyl alcohol over alumina: Dehydration and disproportionation.* Journal of Catalysis, 1983. **82**(2): p. 485-488.

38. Lopez-Sanchez, J.A., et al., *Au–Pd supported nanocrystals prepared by a sol immobilisation technique as catalysts for selective chemical synthesis.* Phys. Chem. Chem. Phys., 2008. **10**: p. 1921–1930.

39. Choudhary, V.R., et al., *A green process for chlorine-free benzaldehyde from the solvent-free oxidation of benzyl alcohol with molecular oxygen over a supported nano-size gold catalyst.* Green Chemistry, 2005. **7**(11): p. 768-770.

40. Su, F.-Z., et al., *Aerobic oxidation of alcohols catalyzed by gold nanoparticles supported on gallia polymorphs.* Catalysis Communications, 2008. **9**(6): p. 1027-1032.

41. Enache, D.I., et al., *Solvent-Free Oxidation of Primary Alcohols to Aldehydes Using Au-Pd/TiO_2 Catalysts.* Science, 2006. **311**(5759): p. 362-365.

42. Miedziak, P.J., et al., *Ceria prepared using supercritical antisolvent precipitation: a green support for gold-palladium nanoparticles for the selective catalytic oxidation of alcohols.* Journal of Materials Chemistry, 2009. **19**(45): p. 8619-8627.

43. Villa, A., C.E. Chan-Thaw, and L. Prati, *Au NPs on anionic-exchange resin as catalyst for polyols oxidation in batch and fixed bed reactor.* Applied Catalysis B: Environmental, 2010. **96**(3–4): p. 541-547.

44. Li, G., et al., *Solvent-free oxidation of benzyl alcohol with oxygen using zeolite-supported Au and Au–Pd catalysts.* Catalysis Letters, 2006. **110**(1): p. 7-13.

45. Haruta, M., et al., *Low-Temperature Oxidation of CO over Gold Supported on TiO_2, α-Fe_2O_3, and Co_3O_4.* Journal of Catalysis, 1993. **144**(1): p. 175-192.

46. Tana, et al., *Influence of Au particle size on Au/CeO_2 catalysts for CO oxidation.* Catalysis Today, 2011. **175**(1): p. 541-545.

47. Moreau, F. and G.C. Bond, *Influence of the surface area of the support on the activity of gold catalysts for CO oxidation.* Catalysis Today, 2007. **122**(3–4): p. 215-221.

48. Xu, R., et al., *Surface structure effects in nanocrystal MnO_2 and Ag/MnO_2 catalytic oxidation of CO.* Journal of Catalysis, 2006. **237**(2): p. 426-430.

49. Tian, W., et al., *Catalytic reduction of NOx with NH3 over different-shaped MnO_2 at low temperature.* Journal of Hazardous Materials, 2011. **188**(1–3): p. 105-109.

Chapter 5

The synthesis of highly crystalline vanadium phosphate catalysts using PAAMA as a structure directing agent

5.1. Introduction

Vanadium phosphate catalysts have been used for the commercial production of maleic anhydride by the oxidation of butane [1-3]. The efficiency of the catalyst highly relies on the method by which the precursor, $VOPO_4.0.5H_2O$, is prepared and the reaction conditions [4, 5]. The morphology and surface area are crucial factors to achieve good catalytic results. Therefore, well controllable synthesis method of the precursor can determine the catalyst performance as it can affect some properties such as the morphology, surface area, the crystallinity, the chemical composition, the phases present in the final catalyst and the reproducibility of the performance. Even simple modification to the preparation method can affect these properties in the final precursor and hence the catalytic performance [6-20].

In recent years, the use of diblock copolymers has increased remarkably in many areas, such as medicine, electronics, ceramics, catalysis, etc [21]. The interest in these copolymers is that they can be used in synthesis to control structure and morphology. Controlling synthesis of materials with a particular shape and structure is a feature of material science particularly catalysis. Diblock copolymers have been employed as structure directing agents in many applications to improve some features of the desirable product. They were used in the synthesis of semiconductors that their properties depend on their shape and size [22]. They also can also be used to promote the crystallization of particular phases. Yu *et al.* [23] displayed that PSMA (2-poly(styrene-alt-maleic acid) could have an application in preventing urolithiasis as it could promote the growth of the tetragonal phase during the formation of CaOx which is easily expelled from the body, over the monoclinic phase which is difficult for the

body to expel and hence, forms kidney stones. Adding a polymer into mortar or concrete can significantly improve the properties of the material [24]. Pore structures are improved, workability is increased and water absorption is decreased. It was found that PSMA enhanced the strength of the material when used into Portland cement due to its promotion to the formation of anhydrous calcium carboxylate over calcium hydroxide [22].

During the preparation of heterogeneous catalysts, preferentially exposing the active plane or preferentially forming the active phase can lead to an increase in selectivity and/or activity. Lin *et al.* [25] illustrated that a diblock copolymer, PSMA, could affect the morphology and crystallinity of a vanadium phosphate catalyst precursor. In this study a more soluble copolymer, poly(acrylic acid-co-maleic acid) (PAAMA), was used to investigate different synthetic routes to the catalyst precursor and to study the effect of higher copolymer concentrations.

5.2 Experimental

5.2.1 Preparation of vanadium phosphate catalysts

The vanadium phosphate hemihydrate ($VOHPO_4 \cdot 0.5H_2O$) precursor was synthesised according to the literature [26] using two different methods denoted the VPO and VPD routes.

5.2.1.1 Preparation of $VOHPO_4.0.5H_2O$ precursor via VPO route

5.2.1.1.1 Standard procedure

The standard vanadium phosphate hemihydrate ($VOHPO_4 \cdot 0.5H_2O$) precursor, P-VPO0, was synthesised via VPO route described in Chapter 2 (Section 2.3.1.1).

5.2.1.1.2 Copolymer modified procedure

The copolymer modified vanadium phosphate hemihydrate ($VOHPO_4 \cdot 0.5H_2O$) precursors, P-VPO5, P-VPO15 and P-VPO25, were synthesised via VPO route described in Chapter 2 (Section 2.3.1.2).

The precursors P-VPO0, P-VPO5, P-VPO15 and P-VPO25 were activated at 400 °C in situ in a flow of 1.7% butane in air until steady state observed to give their respective catalysts, denoted C-VPO0, C-VPO5, C-VPO15 and C-VPO25.

5.2.1.2 Preparation of $VOHPO_4.0.5H_2O$ precursor via VPD route

5.2.1.2.1 Preparation of $VOPO_4.2H_2O$

Vanadium phosphate dihydrate ($VOPO_4 \cdot 2H_2O$) was first synthesised by the standard method without any modification as described in Chapter 2 (Section 2.3.2.1).

5.2.1.2.2 Preparation of $VOHPO_4 \cdot 0.5H_2O$ via $VOPO_4.2H_2O$ using the standard procedure

The standard vanadium phosphate hemihydrate ($VOHPO_4 \cdot 0.5H_2O$) precursor, P-VPD0, was synthesised via VPD route described in Chapter 2 (Section 2.3.2.2).

5.2.1.2.3 Preparation of $VOHPO_4 \cdot 0.5H_2O$ via $VOPO_4.2H_2O$ using copolymer modified procedure

The copolymer modified vanadium phosphate hemihydrate ($VOHPO_4 \cdot 0.5H_2O$) precursors, P-VPD5, P-VPD15 and P-VPD25, were synthesised via VPD route described in Chapter 2 (Section 2.3.2.3).

The precursors P-VPD0, P-VPD5, P-VPD15 and P-VPD25 were activated at 400 °C in situ in a flow of 1.7 % butane in air until steady state observed to give their respective catalysts, denoted C-VPD0, C-VPD5, C-VPD15 and C-VPD25.

5.3 Characterisation

Powder X-ray diffraction (XRD), Scanning electron microscopy (SEM) and Laser Raman spectra were used to characterise the precursor and activated catalyst materials.

5.4 Catalyst testing

The catalyst test was carried out under the following reaction conditions: a gas mixture of 1.7 % butane to air, a gas hourly space velocity of 2000h^{-1}, 0.2 g of catalyst (approx. 0. 3ml), and 400 °C (ramp rate 3 °C min^{-1}). Measurements were taken when stable conversion and selectivity were observed.

5.5 Results and discussion

5.5.1 Catalyst precursor characterisation

5.5.1.1 Characterisation of precursors synthesised via VPO route

The VPO precursors (P-VPO0, P-VPO5, P-VPO15 and P-VPO25) were examined by XRD and the diffraction patterns were found to be typical of $VOHPO_4 \cdot 0.5H_2O$ (Fig. 5.1). The positions of peaks (2 Theta) and planes for the synthesised VPO precursors and the standard reported in the literature [27, 28] are shown in Table 5.1.

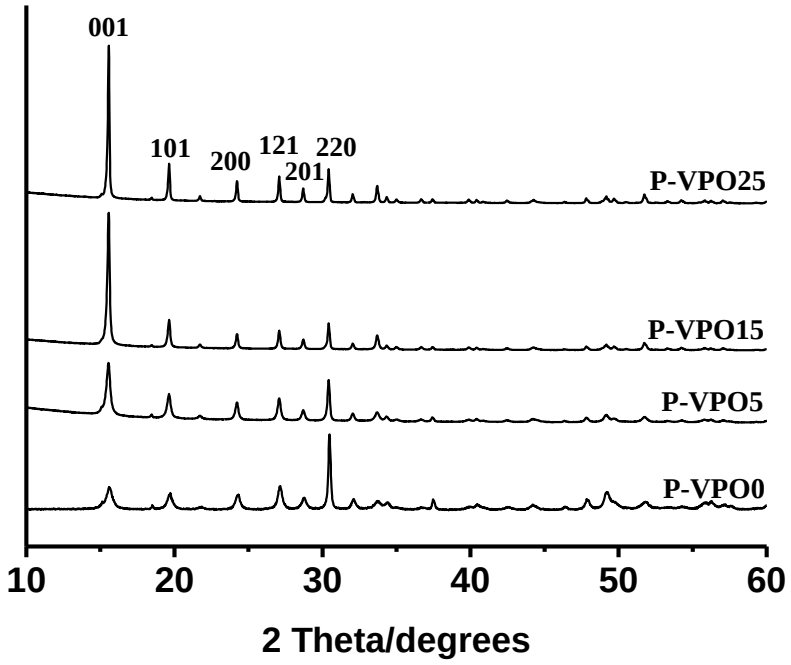

Fig. 5.1 Powder XRD patterns of P-VPO precursors. All can be indexed to $VOHPO_4.0.5H_2O$.

Table 5.1 The XRD reflections of the synthesised VPO precursors and the standard reported in the literature.

HKL	2Θ of $VOHPO_4.0.5H_2O$	
	In the Literature [27, 28]	**Synthesised**
001	15.57°	15.56°
101	19.67°	19.64°
200	24.27°	24.22°
121	27.12°	27.07°
201	28.75°	28.69°
220	30.46°	30.42°

However, the morphology was observed to change as the concentration of PAAMA increased. In the standard precursor, P-VPO0, the (220) reflection was the most intense. This reflection was found to decrease as the concentration of PAAMA added increased, while the (001) reflection increased with PAAMA addition. The different relative intensities of the (001) and (220) reflections have been shown to be characteristic of two distinct morphologies of $VOHPO_4 \cdot 0.5H_2O$ [6, 19, 20, 29]. The pattern with the (220) reflection as the dominant feature is typical of rosette-like structures, whereas the pattern with the (001) reflection as the dominant feature is typical of rhomboidal platelet structures.

SEM analyses confirmed the morphology suggested by the XRD patterns (Fig. 5.2). The standard precursor, P-VPO0 comprises rosette-like morphology, P-VPO5 comprises characteristic rosette-like agglomerates with isolated rhomboidal platelets, P-VPO15 comprises only isolated rhomboidal platelets and P-VPO25 comprises isolated rhomboidal and irregular platelets. Generally, as the concentration of PAAMA in the preparation was increased the number of rosette-like agglomerates decreased and the proportion of platelets increased in agreement with the change in intensity of the (220) and (001) reflections observed in the XRD patterns (Fig. 5.1). This change in morphology can be attributed to the co-polymer behaving as a structure directing agent that prevents the growth of crystals of particular planes, and directs it to the others.

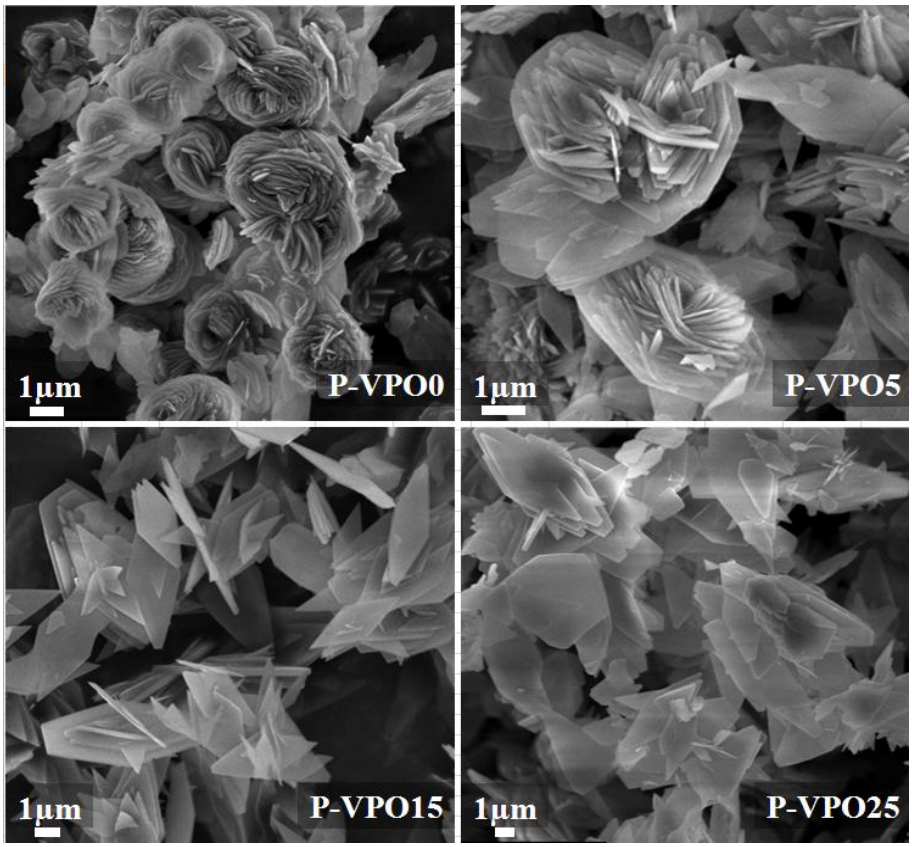

Fig. 5.2 SEM micrographs of P-VPO precursors.

Laser Raman spectroscopy was used to investigate whether there was any PAAMA present in the precursors (Fig. 5.3). However, no PAAMA was detected and the spectra were typical of the $VOHPO_4.0.5H_2O$ [28]. Table 5.2 shows a comparison between the Raman peaks for the synthesised VPO precursors and the standard reported in the literature.

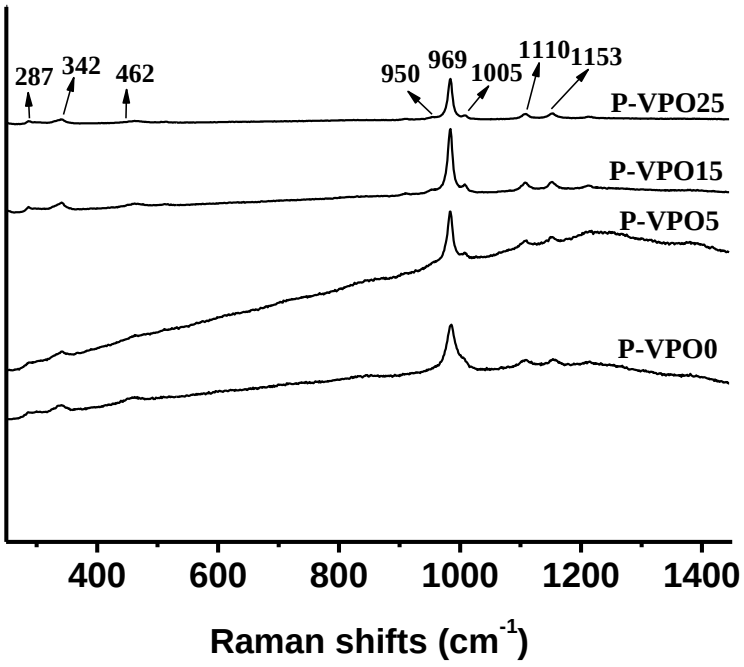

Fig. 5.3 Raman spectra of P-VPO precursors. All can be indexed to $VOHPO_4.0.5H_2O$ and there was no PAAMA present in the precursors.

Table 5.2 Raman peaks for the synthesised VPO precursors and the standard $VOHPO_4.0.5H_2O$ reported in the literature.

In the Literature [28]		**Synthesised**	
Peaks (cm^{-1})	**I/I_o**	**Peaks (cm^{-1})**	**I/I_o**
1154	medium	1153	medium
1109	medium	1110	medium
1007	week	1005	weak
981	very strong	969	Very strong
461	Week	462	weak
339	medium	342	weak
285	week	287	weak

5.5.1.2 Characterisation of precursors synthesised via VPD route

Vanadium phosphate dihydrate, $VOPO_4 \cdot 2H_2O$, was synthesised and then used for the preparation of the VPD hemihydrate precursors. The x-ray diffraction patterns of the synthesised vanadium phosphate dihydrate are shown in Fig. 5.4. All peaks can be assigned to $VOPO_4 \cdot 2H_2O$ [27, 28] and Table 5.3 illustrates the 2 theta and planes for the synthesised dihydrate and the standard reported in the literature.

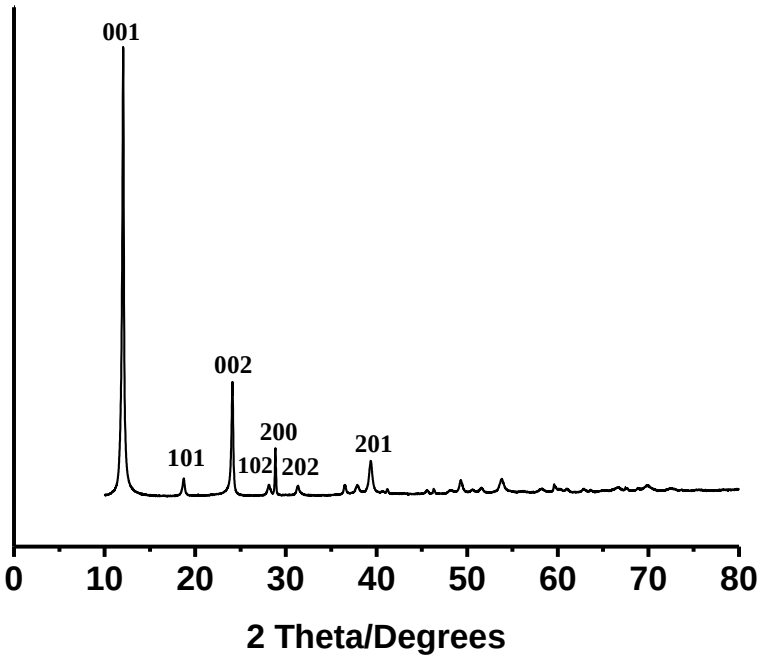

Fig. 5.4 Powder XRD patterns of $VOPO_4 \cdot 2H_2O$.

Table 5.3 The XRD reflections of the synthesised $VOPO_4 \cdot 2H_2O$ and the standard reported in the literature.

HKL	2Θ of $VOPO_4.2H_2O$	
	In the Literature [27, 28]	**Synthesised**
001	12.03°	12.04°
101	18.71°	18.72°
002	24.12°	24.11°
200	28.82°	28.84°
202	31.30°	31.33°
201	39.32°	39.36°

When the PAAMA was used in the reduction step of the vanadium phosphate dihydrate synthesised above it was observed to have a similar effect on the VPD hemihydrate precursors as the VPO materials. XRD confirmed that all precursor materials (P-VPD0, P-VPD5, P-VPD15 and P-VPD25) were $VOHPO_4.0.5H_2O$ phase (Fig. 5.5). As for the VPO precursors, the addition of PAAMA decreased the (200) reflection and increased the (001) reflection characteristic of a change in morphology from rosettes to platelets.

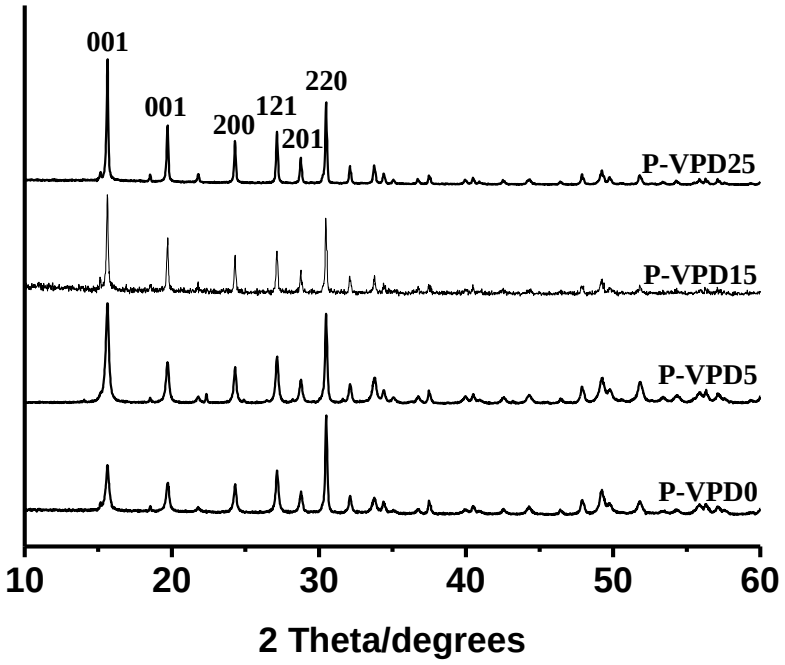

Fig. 5.5 Powder XRD patterns of P-VPD precursors. All precursors can be indexed to $VOHPO_4.0.5H_2O$

SEM analyses of the precursors (Fig. 5.6) confirmed the X-ray diffraction results. P-VPD0 comprised a rosette-like morphology, P-VPD5 comprised mainly of rosette agglomerates, P-VPD15 comprised rosette-like agglomerates with isolated rhomboidal platelets and P-VPD25 comprises isolated rhomboidal platelets. Laser Raman spectroscopy demonstrated that all precursors were typical of the $VOHPO_4.0.5H_2O$ and there was not any PAAMA detected (Fig. 5.7).

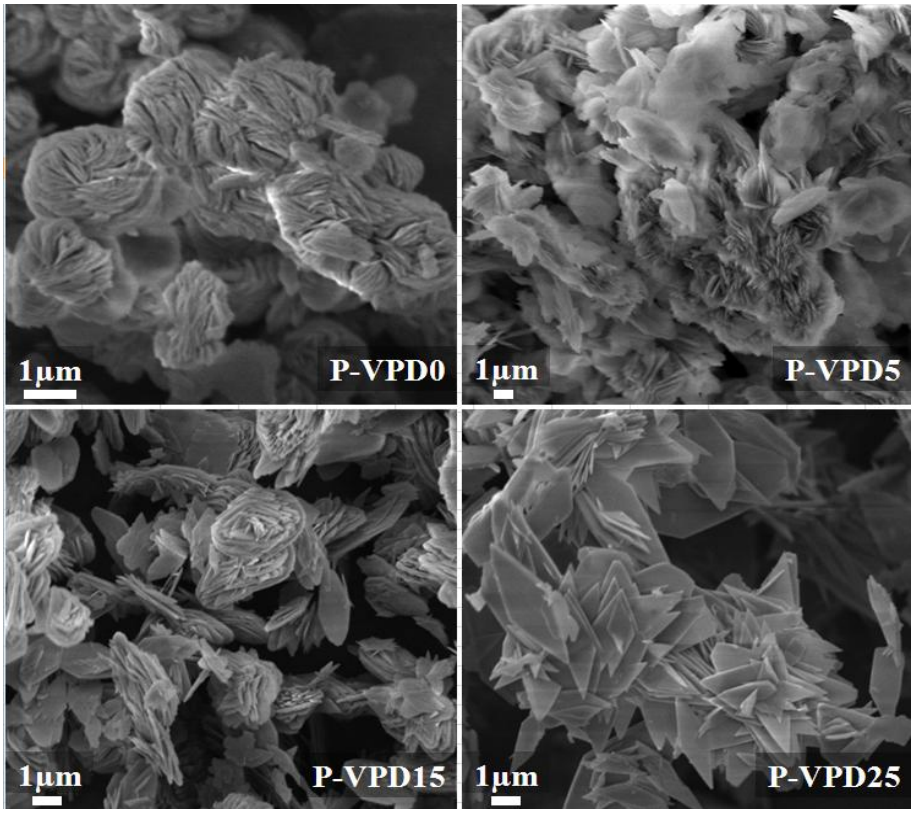

Fig. 5.6 SEM micrographs of P-VPD precursors.

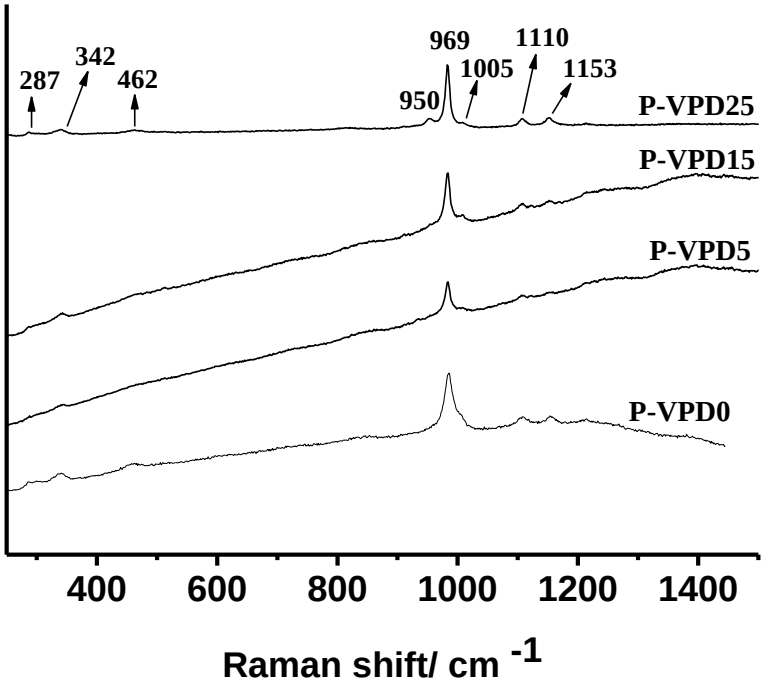

Fig. 5.7 Raman spectra of P-VPD precursors. All can be assigned to $VOHPO_4.0.5H_2O$.

It is apparent in this study that the addition of PAAMA to the precursors prepared *via* either the VPO or VPD route enhances the formation of the rhomboidal platelets and decreases the formation of rosette agglomerations as the concentration of the copolymer increases. For the material prepared without PAAMA the crystals have rough, ill-defined edges leading to hexagonal particles. When PAAMA is added (P-VPO5 and P-VPD15) the hexagonal crystallites become more regular, with well defined edges. When the concentration of PAAMA is increased (P-VPO15 and P-VPD25) only well defined edges of rhomboidal and hexagonal platelets morphology is observed without any presence of rosette agglomerates. Furthermore, the addition of PAAMA increases the

relative intensity of (001) reflection compared to the (220) reflection as the concentration of the copolymer increases. Table 5.4 summarises the effect of PAAMA concentration on the morphology of P-VPO and P-VPD precursors and on the ratio of (001)/(220) reflections.

Table 5.4 The effect of PAAMA concentration on the morphology of P-VPO and P-VPD precursors and the relative intensity of the (001)/ (220) reflections from XRD.

Concentration of PAAMA (g/L)	P-VPO precursor		P-VPD precursor	
	Relative intensity (001)/(220)	Morphology	Relative intensity (001)/(220)	Morphology
0	0.35	rosette-like	0.42	rosette-like
5	1.40	characteristic rosette-like agglomerates with isolated rhomboidal platelets	1.08	characteristic rosette-like agglomerates
15	5.14	isolated rhomboidal platelets	1.35	characteristic rosette-like agglomerates with isolated rhomboidal platelets
25	5.20	isolated rhomboidal and irregular platelets	1.77	isolated rhomboidal platelets

5.5.2 Butane oxidation studies and post-reaction characterisation

5.5.2.1 Butane oxidation studies using the precursors synthesised via VPO route

All precursor materials were activated *in situ* and tested as catalysts for butane oxidation. The precursors prepared *via* VPO route exhibited different catalytic performance. Typically, the performance of a standard catalyst (P-VPO0) (Fig. 5.8a) progressively increases as the $VOHPO_4 \cdot 0.5H_2O$ precursor is progressively transformed to the active catalyst ($(VO)_2P_2O_7$ + some V^{5+} phases) over a period of several days before it reaches a steady state performance [30]. P-VPO5, the precursor that contains characteristic rosette-like agglomerates with isolated rhomboidal platelets, was found to activate in a very short period of time compared to the standard vanadium phosphate materials (Fig. 5.8b). The precursors (P-VPO15 and P-VPO25) also reached steady-state performance quickly (< 10 h) but were found to be less active and selective to maleic anhydride compared to the P-VPO0 and P-VPO5 precursors (Fig. 5.8c and 5.8d).

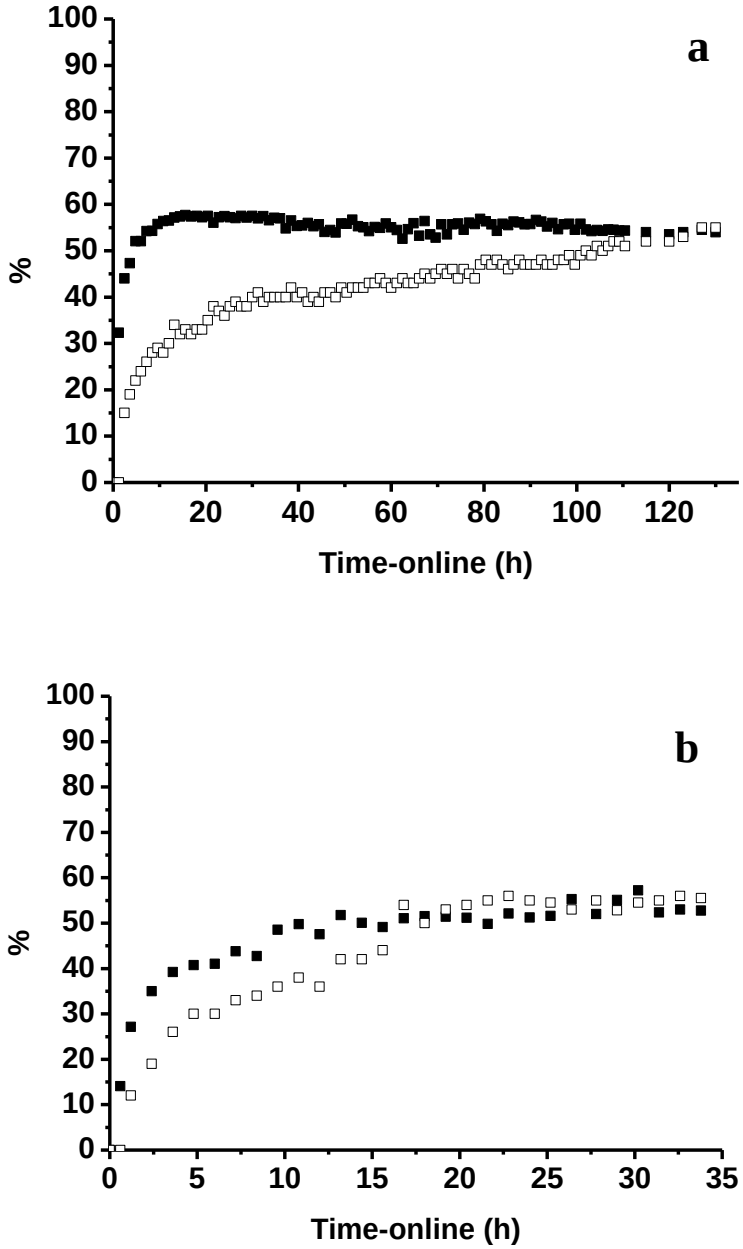

Fig. 5.8 Butane oxidation over: (a) P-VPO0 – steady state performance is reached after >100 h on line; (b) P-VPO5 – steady state performance is reached after < 18 h on line; (c) P-VPO15 and (d) P-VPO25– dramatic decrease in conversion and selectivity. (■) conversion; (□) Maleic anhydride selectivity. 1.7 % Butane in air, 400 °C, 3000 h^{-1} GHSV.

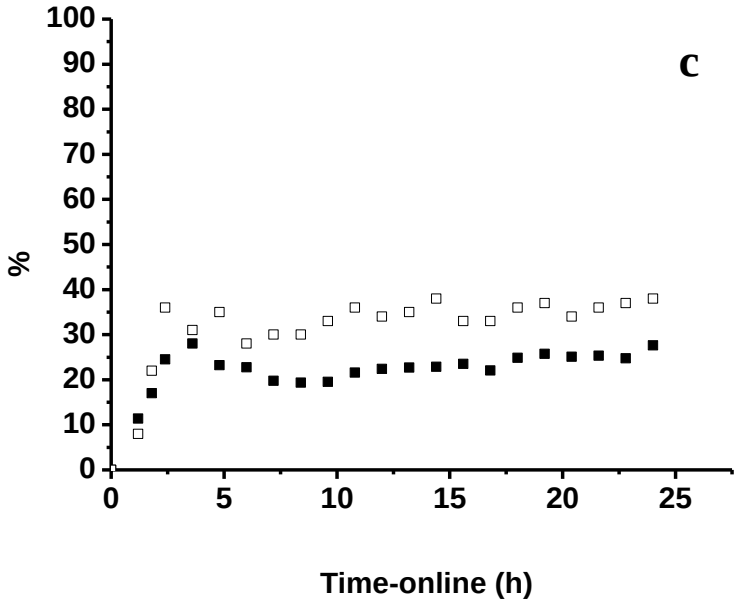

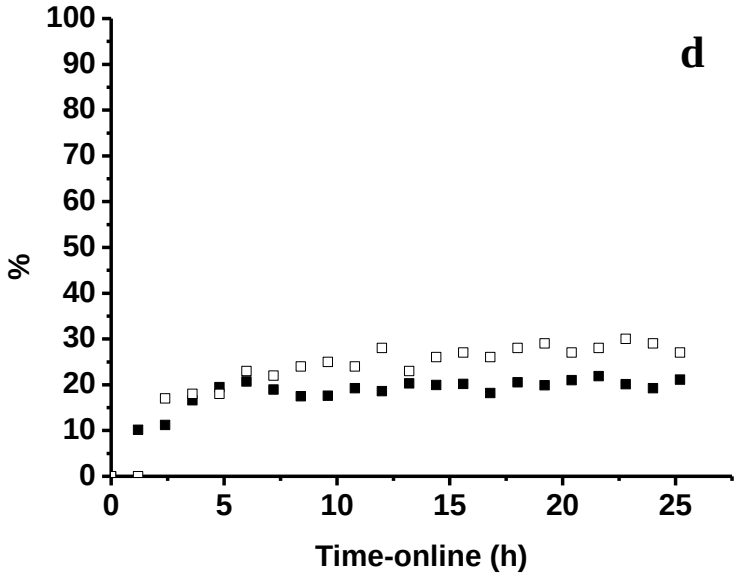

Fig. 5.8 Continued

Table 5.5 shows the normalised rates after 20 h of the reaction and at steady state for each catalyst.

Table 5.5: The normalised rates of VPO catalysts

Catalyst	Surface area (m^2g^{-1})	Rate after 20 h (mole $MAm^{-2}h^{-1}$)	Rate at steady state (mole $MAm^{-2}h^{-1}$)
CVPO0	11	1.7×10^{-5}	2.4×10^{-5}
CVPO5	12	2.2×10^{-5}	2.3×10^{-5}
CVPO15	11	0.8×10^{-5}	0.9×10^{-5}
CVPO25	10	0.4×10^{-5}	0.4×10^{-5}

The variation in catalytic performance can be understood from the characterization of the catalyst after activation. The XRD patterns of the activated catalyst C-VPO5 (Fig 5.9 and Table 5.6) show that the precursor transformed from $VOHPO_4\cdot0.5H_2O$ to $(VO)_2P_2O_7$ which is widely considered to be the active/selective phase for butane oxidation. This transformation has been shown to be topotactic, with the (001) plane of the $VOHPO_4\cdot0.5H_2O$ precursor equivalent to the (200) plane in $(VO)_2P_2O_7$ [19, 31, 32]. Therefore, the high (001)/(220) ratio of P-VPO5 compared with P-VPO0 leads to a $(VO)_2P_2O_7$ XRD pattern with a more intense (200) reflection in C-VPO5 compared to

the standard material. This indicates that the morphology of the precursors is retained and the final catalyst contains thinner platelets of $(VO)_2P_2O_7$ for the materials prepared using the copolymer structure directing agent than for the standard material. The fast activation of P-VPO5 can be attributed to the thinner platelets facilitating the removal of water from the $VOHPO_4 \cdot 0.5H_2O$ lattice during the activation. The precursors P-VPO15 and P-VPO25, which exhibited low catalytic activity, were found to contain a mixture of $(VO)_2P_2O_7$ and α_{II}-$VOPO_4$ phases (Fig. 5.9) [27, 28], which was confirmed by Raman spectroscopy (Fig. 5.10 and Table 5.7) that clearly shows that these two precursors transformed to the α_{II}-$VOPO_4$ [28, 33]. This indicates that the very thin platelet morphology that is achieved with high levels of PAAMA in the synthesis is more prone to oxidation during the activation.

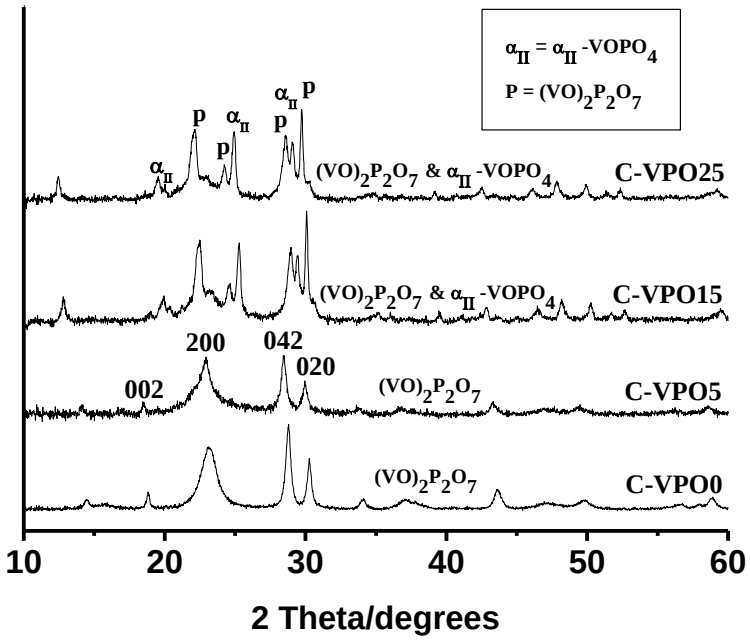

Fig. 5.9 Powder XRD patterns of the activated C-VPO catalysts.

Table 5.6 The XRD reflections of the $(VO)_2P_2O_7$ phase reported in the literature and the activated catalysts in this work.

HKL	2Θ of $(VO)_2P_2O_7$	
	In the Literature [27, 28]	**Catalyst in this work**
002	18.53°	18.55°
200	23.02°	22.95°
042	28.45°	28.44°
020	29.96°	29.94°

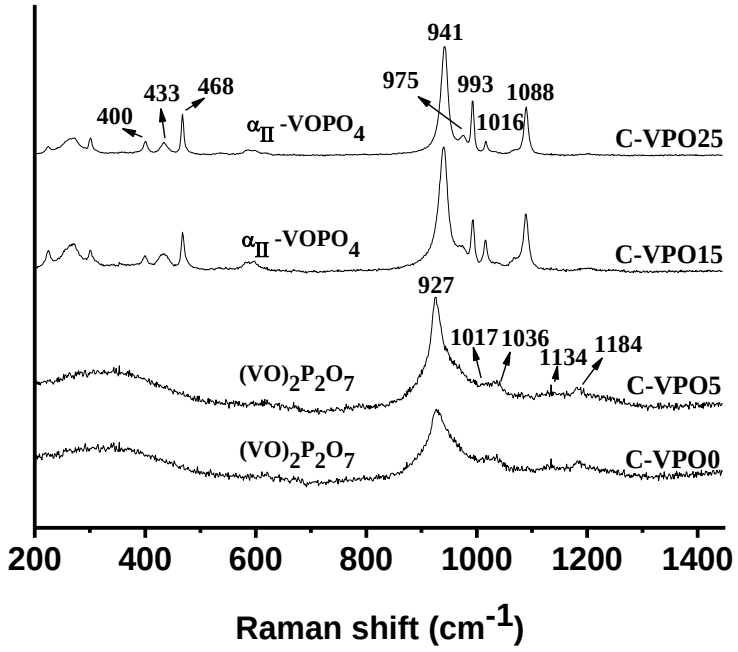

Fig. 5.10 Raman spectra of the activated C-VPO catalysts.

Table 5.7 Raman peaks of the $(VO)_2P_2O_7$ and α_{II}-$VOPO_4$ phases reported in the literature and the activated catalysts in this work.

Raman peaks of $(VO)_2P_2O_7$ (cm^{-1}) [28, 33].		**Raman peaks of α_{II}-$VOPO_4$ (cm^{-1}) [28, 33].**	
In the Literature	**In this work**	**In the Literature**	**In this work**
1182	1184	1089	1088
1135	1134	1015	1016
1035	1036	993	993
1018	1017	974	975
930	927	941	941
		468	468
		434	433
		400	400

SEM micrographs for the post reaction catalysts C-VPO0, C-VPO5, C-VPO15 and C-VPO25 (Fig. 5.11) show the same morphology observed in precursor materials P-VPO0, P-VPO5, P-VPO15 and P-VPO25 (Fig. 5.2) confirming the previous studies that this reaction is topotactic [19, 31, 32]. Lin *et al.* [25] demonstrated from using TEM studies of catalysts prepared with PSMA that, although the interior of the platelets is crystalline, an amorphous rim forms around the edge of the platelet. This is in keeping with the previous studies that the active site for butane oxidation is an amorphous over layer on a crystalline or amorphous bulk support [34-36].

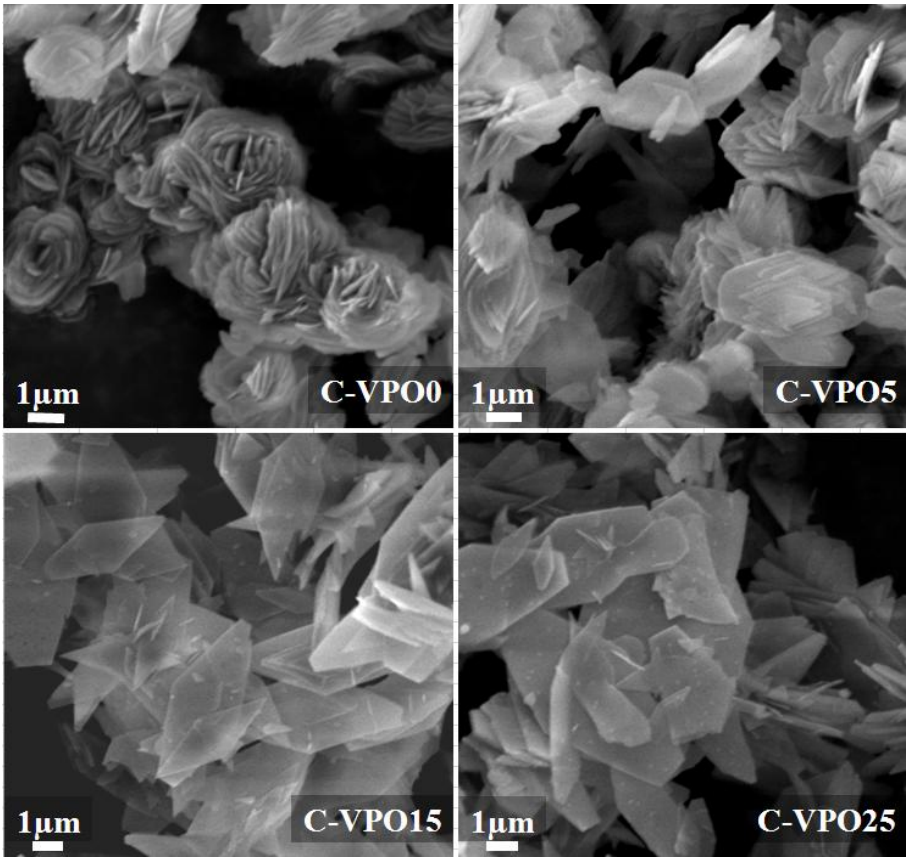

Fig. 5.11 SEM micrographs of C-VPO catalysts

5.5.2.2 Butane oxidation studies using the precursors synthesised via VPD route

The VPD precursors show similar catalytic behaviour. P-VPD0 and P-VPD5 that have a rosette morphology were activated over several days as the $VOHPO_4 \cdot 0.5H_2O$ precursor is gradually transformed *in situ* to the active catalyst ($(VO)_2P_2O_7$ + some V^{5+} phases) (Fig 5.12a and Fig 5.12b respectively). P-VPD15, that contains characteristic rosette-like agglomerates with isolated rhomboidal platelets, activated in a short time compared to P-VPD0 (Fig 5.12c) and achieved a comparable steady state performance after just 15 h on-line.

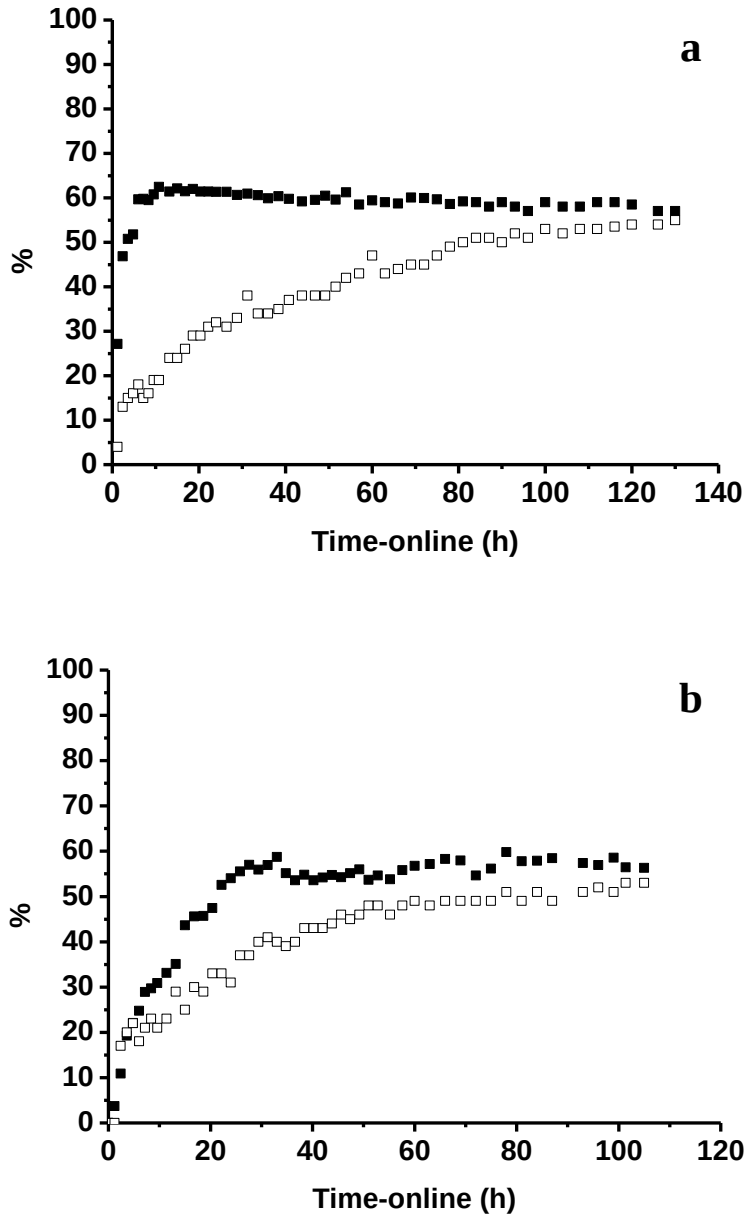

Fig. 5.12 Butane oxidation over: (a) P-VPD0 – steady state performance is reached after >100 h on line; (b) P-VPD5 – steady state performance is reached after > 100 h on line; (c) P-VPD15 – steady state performance is reached after > 15 h and (d) P-VPD25– dramatic decrease in conversion and selectivity. (■) conversion; (□) Maleic anhydride selectivity. 1.7 % Butane in air, 400 °C, 3000 h^{-1} GHSV.

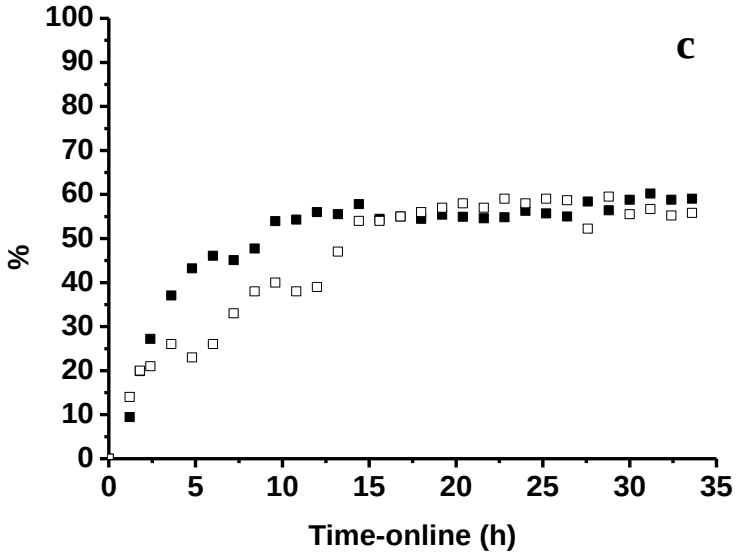

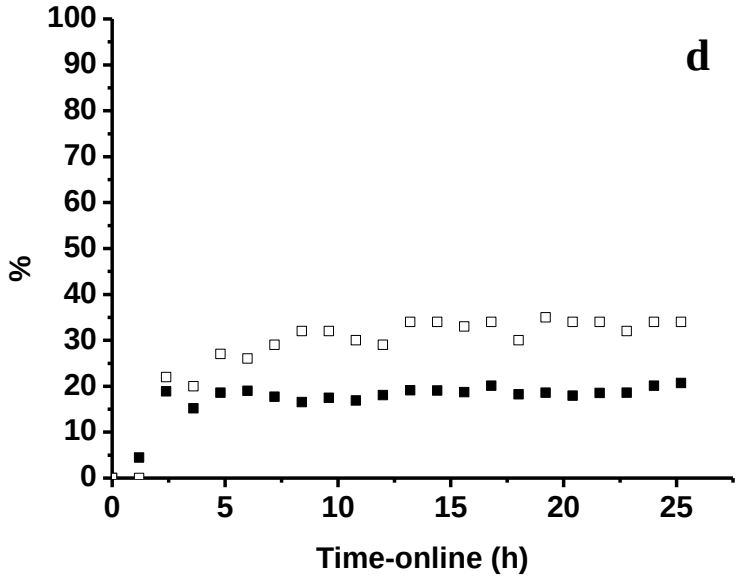

Fig. 5.12 Continued

Table 5.8 shows the normalised rates after 20 h of the reaction and at steady state for each catalyst.

Table 5.8: The normalised rates of VPD catalysts

Catalyst	Surface area (m^2g^{-1})	Rate after 20 h (mole $MAm^{-2}h^{-1}$)	Rate at steady state (mole $MAm^{-2}h^{-1}$)
CVPD0	13	1.3×10^{-5}	2.2×10^{-5}
CVPD5	13	1.2×10^{-5}	2.1×10^{-5}
CVPD15	15	1.9×10^{-5}	2.1×10^{-5}
CVPD25	13	0.5×10^{-5}	0.5×10^{-5}

It is clear from this that C-VPD0, C-VPD5 and C-VPD15 all end up with similar performance, but that C-VPD15 reaches this level much faster than the other catalysts. SEM showed that there is a topotactic transformation and the morphology of the precursors is retained in the active catalysts (Fig. 5.13).

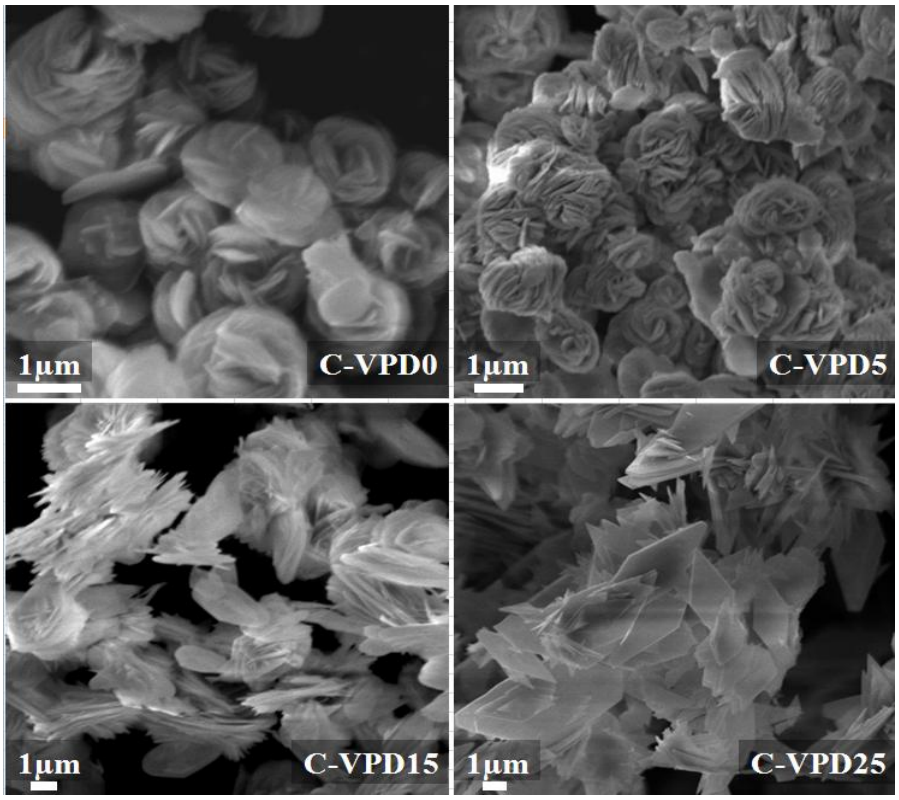

Fig. 5.13 SEM micrographs of C-VPD catalysts.

The XRD patterns for the activated catalysts (Fig. 5.14) display that C-VPD15 catalyst has sharper and more intense (200) reflection of $(VO)_2P_2O_7$ compared to C-VPD0 and C-VPD5 which illustrates the thinner platelet morphology which leads to the fast activation of the precursor. A dramatic drop in conversion and selectivity was observed for C-VPD25 (Fig. 12d) and this was found to contain large amounts of α_{II}-$VOPO_4$ by XRD and Raman spectroscopy (Fig. 5.14 and 5.15), confirming the findings for the VPO catalysts, that a very thin platelet morphology leads to oxidised catalysts.

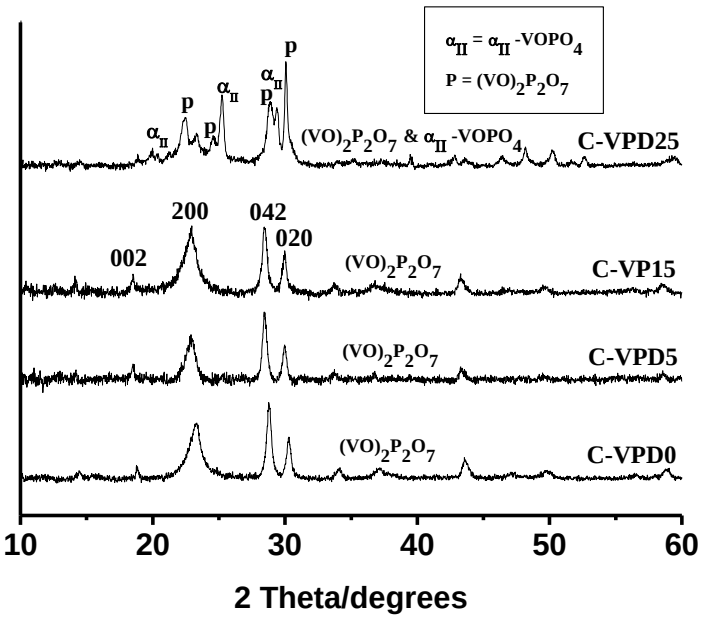

Fig. 5.14 Powder XRD patterns of the activated C-VPD catalysts.

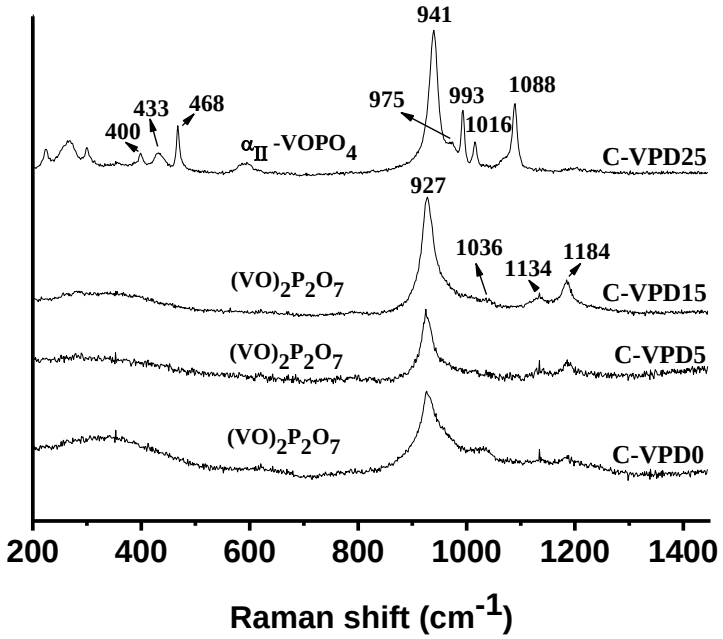

Fig. 5.15 Raman spectra of the activated C-VPD catalysts.

Table 5.9 illustrates a comprehensive summary about the effect of PAAMA concentration on the morphology, structure and hence the catalytic performance of VPO and VPD catalysts.

Table 5.9: The normalised rates of VPD catalysts

Concentration of PAAMA (g/L)	Route	Morphology	Vanadium species	Relative intensity (001)/(220)	Rate × 10^{-5} (mole $MAm^{-2}h^{-1}$)	
					After 20 h	At steady state
0	VPO	Rosette	$(VO)_2P_2O_7$	0.35	1.7	2.4
	VPD	Rosette	$(VO)_2P_2O_7$	0.42	1.3	2.2
5	VPO	Rosette & platelets	$(VO)_2P_2O_7$	1.40	2.2	2.3
	VPD	Rosette	$(VO)_2P_2O_7$	1.08	1.2	2.1
15	VPO	platelets	$VOPO_4$ & $(VO)_2P_2O_7$	5.14	0.8	0.9
	VPD	Rosette & platelets	$(VO)_2P_2O_7$	1.35	1.9	2.1
25	VPO	platelets	$VOPO_4$ & $(VO)_2P_2O_7$	5.20	0.4	0.4
	VPD	platelets	$VOPO_4$ & $(VO)_2P_2O_7$	1.77	0.5	0.5

The results in Table 5.9 clearly demonstrate that only the characteristic rosette-like agglomerates with isolated rhomboidal platelets morphology which has a relative intensity ratio of the (001)/(220) reflections of around 1.4 can activate in a very short time (P-VPO5 and P-VPD15)), and show good performance as catalysts for the selective oxidation of butane to maleic anhydride. It seems that an optimum concentration of the copolymer is needed to form a precursor with these features. However, the thin platelet morphology which is formed by the addition of high concentrations of PAAMA that have a high relative intensity ratio of the (001)/(220) reflections exhibit a poor catalytic performance as the thin plates are easily oxidised to $VOPO_4$.

The higher solubility of PAAMA allowed the use of it in the VPD route as well as the VPO route. In a previous study [25] PSMA could only be used in VPO route as it was found to be insoluble in the alcohol used in the reduction step of $VOPO_4.2H_2O$. Furthermore, by using higher concentrations of PAAMA, a platelet morphology with a high ratio of (001)/(220) reflections can be achieved. Consequently, further investigations of the effect on the catalytic performance and the phases formed after activation can be carried out. In addition, Laser Raman spectroscopy was employed in this study to investigate if any amount of the copolymer was present in the precursors that might affect their activity. The novelty of this work compared with the previous study is showed in Table 5.10.

Table 5.10: The novelty of this work compared to the previous study used different copolymer [25].

		Copolymer	
		PSMA [25]	PAAMA [this study]
Route		VPO route only	VPO and VPD route
Polymer concentration (polymer:V_2O_5)		1:65 Only low concentrations of PSMA were used due its insolubility	1:1 Much higher concentrations of PAAMA could be used due to its solubility
Relative intensity (001)/(220)		1.6 maximum	5.2 could be achieved
Morphology		Rosette-like only	Varied from rosette-like to isolated platelets when high conc. Of PAAMA was used
Surface area (m^2g^{-1})		10-20	10-15
XRD	precursor	$VOHPO_4.0.5H_2O$	$VOHPO_4.0.5H_2O$
	catalyst	$(VO)_2P_2O_7$	Varied from $(VO)_2P_2O_7$ when low concentration of PAAMA was used to $VOPO_4$ at high concentrations
Raman	precursor	Not reported	$VOHPO_4.0.5H_2O$
	catalyst	Not reported	Varied from $(VO)_2P_2O_7$ when low concentration of PAAMA was used to $VOPO_4$ at high concentrations

5.6 Conclusion

Using PAAMA in the preparation of vanadium phosphate catalysts was displayed to affect the morphology of the resultant precursors as well as performance of their corresponding catalysts. It was found that the addition of PAAMA increased the crystallinity of the synthesised precursors and as the concentration of PAAMA increased the morphology altered from a rosette-like to characteristic rosette-like agglomerates with isolated rhomboidal platelets and eventually to isolated platelets. Moreover, the XRD patterns confirmed these results and the relative intensity ratio of the (001)/(220) reflections was found to increase with the addition of PAAMA. This could be ascribed to copolymer acting as a structure directing agent that can interacts with the (001) $VOHPO_4.0.5H_2O$ plane preventing growth in this direction leading to thinner platelets.

When these precursors used as catalysts for butane oxidation they exhibited different activation behaviours. The precursors synthesised using PAAMA which had characteristic rosette-like agglomerates with isolated platelets morphology and a relative intensity ratio of the (001)/(220) reflections of around 1.4 activated much faster in situ to the active catalyst compared to the precursors prepared using the standard methodology. However, those that had isolated platelets morphology and a high relative intensity ratio of the (001)/(220) reflections displayed poor performance as they were oxidised to α_{II}-$VOPO_4$ phases. An optimum concentration of PAAMA is required to control the features of the synthesised precursor to achieve an active catalyst.

5.7 References

1. Hutchings, G.J., *Vanadium phosphate: a new look at the active components of catalysts for oxidation of butane to maleic anhydride.* J. Mater. Chem., 2004. **14**: p. 3385-3395.

2. Hutchings, G.J., *Heterogeneous catalysts-discovery and design.* J. Mater. Chem., 2008. **19**: p. 1222-1235.

3. Guliants, V.V. and M.A. Carreon, *Vanadium-Phosphorus-Oxides: from Fundamentals of n-Butane Oxidation to Synthesis of New Phases.* Catalysis, 2005. **18**: p. 1-45.

4. Cabello Sanchez, F.J., et al., *Effect of Dehydration of $VOPO_4 \cdot 2H_2O$ on the Preparation and Reactivity of Vanadium Phosphate Catalyst for the Oxidation of n-Butane.* Catalysis Letters, 2001. **77**(4): p. 189-192.

5. Hutchings, G.J., et al., *High temperature preparation of vanadium phosphate catalysts using water as solvent.* Phys. Chem. Chem. Phys., 2003. **5**: p. 3525-3533.

6. Hutchings, G.J., et al., *Improved method of preparation of vanadium phosphate catalysts.* Catalysis Today, 1997. **33**(1–3): p. 161-171.

7. Bartley, J.K., R.P.K. Wells, and G.J. Hutchings, *The Unexpected Role of Aldehydes and Ketones in the Standard Preparation Method for Vanadium Phosphate Catalysts.* Journal of Catalysis, 2000. **195**(2): p. 423-427.

8. Lopez-Sanchez, J.A., et al., *High temperature preparation of vanadium phosphate catalysts using water as solvent.* Physical Chemistry Chemical Physics, 2003. **5**(16): p. 3525-3533.

9. Bartley, J.K., et al., *Comparison of vanadium phosphate catalysts derived from $VOPO_4.2H_2O$ prepared from H_3PO_4 and $H_4P_2O_7$.* Physical Chemistry Chemical Physics, 2001. **3**(20): p. 4606-4613.

10. Antonio Lopez-Sanchez, J., et al., *Preparation of high surface area vanadium phosphate catalysts using water as solvent.* New Journal of Chemistry, 2002. **26**(11): p. 1613-1618.

11. Shimoda, T., T. Okuhara, and M. Misono, *Preparation of Vanadium-Phosphorous Mixed-Ooxide (P/V=1) Catalysts and Their Applicaion to Oxidation of Butane To Maleic-Anhydride.* Bulletin of the Chemical Society of Japan, 1985. **58**(8): p. 2163-2171.

12. Poli, G., et al., *The chemistry of catalysts based on vanadium-phosphorous oxides: Note II The role of the method of preparation.* Applied Catalysis, 1981. **1**(6): p. 395-404.

13. Mizuno, N., H. Hatayama, and M. Misono, *One-Pot Synthesis of $VOHPO_4 \cdot 0.5H_2O$ with High Growth of the (001) Plane: An Important Catalyst Precursor of $(VO)_2P_2O_7$.* Chemistry of Materials, 1997. **9**(12): p. 2697-2698.

14. O'Connor, M., F. Dason, and B.K. Hodnett, *Preparation of vanadium phosphorus oxide catalysts: Influence of macroscopic P:V ratio in determining phase composition after calcination.* Applied Catalysis, 1990. **64**(0): p. 161-171.

15. Doi, T. and T. Miyake, *Influence of alcohol solvents on characters of $VOHPO_4 \cdot 0.5H_2O$ prepared from V_4O_9 and ortho-H_3PO_4.* Applied Catalysis A: General, 1997. **164**(1–2): p. 141-148.

16. Miyake, T. and T. Doi, *Importance of a quasistable V_4O_9 to synthesize a highly crystalline $VOHPO_4 \cdot 0.5H_2O$.* Applied Catalysis A: General, 1995. **131**(1): p. 43-54.

17. Guilhaume, N., et al., *Butane Oxidation To Maleic Anhydride On Vpo Catalysts: The Importance Of The Preparation Of The Precursor On The Control Of The Local Superficial Structure*, in *Studies in Surface Science and Catalysis*, P. Ruiz and B. Delmon, Editors. 1992, Elsevier. p. 255-265.

18. Bartley, J.K., et al., *Vanadium(V) phosphate prepared using solvent-free method.* Catalysis Letters, 2001. **72**(1): p. 99-105.

19. Johnson, J.W., et al., *Preparation and characterization of vanadyl hydrogen phosphate hemihydrate and its topotactic transformation to vanadyl pyrophosphate.* Journal of the American Chemical Society, 1984. **106**(26): p. 8123-8128.

20. Horowotz, H.S., et al., *VPO catalysts for oxidation of butane to maleic anhydride: Influence of $(VO)_2H_4P_2O_9$ precursor morphology on catalytic properties.* Applied Catalysis, 1988. **38**(2): p. 193-210.

21. Yu, J., H. Guo, and B. Cheng, *Shape evolution of $SrCO_3$ particles in the presence of poly-(styrene-alt-maleic acid).* Journal of Solid State Chemistry, 2006. **179**: p. 800-803.

22. Singh, N.P. and N.B. Singh, *Interaction between poly(styrene-alt-maleic acid) sodium salt and hydrating Portland cement.* Progress in Crystal Growth and Characterization of Materials, 2006. **52**(1–2): p. 84-90.

23. Yu, J., et al., *Morphological control of calcium oxalate particles in the presence of poly-(styrene-alt-maleic acid).* Journal of Solid State Chemistry, 2004. **177**(10): p. 3368-3374.

24. Chung, D.D.L., *Use of polymers for cement-based structural materials.* Journal of Materials Science, 2004. **39**(9): p. 2973-2978.

25. Lin, Z., et al., *The synthesis of highly crystalline vanadium phosphate catalysts using a diblock copolymer as a structure directing agent.* Catalysis Today, 2010. **157**(1–4): p. 211-216.

26. Hutchings, G.J., et al., *Comments on the nature of the active site of vanadium phosphate catalysts for butane oxidation.* Catalysis Today, 1998. **40**(2–3): p. 273-286.

27. Bordes, E., *Crystallochemistry of V-P-O phases and application to catalysis.* Catalysis Today, 1987. **1**(5): p. 499-526.

28. Guliants, V.V., et al., *The effect of the phase composition of model VPO catalysts for partial oxidation of n-butane.* Catalysis Today, 1996. **28**(4): p. 275-295.

29. Ellison, I.J., et al., *Control of the composition and morphology of vanadium phosphate catalyst precursors from alcohol treatment of $VOPO_4$[middle dot]$2H_2O$.* Journal of the Chemical Society, Chemical Communications, 1994(9): p. 1093-1094.

30. Lombardo, E.A., C.A. Sánchez, and L.M. Cornaglia, *The effect of preparation methods and activation strategies upon the catalytic behavior of the vanadium-phosphorus oxides.* Catalysis Today, 1992. **15**(3–4): p. 407-418.

31. Bawaked, S., et al., *Solvent-free selective epoxidation of cyclooctene using supported gold catalysts: an investigation of catalyst re-use.* Green Chemistry, 2011. **13**(1): p. 127-134.

32. Kiely, C.J., et al., *Structural transformation sequences occurring during the activation of vanadium phosphorus oxide catalysts.* Faraday Discussions, 1996. **105**: p. 103-118.

33. Xue, Z.-Y. and G.L. Schrader, *In Situ Laser Raman Spectroscopy Studies of VPO Catalyst Transformations.* The Journal of Physical Chemistry B, 1999. **103**(44): p. 9459-9467.

34. Hutchings, G.J., et al., *Role of the product in the transformation of a catalyst to its active state.* Nature, 1994. **368**(6466): p. 41-45.

35. Kiely, C.J., et al., *Characterisation of Variations in Vanadium Phosphate Catalyst Microstructure with Preparation Route.* Journal of Catalysis, 1996. **162**(1): p. 31-47.

36. Sajip, S., et al., *in: E.G. Derouane (Ed.), Catalytic Activation and Functionalisation of Light Alkanes*. 1998: Kluwer Academic Publishers.

Chapter 6

Conclusion and future work

6.1 Conclusion

In this study, two of catalytic models were prepared with distinct morphologies namely supported gold catalysts and vanadium phosphate catalysts. The prepared catalysts were characterised and evaluated for particular chemical reactions as it has been addressed. In both models, control of the morphology of the support used in gold catalysts and of the precursors in the case of vanadium phosphate catalysts has been proved to have a crucial role in the catalyst activity.

6.1.1 Gold catalysts

In gold catalysis, it is well documented that the support can have a very important influence in determining the catalyst performance [1, 2]. The morphology and the structure of the support are important as they can possess properties that affect the catalysts activity such as the gold particle size, the dispersion of gold on the support facilitate the redox efficiency of the catalysts [3, 4].

The main objective of this study was to investigate the effect of the morphology and the structure of the support on the catalyst activity. In selected cases, the preparation method of gold catalysts was investigated. The catalysts were examined for the oxidation of benzyl alcohol and carbon monoxide as examples. Ceria supports were prepared hydrothermally over different crystallisation times by reacting L-Asparagine and $CeCl_3.7H_2O$ at 160 °C. SEM microscopy illustrated that the morphology of the prepared ceria differed considerably with the crystallisation time. The ceria prepared at 2 h had a spherical morphology whereas a foam structure formed for the samples

prepared at crystallisation time from 4 to 48 h. However, the sample prepared after 4 h possessed the highest surface area and was the most porous structure. As the crystallisation time increased the foam structure became less porous and eventually collapsed. Nano-crystals of gold were deposited by sol-immobilisation on all ceria foams as well as two commercial samples of ceria for comparison purposes. Gold catalysts supported on the foamCeO_2 exhibited greater performance than Au/commercialCeO_2 catalysts for the solvent-free oxidation of benzyl alcohol using molecular O_2 as an oxidant. The activity of Au/foamCeO_2 catalysts was found to depend on the crystallisation time of the foam and Au/foamCeO_2-4h illustrated the best activity. Re-use of Au/foamCeO_2-4h was studied as it showed the best performance and the catalyst was completely reusable which is beneficial in terms of green chemical operation. STEM microscopy was employed to investigate the gold size distribution for two catalysts [i.e. Au/CeO_2 (Aldrich) and Au/foamCeO_2-4 h samples]. The mean size of the gold nanoparticles was 2.2 nm when added to the commercial ceria while it was 8 nm for the gold nanoparticles when supported on ceria foam although the same Au sol was used for both samples. The STEM results clearly showed that the support can play an important influence in gold catalysis as the catalyst with the larger mean size (Au/foamCeO_2-4h) exhibited the best activity. TPR analysis was used to investigate the reactivity of the ceria for foamCeO_2-4h and the commercial standard (Aldrich) along with their corresponding Au/CeO_2 materials. TPR analysis confirmed that the foamCeO_2-4h has a greater surface reducibility compared to the commercial one and the addition of Au increased the reducibility further. This indicates that foam ceria has more surface oxygen available which makes it ideal for oxidation reactions. The

Au/foamCeO_2 catalysts were found to perform well (showed higher activity and complete reusability) for benzyl alcohol oxidation using a green process and the superiority is considered to be related to the support.

In Chapter 4, MnO_2 was prepared by the hydrothermal reaction of $MnSO_4.H_2O$ and $(NH_4)_2S_2O_8$ at 120 °C. The effect of the crystallisation time, varied from 6-240 h, on the structure and morphology of the resultant MnO_2 was studied. The phase and the morphology of MnO_2 were found to be time dependent. Powder XRD patterns indicated that the samples were mainly α-MnO_2 for the samples prepared at lower crystallisation time, 6-24 h, and as the crystallisation time increased, above 24 h, β-MnO_2 formed and persisted for the longer crystallisation times (72-240 h). The morphology also changed remarkably with the crystallisation time. The SEM showed that a micro-spherical structure formed over 6 to 12 h and the spheres started to collapse by increasing the crystallisation time above 12 h until the nanowire structure totally formed for 72-240 h samples. The surface area was much higher for the microsphere structure, 6-12 h samples, than the nanowire, 72-240 h and it was found to notably decrease as the crystallisation time increased. Generally speaking, lower crystallisation time produces α-MnO_2, microsphere structure and higher surface area while as the time increased β-MnO_2, nanowire structure and low surface area were produced. Nano-particles of gold were deposited on all MnO_2 materials and the effect of preparation method of gold on the oxidation of benzyl alcohol was investigated. In addition CO oxidation was performed with the Au/MnO_2-12h catalyst. Four different methods were used to add gold onto MnO_2 materials namely impregnation (IM), sol-immobilisation (SI), reflux

sol-immobilisation (RSI) and deposition precipitation (DP). The SI displayed the best performance towards benzyl alcohol while the DP and then RSI were the best for CO oxidation. The IM method was found to be very poor towards these reactions. DP produced smaller Au particles than the other preparation methods (mean value of 2.5 nm) which is very crucial for CO oxidation as the smaller Au particles provide facilitate a strong Au-MnO_2 interaction and provide effective adsorption of CO [5, 6]. RSI exhibited much better performance towards CO oxidation than SI due to the facile removal of PVA from the RSI catalysts [7]. The effect of the crystallisation time of the prepared MnO_2 and their phases on the activity of their corresponding Au catalysts was examined. For all preparation methods, SI, RSI and DP, it was found that α-MnO_2 microspherical catalysts (6-12 h) exhibited better catalytic activity for the oxidation of benzyl alcohol than β-MnO_2 nanowires catalysts (72-240 h). However, the β-MnO_2 nanowires catalysts possessed the greater performance for CO oxidation and the Au/MnO_2-96h was found to be the best. It was considered that the Au particle size and the TPR analysis, which indicated that the Au nanoparticles were found to be much smaller in case of β-MnO_2 nanowires catalysts. TPR analysis showed that the surface was more easily reduced for the β-MnO_2 nanowires catalysts compared to α-MnO_2 microspheres ones because of the smaller Au particles presented in β-MnO_2 nanowires catalysts that led to a stronger Au-MnO_2 interaction that facilitated the adsorption of CO and the surface reduction with oxygen species provided by the support. Generally, the preferred morphology and phase for benzyl alcohol oxidation were α-MnO_2 microspheres catalysts whereas the preferred morphology and phase for CO oxidation were β-MnO_2 nanowires due to the smaller Au particles as well as the ease of their

surface reduction. The SEM confirmed that the morphology structure of these catalysts whether micro-spherical or the nanowire-type were robust and stable under stirring condition and they were fully reusable.

The results in Chapter 3 and Chapter 4 demonstrate that the support, its morphology and phase in this case, can play an essential role in gold catalysis as it can determine the gold particle size, gold distribution on it and the surface reducibility.

6.1.2 Vanadium phosphate catalysts

Vanadium phosphate catalysts are used commercially for the production of maleic anhydride by the oxidation of n-butane. The vanadyl pyrophosphate phase, $(VO)_2P_2O_7$, is considered the main active phase in the vanadium phosphates catalysts and this phase is derived from the activation of its hemihydrate precursor; $VOHPO_4.0.5H_2O$. The transformation of the $VOHPO_4.0.5H_2O$ precursor to the active catalyst $(VO)_2P_2O_7$ is topotactic as a result the morphology and surface area are dependent on those of the precursor. Therefore, to attain an active catalyst requires a careful preparation of the precursor $VOHPO_4.0.5H_2O$. Many studies have been reported regarding the influence of the precursor morphology on the catalyst activity as it can determine the catalytic performance for n-butane oxidation [8-11].

In Chapter 5, poly (acrylic acid-co-maleic acid) copolymer (PAAMA) was used as a structure directing agent. This polymer has been was shown to be very effective for altering the morphology and the structure of the prepared hemihydrate precursors via

both VPO and VPD routes. It was found that all VPO and VPD precursors were $VOHPO_4 \cdot 0.5H_2O$ when examined by XRD and there was not any PAAMA present in the precursors as confirmed by Laser Raman spectroscopy. When the concentration of PAAMA was increased the (001) reflection was found to increase while the (220) reflection decreased with PAAMA addition. SEM analysis confirmed the observations from the XRD patterns and it was found that as the concentration of PAAMA increased the morphology altered from a rosette-like (P-VPO0 and P-VPD0) to characteristic rosette-like agglomerates with isolated rhomboidal platelets (P-VPO5, P-VPD15) and eventually to isolated platelets (P-VPO15, P-VPO25 and P-VPD25). The alteration in the structure and morphology of the vanadium phosphate precursors led to different activation behaviours when they were used for the partial oxidation of butane to maleic anhydride. The precursors synthesised using PAAMA which had characteristic rosette-like agglomerates with isolated platelet morphology (C-VPO5 and C-VPD15) which activated *in situ* much faster to the active phase $(VO)_2P_2O_7$ and the steady state of conversion and selectivity was achieved in a very short time compared to the standard precursors (C-VPO0 and C-VPD0). However, the platelet morphology (C-VPO15, C-VPO25 and P-VPD25) exhibited a poor catalytic performance as they were oxidised to α_{II}-VOPO4 rapidly as confirmed by XRD and Raman spectroscopy. Therefore, it has been concluded that an optimum concentration of PAAMA is required to control the morphology and the structure of vanadium phosphate catalysts that can be more effective for butane oxidation.

6.2 Future work

6.2.1 Gold catalysts

6.2.1.1 Au/CeO_2 foam

- In this work, only the effect of the reaction time on the ceria morphology has been investigated. The effect of the other factors such as the molar ratio of the reactants, L-Asparagine and Cerium (III) chloride heptahydrate $CeCl_3.7H_2O$, and the reaction temperature could produce interesting morphologies of ceria rather than foam and then use them as supports for gold catalysis.
- Study other preparation methods of gold that could work in gas phase reactions like deposition precipitation method.
- Use copolymers such as poly (acrylic acid-co-maleic acid), which used as a structure directing agent in vanadium phosphate catalysts, in the preparation of metal oxides.

6.2.1.2 Au/MnO_2 nanowire microspheres

- Investigate the other factors such as the molar ratio between the reactants, hydrated manganese sulfate $MnSO_4.H_2O$ and ammonium persulfate $(NH_4)_2S_2O_8$ and the reaction temperature on the morphology of the resultant MnO_2.

- Examine whether the same preparation methodology of MnO_2 support can be applied on the other metals using their corresponding hydrated metal sulfate such as iron (II) sulfate hydrate ($FeSO_4.xH_2O$), magnesium sulfate hydrate

($MgSO_4.xH_2O$), copper (II) sulfate hydrate ($CuSO_4.xH_2O$) and vanadium (IV) oxide sulfate hydrate ($VOSO_4.xH_2O$).

6.2.2 Vanadium phosphate catalysts

- Use other di-block copolymers or additives that could behave as structure directing agents and study the influence of adding them on the morphology and the structure of the VPO precursors and on their performance as catalysts for butane oxidation.
- Apply this methodology, the addition of copolymer, on other catalytic systems especially the mixed metals oxide.

6.3 References

1. Bond, G.C., C. Louis, and D.T. Thompson, *Catalysis by Gold*. Catalytic Science Series, ed. G.J. Hutchings. Vol. 6. 2006, London: Imperial College Press.

2. Huang, J., W.-L. Dai, and K. Fan, *Remarkable support crystal phase effect in Au/FeO_x catalyzed oxidation of 1,4-butanediol to γ-butyrolactone.* Journal of Catalysis, 2009. **266**(2): p. 228-235.

3. Carrettin, S., et al., *Nanocrystalline CeO_2 Increases the Activity of Au for CO Oxidation by Two Orders of Magnitude.* Angewandte Chemie International Edition, 2004. **43**(19): p. 2538-2540.

4. Huang, X.-S., et al., *Morphology effects of nanoscale ceria on the activity of Au/CeO_2 catalysts for low-temperature CO oxidation.* Applied Catalysis B: Environmental, 2009. **90**(1–2): p. 224-232.

5. Haruta, M., et al., *Low-Temperature Oxidation of CO over Gold Supported on TiO_2, α-Fe_2O_3, and Co_3O_4.* Journal of Catalysis, 1993. **144**(1): p. 175-192.

6. Tana, et al., *Influence of Au particle size on Au/CeO_2 catalysts for CO oxidation.* Catalysis Today, 2011. **175**(1): p. 541-545.

7. Lopez-Sanchez, J.A., et al., *Facile removal of stabilizer-ligands from supported gold nanoparticles.* Nat Chem, 2011. **3**(7): p. 551-556.

8. Hutchings, G.J., et al., *Improved method of preparation of vanadium phosphate catalysts.* Catalysis Today, 1997. **33**(1–3): p. 161-171.

9. Griesel, L., et al., *Preparation of vanadium phosphate catalysts from $VOPO_4{\cdot}2H_2O$: effect of $VOPO_4{\cdot}2H_2O$ preparation on catalyst performance.* Journal of Molecular Catalysis A: Chemical, 2004. **220**(1): p. 113-119.

10. Kamiya, Y., et al., *Microstructures of V-P-O catalysts derived from $VOHPO_4{\cdot}0.5H_2O$ of different crystallite sizes.* Journal of Molecular Catalysis A: Chemical, 2004. **220**(1): p. 103-112.

11. Lin, Z., et al., *The synthesis of highly crystalline vanadium phosphate catalysts using a diblock copolymer as a structure directing agent.* Catalysis Today, 2010. **157**(1–4): p. 211-216.